

SOME STUDIES ON SPRAY CHARACTERISTICS OF ALTERNATIVE FUEL AND THEIR EFFECT ON COMBUSTION, PERFORMANCE AND EMISSIONS

**A Thesis submitted to the Delhi Technological University, Delhi in
the fulfillment of the requirements for the award of the degree of**

DOCTOR OF PHILOSOPHY

in

Mechanical Engineering

by

**PREM SHANKER YADAV
(2K18/PhD/ME/34)**

Under the supervision of

**Dr. RAGHVENDRA GAUTAM
(Assistant Professor)**



**Department of Mechanical Engineering
Delhi Technological University
Shahbad Daulatpur Bawana Road
Delhi – 110042, INDIA
June 2023**

**© DELHI TECHNOLOGICAL UNIVERSITY-2023
ALL RIGHTS RESERVED**

DECLARATION

I hereby declare that the thesis entitled "**SOME STUDIES ON SPRAY CHARACTERISTICS OF ALTERNATIVE FUEL AND THEIR EFFECT ON COMUSTION, PERFORMANCE AND EMISSIONS**" is an original work carried out by me under the supervision of Dr. Raghvendra Gautam, Assistant Professor, Mechanical Engineering Department, Delhi Technological University, Delhi. This thesis has been prepared in conformity with the rules and regulations of the Delhi Technological University, Delhi. The research work reported, and results presented in the thesis have not been submitted either in part or full to any other university or institute for the award of any other degree or diploma.

(Prem Shanker Yadav)

2K18/PhD/ME/34

Research Scholar

Mechanical Engineering Department

Delhi Technological University

Delhi-110042

Date:

Place: Delhi

CERTIFICATE

This is to certify that the work embodied in the thesis entitled **“SOME STUDIES ON SPRAY CHARACTERISTICS AND THEIR EFFECT ON COMBUSTION, PERFORMANCE AND EMISSIONS”** by **Prem Shanker Yadav**, (Roll No.- **2K18/PhD/ME/34**) in partial fulfilment of requirements for the award of Degree of **DOCTOR OF PHILOSOPHY in Mechanical Engineering**, is an authentic record of student’s own work carried by him under my supervision.

This is also certified that this work has not been submitted to any other university or institute for the award of any diploma or degree.

(Dr. Raghvendra Gautam)
Assistant Professor
Mechanical Engineering Department
Delhi Technological University
Delhi-110042

Dedicated to my

Parents

&

Wife

ACKNOWLEDGEMENT

At the very outset of this thesis, I would like to express my sincere and heartfelt gratitude to my learned guide Dr Raghavendra Gautam, under whose esteemed supervision I had accomplished the present research work. Without his panegyric efforts, active participation, ever helping attitude and cooperation, I would not have made headway in my work. His constant encouragement and 'never give up' perspective, especially during difficult times, have always led me to become a good researcher. I am especially grateful to my mother Smt. Indravati Devi, who have supported me emotionally. I would also like to extend my gratitude to Prof. S.K. Garg, Head, DRC Chairman, Prof. M.M Hasan, Jamia Millia Islamia New Delhi, Prof. Gian bhusan NIT Kurushetra, Prof. R C Singh DTU Delhi, Prof. Naokant Deo DTU Delhi, Dr Olawole Kuti, Senior Lecturer in Mechanical Engineering, Manchester Metropolitan University, UK, Dr. Atul Dhar, Associate Professor School of Engineering, Indian Institute of Technology Mandi, Professor (Emiritus) S N Singh IIT Delhi, Dr. Rajesh Kumar, Assistant Professor, NIT kurushetra, Dr. Anup kumar, Associate professor, IMT Nagpur for their guidance and unwavering support.

I owe a debt of appreciation to the supportive colleagues DTU, Delhi; in particular, Dr. Roshan Raman, Assistant Professor, The Northcap University, Mr. Kirat Singh, Researcher, Co-Founder of Nextup Robotics Pvt. Ltd. and existing researcher of centre for advance studies in vehicle diagnostic in research in automobile engineering lab Mr. Saket Kumar and Mr. Manoj Kumar for their valuable guidance, persistent help and support. Besides, this journey would not have been possible without the blessings and support of my family. I am especially grateful to my son, who have supported me for concentrating in research work. Thank you for teaching me that my job in life was to learn, be happy, and know and understand myself; only then could I know and understand others. I am also indebted to my brother-in-law Anil Kumar

who always extended help whenever required. My sincere respect and gratitude to Father-in-law as well for showering their blessings on me forever. Finally, I am falling short of words to express my deepest gratitude towards my wife, Mrs. Sunita Yadav. Affection, motivation, guidance and moral support extended by her at every step of this journey is unforgettable; hence, I owe much to her. I know how beholden to you I am for not giving due attention and time during my Ph.D. journey. In addition, there are many more person who knowingly and unknowingly contributed in making my work easier and a real success. I take this opportunity to express word of thanks to all of them. Last but not least, I praise and thank the Almighty for his shower of blessings, providing me self-motivation, focus, enthusiasm and patience to complete the research work successfully.

(Prem shanker Yadav)

ABSTRACT

At present, India is the fourth chief-importer of petroleum and crude products. Owing to the inadequate resource availability, India chiefly relies on its import, leading to fluidity of its overseas exchange. Abrupt hike in neat diesel fuel within a year in India isn't well-received in agricultural domain, especially by farmers and agronomists. Over and above, it's prognosticated that soaring energy requirements would increase petroleum diesel by 6-7% in the impending two decades. Expanded production of WCO causes serious waste disposal issues. In most situations, this waste oil discharges into water bodies. It degrades the water quality, and this contaminated water can cause many health issues. Further, oxygen deficiency in combustion of diesel fuel encourages the carbon emissions. Most of waste oils are generated from edible oils after frying or cooking operations. Approximately 70–80% of the total cost of biodiesel production is associated with feedstock cost, so the cost of biodiesel production could be reduced to 60–70% if waste cooking oil (WCO) is used as feedstock. The use of WCO as a biodiesel feedstock can mitigate issues such as water contamination and drainage systems blockages, which required additional cleaning. It is found to be a highly efficient way to deal with disposal issues with the partial fulfillment of the world's energy demand. Therefore, the current research exhibits the conversion of waste cooking oil to diesel like fuel through transesterification method and experimental and computational study were performed to study the spray characteristics and combustion characteristics. Further, the study has been carried out in four different phases.

The first phase consists of selection and production of biodiesel from waste cooking oil. The reaction parameters such as reaction temperature, reaction time, catalyst concentration and alcohol to oil molar ration were varied to get maximum yield. Where, the optimized parameters were 120min reaction time, 120⁰C reaction temperature and 1:6 oil to alcohol molar ratio. Then, the approval experiment was performed using above reaction parameter and found 89.5%

conversion efficiency. The physico- chemical properties like density, viscosity, surface tension, calorific value, distillation temperature etc. were estimated and got the value within the limit as per ASTM standards.

The second phase of work contains mixing of biodiesel with diesel in different proportions and spray visualization was performed to validate the computational model. the computational study consists of linear instability sheet atomization model and Taylor's analogy and that imparted the acceptable agreement with standard data and the deviation presented was within 5% limit. The grid convergence test was also performed and found to be 1.96 million cells with residual of 10^{-6} to converge the solution. The results showed that as the injection pressure increases from 110MPa to 160MPa, the spray tip penetration was increases while the spray cone angle decreases with constant ambient pressure. The maximum increase in tip penetration was recorded by 19.86% for B100, while highest decrease in cone angle was seen by 6% for B100, however, the lowest in both conditions is for diesel fuel. The reduction in sauter mean diameter from 110MPa to 160MPa was observed for B25 by 33% followed by B100 and diesel.

The third phase of testing consist the determination of rheological properties especially surface tension. Since, the surface tension of biodiesel is depending on production process and also it plays a major role in atomization characteristics and combustion characteristics. The theoretical and experimental investigation on fuels such as soyabean, jatropha, Karanja, Palm, rapeseed, sunflower was done at wide range of temperature. The results showed that Gibbs free model exhibited lowest error 1.6-6.8% than Dalton type mass average model (9.52-14.16%) and Macleod – sudgen model (3.2-12.1%) at wide range of working temperature. The modification in double bonds in unsaturated FAME able to improve the accuracy towards standard data.

The last phase of investigation is to examine spray combustion characteristics of waste cooking oil (WCO) using swirl nozzle (SN) and conventional nozzle (CN) with same cross-

section area. Surrogates of WCO were used in simulation such as n-heptane, methyl decanoate and methyl-9-decenoate. The computation consists Eulerian- Lagrangian approach to emphasize multiphase flow and linearized instability sheet atomization model model, Taylor analogy break up model to identify atomization, film formation and sheet breakup. Further, to identify the model's strength, validation of spray tip penetration, and kinetic solver for heat release rate and maximum temperature was accomplished against experiment and previous work and that permitted for further investigation at all injection pressures. The cool flame temperature was identified by formaldehyde (CH_2O) species, where main ignition was by formation of OH species. The results revealed that evaporative spray tip penetration through SN was little lower than CN at all injection pressures (100 MPa, 200 MPa, 300MPa), however, cone angle was higher for same. Axial and circumferential motion of spray volume exhibited early disintegration of fuel jet and that causes more air entrainment. Generation of OH^* has been considered for ignition, lift-off and combustion. SN showed decrease in ignition delay by 3.26%, 4.65% and 8.97% and lift-off length by 1.78%, 5.88% and 8.43% at 100 MPa, 200MPa and 300MPa respectively as compared to CN, and this is due to shorter primary break-up length in SN. An Increment in Heat release rate and Temperature was observed for SN than CN, and also soot was reduced by 3.20%, 4.81% and 6.72% with increase in injection pressure from 100MPa to 300MPa. This is due to better air -fuel mixing through swirl nozzle as compared to conventional nozzle. It was observed that influence of SN became strong with increasing injection pressure because rheological properties of WCO were decreased at ultra-high injection pressures.

LIST OF CONTENT

		Page. No
		Declaration
		i
		Certificate
		ii
		Acknowledgement
		iv
		Abstract
		vi
		List of contents
		ix
		List of figures
		xii
		List of plates
		xiv
		List of tables
		xv
		Nomenclature
		xvi
CHAPTER 1		Introduction
		1 - 13
1.1.		Motivation of current work
		1
1.2.		Energy Scenario
		2
1.3.		Environmental Issues
		5
1.4.		Technological Advancement and Alternative Fuels
		7
1.5		Role of spray characteristics
		9
1.6		Organization of chapters in Ph.D. thesis
		11
CHAPTER 2		Literature Review
		14-42
2.1		Introduction to spray characteristics of fuel
		14
	2.1.1	Primary Breakup
		16
	2.1.2	Secondary Breakup
		17
	2.1.3	Coalescence and Collision
		18
	2.1.4	Evaporation
		19
2.2		Nozzle geometry
		20
	2.2.1	Elliptical
		20
	2.2.2	Triangular
		23
	2.2.3	Conical
		23
	2.2.4	Round inlet
		24
	2.2.5	Square and Rectangular orifice
		24
	2.2.6	Swirl Injector
		25
2.3		
		27
	2.3.1	Injection pressure
		28
	2.3.2	Ambient density
		29
	2.3.3	Injection timing
		29
2.4		Review of AFs Properties
		30
	2.4.1	Density
		30
	2.4.2	Kinematic Viscosity
		30
	2.4.3	Surface Tension
		30
	2.4.4	Flash point
		31

Table of Contents

	2.4.5	Cetane No	31
	2.4.6	Heating Value	32
2.5		Production of biodiesel	32
	2.5.1	Transesterification	35
2.6		Outcome of Literature Review	37
2.7		Research Gap Analysis	39
2.8		Problem statement	40
2.9		Research Objectives	41
CHAPTER 3		METHODOLOGY AND SYSTEM DEVELOPMENT	43-85
3.1		Introduction	42
3.2		Waste cooking as feedstock	44
	3.2.1	Evaluation of Free Fatty Acid (FFA) content and Acid number	47
3.3		Preparation of waste cooking oil biodiesel	48
	3.3.1	Acid-Catalyzed esterification	48
	3.3.2	Base-catalyzed Esterification	49
3.4		Determination of physico-chemical properties	50
	3.4.1	Density	50
	3.4.2	Kinematic viscosity	51
	3.4.3	Calorific Value	51
	3.4.4	Flash Point	52
	3.4.5	Cetane Number	53
	3.4.6	Carbon Residue	53
	3.4.7	Distillation	54
	3.4.8	Oxygen Content (wt%)	54
	3.4.9	Copper strip Corrosion	56
3.5		Cold Flow Properties	56
	3.5.1	Cold Point & Pour Point	56
	3.5.2	Cold Filter Plugging Point (CFPP)	57
3.6		Experimental set-up to measure spray characteristics	58
	3.6.1	Experimental error and Uncertainties analysis	59
3.7		Swirl Injector	61
3.8		Experimental set-up to measure surface tension of biodiesels	63
3.9		Engine trial setup	64
3.10		Computational Technique	65
	3.10.1	Meshing of computational volume	67
3.11		Numerical simulation	69
	3.11.1	Continuous Phase Air	69
	3.11.2	Discrete Phase	71
	3.11.3	Break-up and atomization	71
	3.11.4	Droplet Evaporation	74
	3.11.5	Cavitation Modelling	75
3.12		Model description of surface tension of biodiesels	79
	3.12.1	The parachor based macleod-sudgen model	79
	3.12.2	The gibbs free energy model	82

Table of Contents

	3.12.3	The dalton type mass average model	84
CHAPTER 4		RESULTS AND DISCUSSION	85-122
4.1		Physico-chemical properties	86
	4.1.1	Density	86
	4.1.2	Kinematic viscosity	87
	4.1.3	Distillation Data	88
4.2		Model Validation	89
4.3		Grid Independence Test	90
4.4		Results and Discussion	91
	4.4.1	Spray Tip Penetration and Cone angle	91
	4.4.2	Sauter Mean Diameter	95
	4.4.3	Parachor Based model	96
	4.4.4	Prediction of surface tension using Gibbs free energy model	99
	4.4.5	Dalton type mass average model	101
4.5		Grid convergence study	102
4.6		Validation	104
4.7		Evaporative spray characteristics	107
4.8		Air Entrainment	107
4.9		Ignition Delay	110
4.10		Flame lift-off length	112
4.11		Heat Release Rate and Maximum Temperature	113
4.12		Emission	118
CHAPTER 5		CONCLUSION AND FUTURE SCOPE	122-125
5.1		Conclusions	122
5.2		Scope of Future Work	125
References			126-141
List of Publications			142
Biographical Sketch			143
Curriculum Vitae			144

LIST OF FIGURES

S.NO.	Caption	Page No.
Figure 1.1.	The world's oil production from 2021-2022, December	3
Figure 1.2.	The liquid oil consumption in various sector from 2021-2022 December in India	3
Figure 1.3.	CO ₂ gas emissions from different countries in year 2020 and 2021	6
Figure 1.4.	Complications associated with alternative fuel during use in Internal combustion engine	9
Figure 1.5.	Flow diagram of spray, combustion and emission characteristics	11
Figure 2.1.	Different stages of spray of biodiesel at high pressure	15
Figure 2.2.	Secondary breakup of jet in terms of We	17
Figure 2.3.	Disintegrations of jet in terms of Re, Z and gas density	17
Figure 2.4.	Collision and separation of droplets	19
Figure 2.5.	Collision and separation of droplets	19
Figure 2.6.	Evaporative region of droplet	20
Figure 2.7.	Nozzle with sharp contraction at exit	21
Figure 2.8.	Axis switching of spray jet	22
Figure 2.9.	Nozzle inlet without rounding	24
Figure 2.10.	Nozzle inlet with rounding	24
Figure 2.11.	Chemical reaction associated with production of biodiesel	36
Figure 3.1.	Flow chart of research methodology	44
Figure 3.2.	Vegetable oil consumption worldwide	46
Figure 3.3.	Process to produce biodiesel from WCO	49
Figure 3.4.	Experimental set up of visualization of spray characteristics of fuel	59
Figure 3.5.	Cross-sectional view of the pressure swirl nozzle	62
Figure 3.6.	Geometrical specification of slot in pressure swirl nozzle	62
Figure 3.7.	No of slots in the cross-section	63
Figure 3.8.	Ring of the Du Nouy ring tensiometer	63
Figure 3.9.	Du Nuoy ring tensiometer	63
Figure 3.10.	Engine trail setup	65
Figure 3.11a.	3-D view of the computational volume	68
Figure 3.11b.	Side view of computational model with boundary conditions	68
Figure 3.12.	Meshing of computational volume	68
Figure 3.13.	Flow chart depicting the spray characteristics	75
Figure 4.1.	Density Vs test fuel samples	87
Figure 4.2.	Kinematic viscosity Vs test fuel samples	88
Figure 4.3.	Grid Independence test summery	91
Figure 4.4.	Spray tip penetration of fuels B100, B25, D at 110 MPa	92
Figure 4.5.	STP vs ASOI for fuel B100, B25, D at 160 MPa	93
Figure 4.6.	SCA vs ASOI of fuels B100, B25 and D at 110 MPa	94
Figure 4.7.	SCA vs ASOI for fuels B100, B25 and D at 160 MPa	94

List of Figures

Figure 4.8.	SMD vs Injection Pressure at 110 MPa, 160 MPa for test fuels	95
Figure 4.9.	Mol.wt, density, Prachor(Allen and Knotts) vs test fuels	96
Figure 4.10.	Surface tension (Allen and Knotts) vs test fuels	97
Figure 4.11.	Experimental vs measured by Allen's and Knotts's parachor	98
Figure 4.12.	Surface tension (Jatropha, karanja, and soybean) vs temperature	100
Figure 4.13.	Surface tension (rapeseed, sunflower, palm) vs temperature	100
Figure 4.14.	Surface tension through Dalton model	102
Figure 4.15.	Grid independence test with the comparison of experimental and predictive spray characteristics	105
Figure 4.16.	Computer model validation with study of (Wang et al.,2010)	106
Figure 4.17.	Theoretical validation of evaporative tip penetration	106
Figure 4.18.	Evaporative STP vs ASOI at 100, 200, 300MPa with CN and SN heometry.	109
Figure 4.19.	SCA vs ASOI for CN and SN at different injection pressures.	109
Figure 4.20.	Mass of air entrained vs STP for CN and SN at different injection pressures	110
Figure 4.21.	Ignition delay vs Injection Pressure for CN and SN with injection pressure from 100MPa to 300 MPa.	111
Figure 4.22.	Variation of OH* flames of SN with injection pressure from 100MPa to 300 MPa.	113
Figure 4.23a.	HRR vs Time for CN and SN for injection pressure 100 MPa	114
Figure 4.23b.	HRR vs Time for CN and SN for injection pressure 200MPa	115
Figure 4.23c.	HRR vs Time for CN and SN for injection pressure 300MPa	115
Figure 4.24a.	Temperature vs Time of spray through OH species of CN at 100MPa	117
Figure 4.24b.	Temperature vs Time of spray through OH species of CN at 200MPa	117
Figure 4.24c.	Temperature vs Time of spray through OH species of CN at 300MPa	117
Figure 4.25a.	Temperature vs Time of spray through OH species of SN at 100MPa	117
Figure 4.25b.	Temperature vs Time of spray through OH species of SN at 200MPa	117
Figure 4.25c.	Temperature vs Time of spray through OH species of SN at 300MPa	117
Figure 4.26.	Graphic representation of the phenomenological soot model	119
Figure 4.27a.	Soot vs time of CN and SN for injection pressure 100-100MPa	119
Figure 4.27b.	Soot vs time of CN and SN for injection pressure 100-200MPa	120
Figure 4.28c.	Soot vs time of CN and SN for injection pressure 100-300MPa	120

LIST OF PLATES

S.NO.	Caption	Page No.
Plate 3.1.	Density meter	52
Plate 3.2.	Viscometer	52
Plate 3.3.	Bomb calorimeter	52
Plate 3.4.	Flash point tester	52
Plate 3.5.	Distillation setup	55
Plate 3.6.	Carbon residue tester	55
Plate 3.7.	CHNS/O Elemental Analyzer	55
Plate 3.8.	Copper strip corrosion tester	55
Plate 3.9.	Cloud point and Pour point apparatus	57
Plate 3.10.	Cold filter plugging point apparatus	57

List of Tables

S.No.	Caption	Page No.
Table 2.1.	Spray characteristics, performance and emission characteristics of various nozzle geometry	26
Table 2.2.	Properties of diesel and alternative fuel used in CI engine	33
Table 2.3.	Effect of rheological property, injection parameter on spray, combustion, performance and emission characteristics	34
Table 3.1.	Fatty acid composition of waste cooking oil	45
Table 3.2.	Uncertainty analysis of experimental setup	60
Table 3.3.	Eulerian- langrangian approach for multiphase flow	66
Table 3.4.	Breakdown of surrogates of WCO with devising from main components of biodiesel	77
Table 3.5.	Parachor values by Knotts and Allen of each FAMES	80
Table 3.6.	Increment to parachor/structural contribution	81
Table 4.1.	Properties of test fuel	89
Table 4.2.	Error study for the parachor based model (knotts parachors') and Allen parachors' with calculated surface tension	98
Table 4.3.	Average number of double bonds, carbon atoms and surface tension using Gibbs model at 40°C	100
Table 4.4.	Error estimation using Gibbs energy model (at 313K)	101
Table 4.5.	Error estimation (Dalton type mass average model) at 313K	102
Table 4.6.	Simulation parameter	103

NOMENCLATURE

CI	Compression Ignition
CO ₂	Carbon Dioxide
CO	Carbon Monoxide
HC	Hydrocarbon
NO _x	Oxides of Nitrogen
PM	Particulate Matter
SO ₂	Sulphur Dioxide
mb/d	Million barrel per day
ICE	Internal Combustion Engine
EVs	Electric Vehicles
HEV	Hybrid Electric Vehicle
BEV	Battery Electric Vehicle
GHG	Green House Gas
CH ₄	Methane
BS	Bharat Stage
g/km	Gram Per Kilometer
PPM	Parts Per Million
AFs	Alternative Fuels
WCO	Waste Cooking Oil
MT	Metric Ton
FFA	Free Fatty Acid
CFD	Computational Fluid Dynamics
BTH	Brake Thermal Efficiency
IMEP	Indicated Mean Effective Pressure
BSFC	Brake Specific Fuel Consumption
MMT	Million Metric Ton
ml	Milli Liter
gm	Gram
Mol. wt	Molecular Weight
WCOME	Waste Cooking Oil Methyl Ester
KJ/Kg	Kilo Jule Per Kilogram
CN	Cetane Number
TCD	Thermal Conductivity Detector
hrs	Hours
Hz	Hertz
ms	Milli Second
µm	Micrometer
KW	Kilo Watt
rpm	Revolution Per Minute
RANS	Reynolds average Navier stroke
C ₂ H ₂	Acetylene
FAME	Fatty Acid Methyl Ester
T	Temperature
ΔG	Gibbs Free Energy

ΔH	Enthalpy
ΔS	Entropy
M	Molecular Weight
ρ_l	Liquid Density
ρ_v	Vapor Density
ρ_g	Gas Density
DEC20	Diesel (80%) +Di-ethyl carbonate (20%)
B100	Biodiesel (100%)
B25	Diesel (75%)+Biodiesel(25%)
D	Diesel
STP	Spray Tip Penetration
SCA	Spray Cone Angle
SMD	Sauter Mean Diameter
ASOI	After Start of Injection
P_{inj}	Injection Pressure
P_{amb}	Ambient Pressure
mN/m	Milli Newton per Meter
CH ₂ O	Formaldehyde
O ₂	Oxygen
HRR	Heat Release Rate
CN	Conventional Nozzle
SN	Swirl Nozzle
CH ₃	Methanide
C ₂ H ₄	Ethylene
C ₃ H ₃	Cyclopropenyl radical
C ₅ H ₅	Cyclopentadienyl
ID	Ignition Delay
LISA	Linear Instability Sheet Atomization
TAB	Taylor Analogy Breakup Model
CFD	Computational Fluid Dynamics
Wt%	Percentage of Weight
KOH	Potassium Hydroxide
PTSA	P-toluenesulfonic Acid
UHC	Unburnt Hydrocarbon
GC	Gas Chromatography
PSI	Pound per Square Inch
hp	Horse Power
DNS	Direct Numerical Simulation
We	Weber Number
Re	Reynolds Number
mg	Milli Gram

INTRODUCTION

Overview

This chapter consists of research background which starts with the motivation of current study as well as the energy situation of India. Moreover, the environmental issues associated with exhaust emissions and their consequences on health are also discussed. Subsequently, the alternative solution is also suggested to alleviate harmful pollutants using advanced technology and alternative fuel. This also highlights the role of spray characteristics on combustion, performance and emissions in diesel engine. At the end of the chapter, the outline of the thesis is presented.

1.1. Motivation of current work

The nation's growth primarily relies on adequate energy availability as well as advanced technologies. Right now, the conventional fossil fuels fulfil the energy requirement, however, the depletion of fossil fuels and increasing demand of energy, researchers are moving towards better fossil fuels. The major consumer of energy is industrial sector followed by transportation and agriculture. The compression ignition (CI) engine with superior thermal efficiency with higher compression ratio has become an important segment of modern life. However, diesel engine emits the harmful emissions like carbon dioxide (CO₂), carbon monoxide (CO), smoke, oxides of nitrogen (NO_x), particulate matters (PM), sulphur dioxide (SO₂) etc. These harmful gases pose health hazard to human health which directly link to lung infection and breathing problems. Furthermore, they are primarily associated with global warming, environmental degradation, ozone layer depletion, and natural catastrophe. Therefore, there is need of improvement in combustion technology. In this regard, the improvement in spray characteristics of fuel

can be a promising way to assuage this harmful emission without affecting performance of engine. The aim of current work is to enhance the spray characteristics of alternative fuel to reduce exhaust emission and enhance thermal efficiency of engine.

1.2. Energy Scenario

Energy consumption and the use of innumerable fuel have become an unavoidable feature of rapidly growing countries like India. Also, industrialization and faster modernization have escalated the fuel consumption in different spheres such as domestic, agriculture, transport etc. The worldwide transportation is mainly petroleum products which maintain the faster pace of the world. India, a nation with CI engine motivated economy, consumed around 88.2 billion litres of diesel fuel, 37.2 billion liters of petrol. The demand of 34% of energy in India is fulfilled through crude oil, where 83% of crude oil is imported through foreign exchange and huge exchange of foreign currencies create an economic instability in the country (MOPNG, Annual Report 2022). The world oil production is shown in Figure 1.1 from 20-2022, December. Thereby, price fluctuation of oil in global market affects the Indian economy significantly. The industrial sector, a largest energy centric industry constitutes around 41% of total energy consumption. Where, per capita energy usage was 2.58% in the period of 2011-12 to 2020-21 (Energy Statistics, 2022). The liquid oil consumption in different sectors is shown in Fig. 1.2. The demand of energy for India's growth rate is 3% higher than other countries (BP Energy Outlook, 2022).

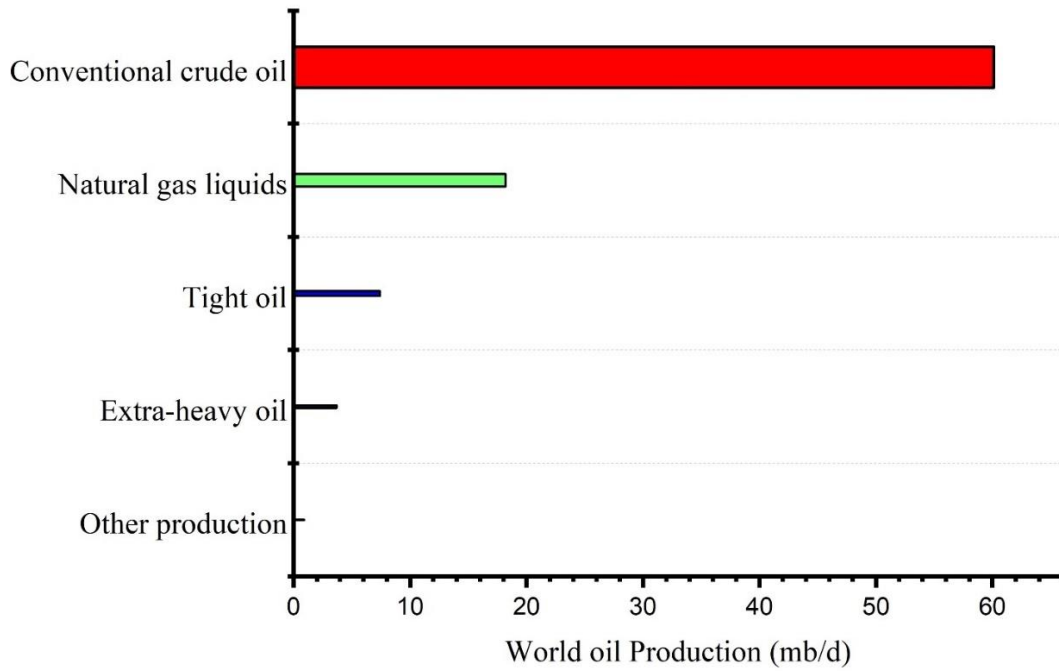


Figure 1.1: The world oil production from 2021-2022, December (World Energy Outlook-IEA, 2022).

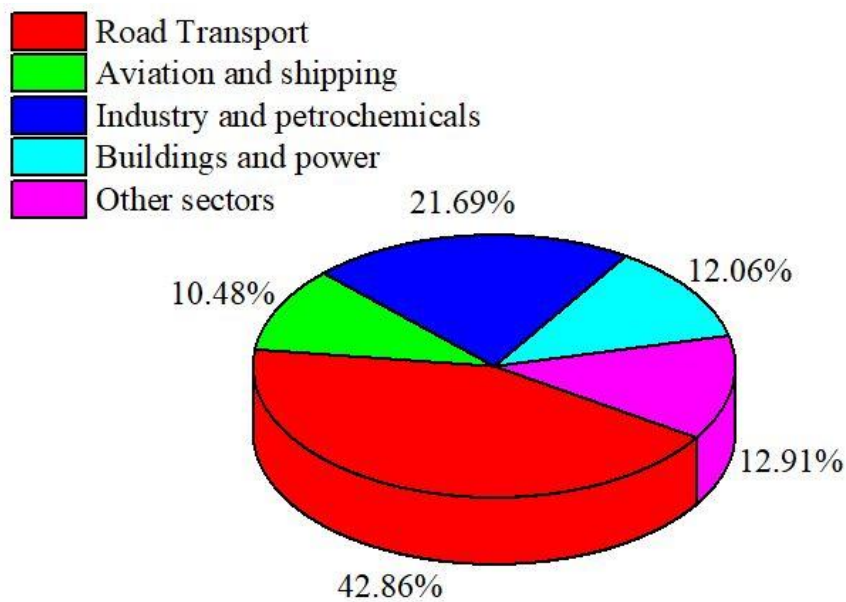


Figure 1.2: The liquid oil consumption in various sector from 2021-2022 December in India (Diesel Net, 2022).

The fast demographic expansion and technological advancement have changed the mindset of living standard in developing countries like India over the last decades. Now, the personal vehicle is treated as essential commodities rather than luxury item. Consequently, rise of 22.48% in car production as well as 9.67% in truck production were recorded in from 2010-11 to 2020-21 respectively in India (World Energy Outlook-IEA, 2022). Due to versatile behaviour of diesel engine, India constitutes majority of diesel engine followed by petrol engine. Though, these engines have major contribution in harmful emissions, thereby, there is necessity to search substitute of petroleum-based diesel and technological development in engines to cut these destructive emissions of the atmosphere. Currently, the standing of internal combustion engine (ICE) has been negatively impact by its harmful emission and that menaces the capability of technology to improve significantly and their contribution towards decrease of emissions through transportation sector. In reaction, policy makers on emissions have given proposals to replace IC engines with electric vehicles (EVs) with planned goals to drastic reduction in emissions and fuel consumption. The impediment still faced by suggested alternatives like EVs drove by batteries that have high cost, weight and more limitations. Further, these are driven with renewable fuels such as solar and wind and which are currently represent only a small fraction of energy supply throughout the world (Kalghatgi G, 2018). Therefore, future mobility will be depending on mix of solutions such as hybrid and electric vehicles (HEV and BEV), fuel cell electric vehicle involving conventional vehicles and the demand of above vehicles will be depend on specific applications like cost, city, and country (Sharma et al., 2019). Thus, there will be an important role of combustion engine whether for transportation, power generation or electrified power train.

1.3. Environmental Issues

From the past decades, researchers have found that environmental deprivation at faster rate has become a foremost concern for entire world. Presently, world released 24,785 million tons of CO₂ emissions and on that India contributed 2472 million tons of carbon dioxide in the year 2021-22 (World Energy Outlook-IEA, 2022). Further, worldwide 28% CO₂ emissions alone generated from petroleum fuels in the year 2022 (Diesel Net: Engine & Emission Technology, 2022). Figure 1.3 shows the CO₂ gas emissions from major emitter countries in the years 2020, 2021. While, it was observed that 45% CO₂ emissions accounted in year 2022 through crude oil. Thus, the faster rise in CO₂ concentration induces to global warming cause of greenhouse gas (GHG) effect.

The greenhouse gases mainly constitute CO₂, methane (CH₄), and water vapor at major concentration level. Other than that, nitrous oxide, ozone, fluorinated gases also contribute for GHG effect to little extent (World Energy Outlook-IEA, 2022). GHG absorbs radiation returning from the surface of Earth and again return to the Earth, the above phenomena disturb the radiation balance. Consequently, there is a drastic change in climate pattern and that causes ecological imbalance, ocean tides, changes in sea level, and occasionally calamities (Emissions Gap Report, UN Environment Programme, 2022). However, an effort has been made by Indian government to reduce vehicle pollution from year 2000 by implementing the various Bharat stages (BS) emission norms I to V. Again, they have implemented the BS-VI emission norm from April 2020 for lowering automobile emissions.

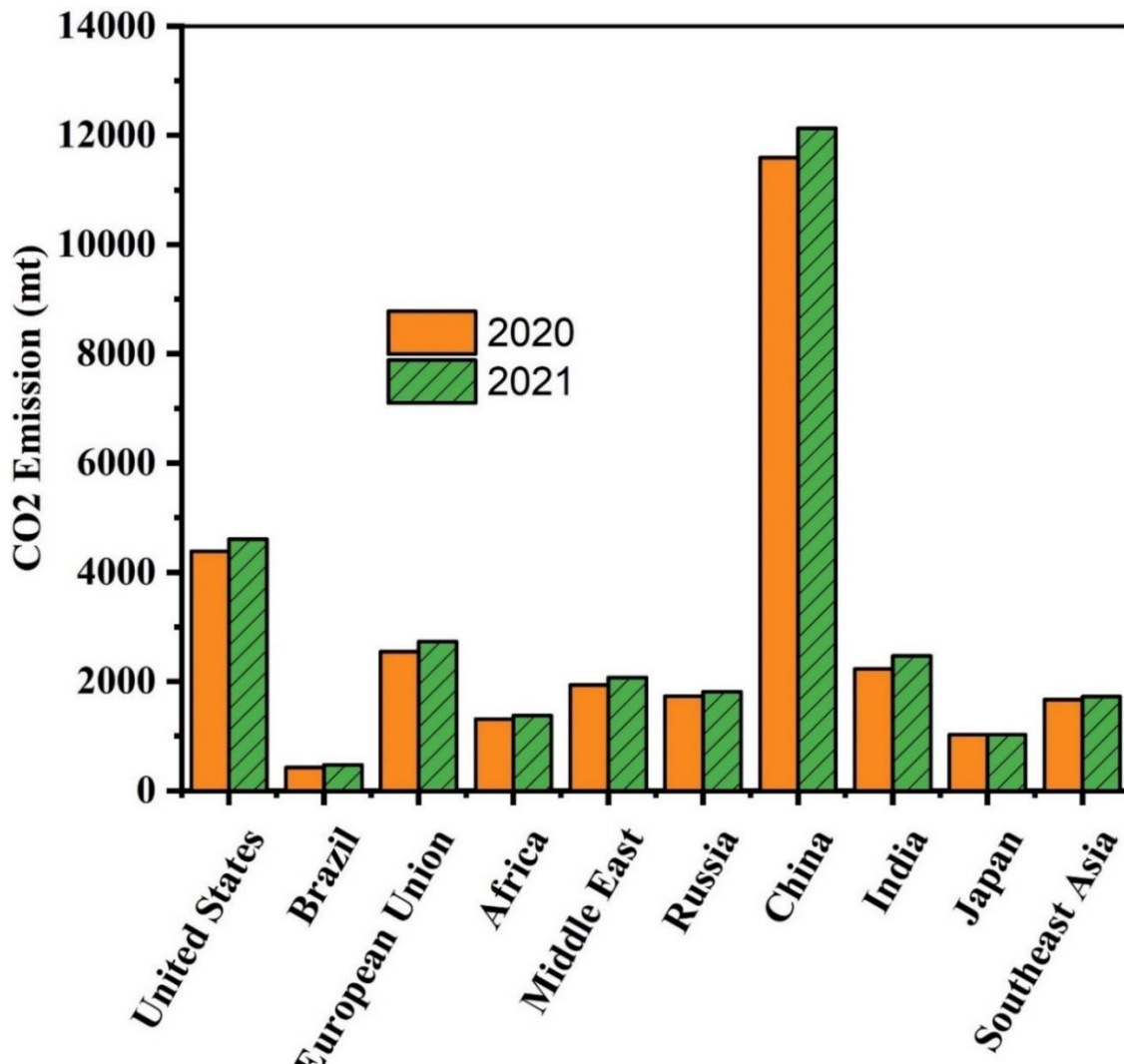


Figure 1.3. CO₂ gas emissions from different countries in year 2020 and 2021 (World Energy Outlook-IEA, 2022).

The emission standard for diesel vehicles is NO_x : 0.06; CO : 0.05; NO_x+ HC: 0.17 (in g/km); S in Fuel: 10ppm. The stringent emission norms have forced to engine manufacturer for modification in hardware of engine or fuel.

Moreover, diesel engines with recent new technology such as selective catalytic reduction (SCR), lean NO_x trap (LNT), and diesel particulate filters (DPF) are capable to restrict emissions but is expensive to implementing with BS-VI norms (Diesel Net: Engine & Emission Technology, 2022). Therefore, to diminish the issues i.e environmental degradation

and diminution of fossil fuels, the engine researchers have made effort to search alternative fuel and technological improvement in future. So, implementation of alternative fuels could be effective way to lower down the emission level and also solve the mission of clean environment in India.

1.4. Technological Advancement and Alternative Fuels

The issues of environmental deterioration and diminution of fossil fuels have eagered the engine researchers and manufacturer to make policy for better replacement of diesel fuel. Further, the recommended fuel could not only meet the diesel norms but also readily available, economical, and does fulfil the standard emission norms. Thus, the clean burning, sustainable fuel can be replaced by non-conventional ways, and this is considered as alternative fuel. Alternative fuels (Afs) exhibit some key benefits such as less harmful emission, naturally sustainable and easily available like edible and non-edible feedstock (AK Agarwal, 2007). Over that, biodiesels attract more in AFs since can use in CI engine with or without modification. Biodiesel is produced from numerous feedstocks namely edible and non-edible oil, waste cooking oils, and animal fats. Presently, edible oil has been the pivotal source accounting 95% of biodiesel production, intensifying food scarcity and escalating production costs. Though, nonedible feedstock like Karanja, jatropha nana, jatropha curcas Calophyllum inophyllum, etc are economic as well as environment friendly have since grown in wasteland (Gautam et al., 2022). The consumption of waste oil produced from different food processing industries is the requirement in the future. Since, maximum amount of waste oil generates after cooking or frying oil of edible oil and the percentage share is shown in Figure. 1. The 70-80% cost of biodiesel is accounted with the cost of feedstock. Therefore, 60-70% cost of biodiesel production could be reduced through using waste cooking oil as a feedstock (Carus, 2019). India constitutes the 2nd largest consumption and largest importer of cooking oil in the world. Consequently, largest volume production of waste cooking oil (WCO) causes disposal issue such as water contamination in rivers and soil, drainage problem and that can rise many

health issues. The efficient way to mitigate above problem is to use WCO as a feedstock for partial fulfilment of energy demand (Mittelbach and Remschmidt, 2006).

Further, the goal set by the government of India to blend 5% biodiesel in diesel by 2030 is fulfilled by collecting 5MT of WCO per year. However, the collected WCO contains high free fatty acid (FFA) and water content due to mixing of water during frying operation (Singh et al., 2021) and that increases acidity and viscosity of WCO biodiesel. The worldwide acceptance of biodiesel is due to its advantages over diesel fuel including high cetane number, minuscule fragment of sulfur content, aromatics, ameliorated lubricity, and oxygen content of about 10-12% by weight which prevents deleterious emissions and contaminants. The impediments for anticipated scientific progress includes NO_x emissions, injector deposits, poor atomization, heterogeneous mixture, and filter plugging in a colder environment as shown in figure. 1.4 (Yadav et al., 2021). The disadvantages of biodiesel are high rheological properties mainly density, viscosity and surface tension of biodiesel which prohibits the use in CI engine. However, there are several ways to alleviate such problems like blending, modification in fuel and injector, mixing of nano additives etc. Spray characteristics of fuel is mainly influenced by rheological properties of fuel, injection pressure and ambient condition of the constant volume chamber and fuel-air mixing generally depends on spray behaviour of fuel. Consequently, the combustion, performance and emission follow the trend of spray behaviour.

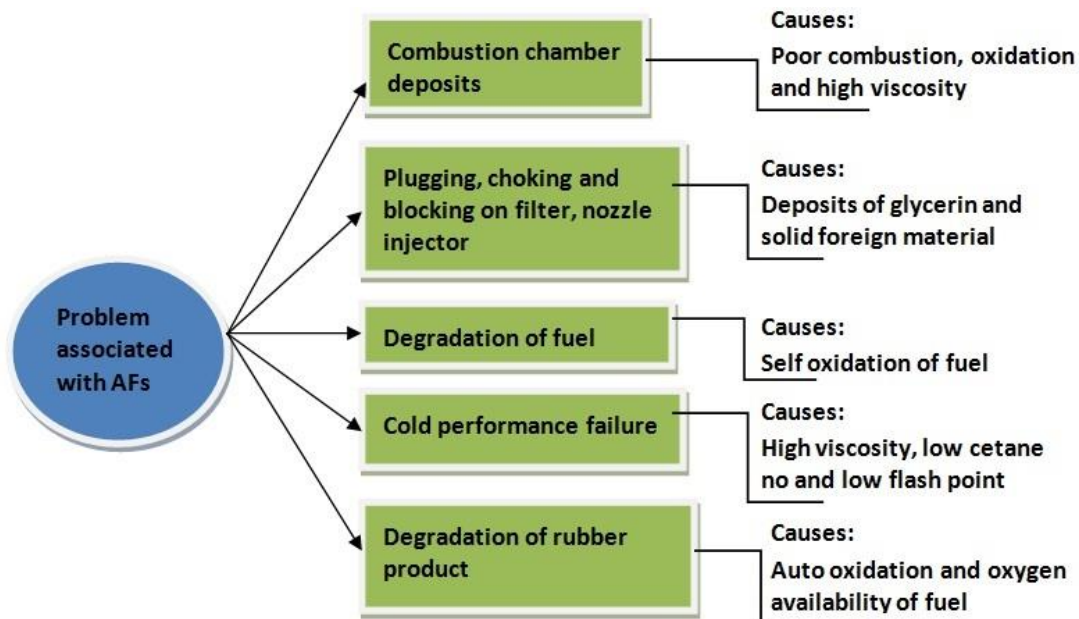


Figure 1.4: Complications associated with alternative fuel during use in Internal combustion engine (Yadav et al., 2021)

Literature shows that most of the research work is based on low injection pressure with conventional nozzle. Whereas future demand of engine manufacturer is that with a high injection pressure. A low injection pressure engine has major challenges for poor atomization characteristics of biodiesel and that leads to inferior combustion, performance and emissions (Yu et al., 2018,2019; Sharma and Fang, 2015). Even conventional nozzle with circular cross-section passes through less atomization characteristics than non-circular cross-section. Swirl nozzle with similar cross-section of conventional nozzle could be used to improve spray characteristics of fuel. The wall impingement problem of combustion chamber can be solved using swirl nozzle. Additionally, high injection pressure is able to promote earlier disintegration into droplets from spray plume (Yadav and Gautam, 2022). However, injector deposits are still a challenge of biodiesel fuel for longer run of CI engine.

1.5. Role of spray characteristics

Spray disintegration phenomenon constitutes a major role in IC engines. When the fuel jet moves away from the nozzle, the forces such as drag, inertia, and the properties like viscosity, surface tension dominant on spray jet and that causes deformation and finally breakup in jet. Spray and atomization characteristics of fuel exhibit different behaviour, is due to injection quantity, injection timing and injection pressure, ambient condition in combustion chamber. Rate of breaking liquid jet into droplets promotes air-fuel mixing followed by evaporation, and this is better way to control combustion characteristics. Therefore, engine experts are more prone to study the spray behaviour of jet fuel and their impact on combustion characteristics. Since past decades, various experimental procedure applied to capture spray images with thermos-fluid-dynamic condition. The current instruments range do not meet the current required range of engine parameters. So, the researchers have bend towards simulation such as computational fluid dynamics (CFD), which is very strong and useful tool for critical examination of multi-phase flow as well as combustion characteristics. The influence of spray characteristics and atomization characteristics are represented in Figure. 1.5

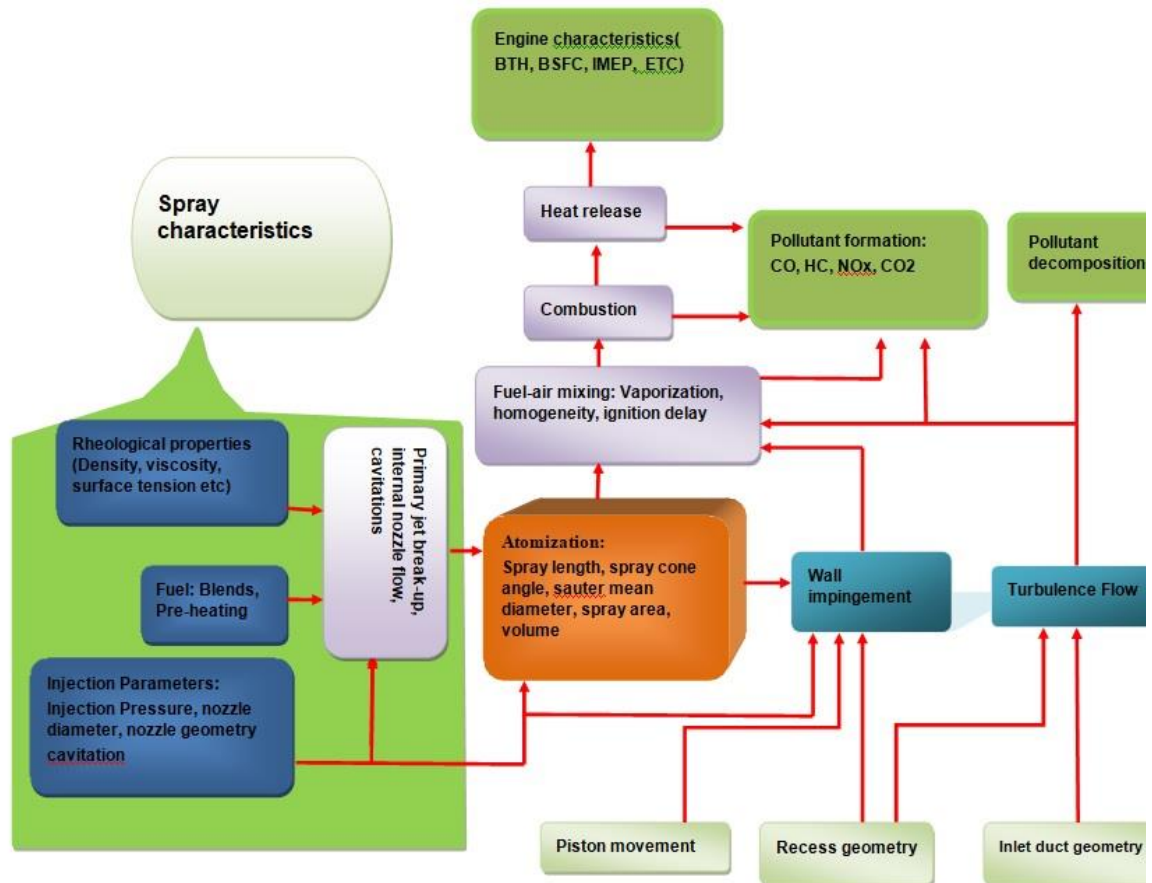


Figure 1.5: Flow diagram of spray, combustion and emission characteristics.

1.6. Organization of chapters in Ph.D. thesis

This thesis entitled “Some study on spray characteristics of alternative fuel and its effect on combustion, performance and emissions” consists of five chapters:

Chapter 1 presents the overview of current research. It begins with motivation for selecting the area of research, current scenario of energy in India, economic relevance and diesel engines. The subsequent section explains the importance of alternative fuels particularly the current status of biodiesel and availability in India. It is then continued with problems associated with alternative fuel during application. Lastly, the chapter 1 ends with the role of spray characteristics, combustion and performance characteristics of diesel engine.

Chapter 2 incorporates the brief literature survey that provides a summary of physico-chemical properties, spray characteristics, various nozzle geometry, injection parameter, thermodynamic parameter and diesel, biodiesel. The work available in literature are based on challenges associated to technological development in diesel engine and serviceability of biodiesel and their blends in diesel engine. Further, the review also focused on the studies of modelling of spray, injection and ambient condition in the constant volume chamber.

Chapter 3 discusses the processes to generate biodiesel from feedstock. The methodology applied to measure the physico-chemical properties is explored in detail. Furthermore, the system development to visualize the spray characteristics, measurement of surface tension and also engine trials have also been described thoroughly. The computational study has been performed to analyze the complexity of spray by selecting a constant volume chamber as the solution domain before the discretizing it with appropriate meshing. The model was applied to examine the spray behavior at different operational conditions. Lastly, the range, uncertainty and accuracy of instruments are also presented in this chapter.

Chapter 4 exhibits the comprehensive investigation on the results attained from the experimental work, characterization techniques and theoretical assessment carried out in the current study. The argument is elaborated based on the findings from computational work and also comparing them with experimental results and findings from the open literature. Furthermore, identification of model's strength has been explored through validation of spray and combustion characteristics. Finally, spray and combustion characteristics were analyzed from swirl injector using waste cooking oil biodiesel, biodiesel- diesel and diesel fuel.

Chapter 5 contains the summary. The logical outcomes are drawn from the results abstained from the study. Recommendation for future work have been suggested.

LITERATURE REVIEW**Overview**

The improvement in spray characteristics of fuel is one of the effective ways to enhance the combustion, performance and emission characteristics. This chapter explores a literature study on various techniques to enhance the spray behavior in the constant volume chamber of combustion ignition engine. Further, this also discusses the little modification in fuel injector and their influence on spray characteristics, combustion and emission characteristics in the CI engine. It is also explained the impact of biodiesel as a test fuel in diesel engine to spray phenomenon, and engine parameters. Finally, different works have been discussed on modelling and simulation of spray and combustion and the objectives have been drawn from the research gap of literature review.

2.1. Introduction to spray characteristics of fuel

Spray crumbling phenomena play an vital role in air-fuel mixing in combustion ignition engines. When the spray jet moves away from injector tip, different kind of forces such as drag, inertia, viscosity and surface tension acts on fuel spray and that leads to deform and finally breakup (Krishna et al., 2019). Spray characteristics of fuel exhibits STP, SCA, spray volume and spray area and these parameters primarily depend on injection timing, injection pressure, ambient pressure and injection quantity of fuel in combustion chamber. The spray tip penetration is defined as the distance between the nozzle tip to the farthest point of spray along the spray axis, and the cone angle is the angle between two tangent lines at injector tip up to half of spray length (Boggavarapu and Ravikrishna, 2013). Early disintegration of spray after the nozzle exits prone to smaller droplets which promotes rapid

evaporation followed by excellent air-fuel mixing. Thus, this is a better way to control combustion characteristics (Gautam et al., 2022). When, the fuel jet comes out from the nozzle at high velocity, the jet breaks up into ligaments and then droplets. The denser spray region constitutes the cone shape, and the volume fraction is formed by liquid droplets with gaseous surrounding as shown in Figure 2.1. This phenomenon primarily depends on injector outlet geometry. The spray cone consists of thicker to thinner zones with gas occupied volume. Thicker zone exhibits droplet-droplet interaction cause of little relative distance which is known as collision and coalescence and at last thin zone appears where volume fraction is very small and surrounded by denser gases (Reitz, R. D, 1996). The jet fuels leave from injector divide the spray into two regions which are primary breakup and the secondary breakup.

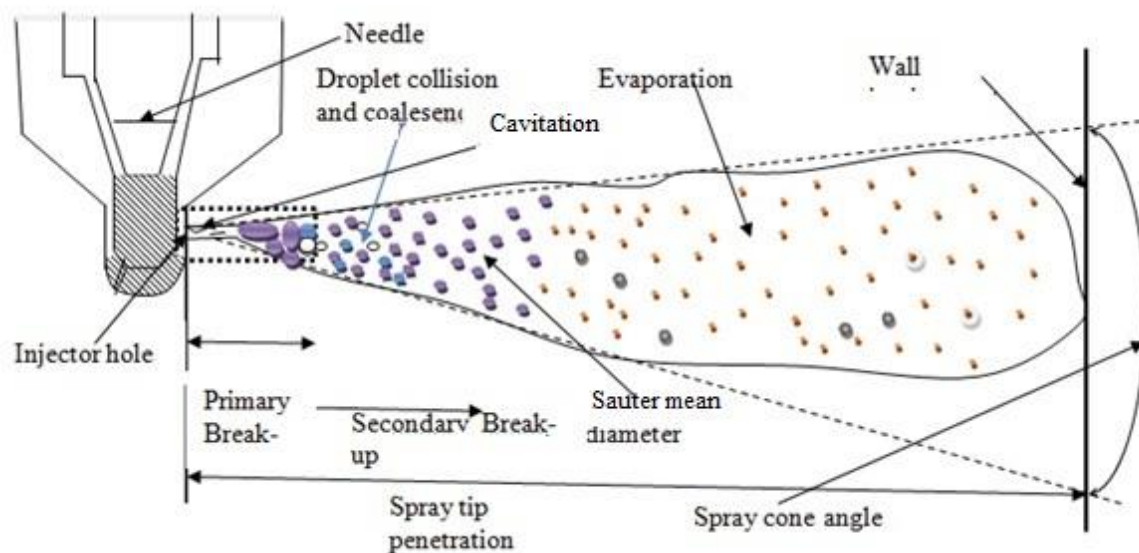


Figure 2.1 Different stages of spray of biodiesel at high pressure (Boggavarapu and Ravikrishna, 2013)

2.1.1. Primary Breakup

Primary breakup consists of splitting of jet fuel leaving from nozzle exit into droplet formation as shown in figure 2.1. This phenomenon occurs at high pressure drop across nozzle, which provides acceleration to spray volume. This creates high strength of turbulence between liquid and gaseous interface and that causes destabilization in fuel spray (Reitz, R. D, 1996).

Furthermore, cavitation phenomenon occurs inside the nozzle, and this happens when static pressure is below the vapor pressure of fuel. Cavitation causes choking of mass flow and that occurs at the throat at constant pressure. Thus, these processes exhibit through formation and growth followed by collapse, break-off. The bubble rings are generated at the entry of injector and spread throughout circle wall. It then collapses in spray jet and that promotes an early breakup and disintegration of jet fuel from the original stage and this also improves the secondary disintegration stage (Stiesch, G.,2003). The four spray regimes namely Rayleigh, First wind-induced, second wind-induced and atomization regimes are dependent on dimensionless number like Ohnesorge (Z) number, Reynolds (Re) (Czerwonatis and Eggers, 2001; McKinley and Renardy, 2011) in Rayleigh breakup, low injection velocity is driven by surface tension and liquid inertia forces, and it reveals that nozzle diameter is smaller than initially generated droplets. Additionally, the regime of the first wind shows gas-phase dominance and major disturbances occur on gas-liquid interface and that causes breakup and the nozzle size is smaller than droplet size. When the pressure drop increases across the injector, the second wind induced regime presents with a significant dominance of aerodynamic force. The liquid surface accounts for more commotions with shorter wavelength and that results in a smaller droplet size. Lastly, the atomization

regimes consist of high injection pressure along with high gas density, where spray takes a conical shape, the nozzle diameter is larger than the droplet diameter when the breakup begins as the fuel jet gets away from the injector tip. The effect of gas density towards the breakup regimes are shown in figure 2.3 (Reitz R. D, 1978).

$$We = \frac{\rho_l U_0^2 D}{\sigma} \dots\dots (2.1), Re = \frac{\rho_l U_0 D}{\mu_l} \dots\dots (2.2), Oh = \frac{\mu_l}{\sqrt{\rho_l D \sigma}} \dots\dots (2.3)$$

where σ , μ_l , ρ_l , shows surface tension, viscosity and density respectively

2.1.2. Secondary Breakup

As the jet passes farther away from injector tip then secondary breakup occurs, and the aerodynamic forces act on droplets' surface through the surrounded turbulent gases. The surface energy of droplet is dominated by aerodynamic forces which promotes the disintegration into finer droplets (Wierzba A. 1990). Secondary breakup is clearly understood by Weber number (We) as shown in figure 2.2.

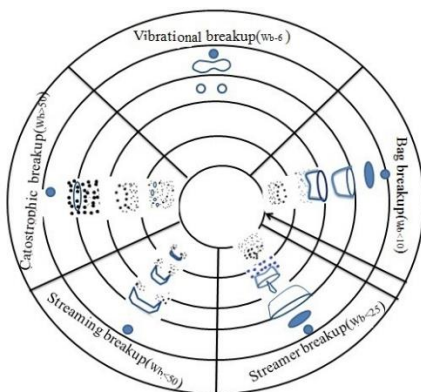


Figure 2.2. Secondary breakup of jet in terms of We (Wierzba, A., 1990).

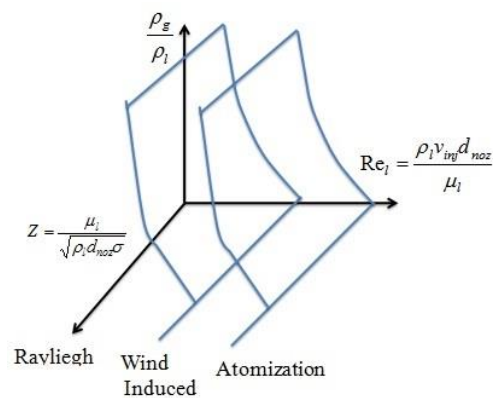


Figure 2.3. Disintegrations of jet in terms of Re, Z and gas density (Reitz R. D, 1978).

Further, the energy transfers from droplets to ambient air occurs and that makes evaporation in secondary breakup. So, the balanced air-fuel mixture can attain through this fundamental method. The incorrect air-fuel mixture reasons rapid or reduced evaporation that results a futile combustion and generation of hazardous emission (Reitz and Bracco, 1990; Wierzba and Takayama, 1988). The volume of combustion chamber where large no of droplets are available passes through collision. This phenomenon happens little or more during mixture generation and generally depends on relative velocity and local void fraction (Qian and Law, 1997; Georjon and Reitz, 1999).

2.1.3. Coalescence and Collision

As, the droplets approach near each other, the high-pressure region creates between droplet's gap and that causes flattening of droplet surface and conversion of kinetic energy (KE) to surface tension energy of droplets takes place. However, a partial loss in KE is imparted by turbulence of gas between the gas and self-motion of droplets (Qian and Law, 1997). Furthermore, when the gap size between the droplets encounters the molecular interaction range, bounce and coalescence processes occur due to rheological properties of fuel, Weber number, and behavior of gases (Shlegel et al., 2020). Since, head-on collision between two droplets and high momentum of droplets, the droplet deformation passes through viscous loss which overcome the gas film's resistance and form coalescence in droplets. The collision occurs in two way- firstly off-center and secondly tangential, normal force creates the resistance of gas films in first one while rotational motion attains through second one. Here, the inertia of the droplets decreases whose strength reduces and the internal motion of droplets is subsequently lowered. But, the tangential impacts of droplets provide centrifugal action and that behaves like spring – mass system and finally gets breakup since surface tension energy is surpassed by the rotational kinetic energy (Jiang et

al., 1992). The different regions of coalescence and collision are shown in Figure. 2.4 and Figure 2.5.

2.1.4. Evaporation

The evaporation of droplets occurs due to heat transfer between the surrounding air and droplets. Where, droplets acquire thermal energy through surroundings and then these droplets evaporate (Markadeh et al., 2020). As a result, the radius of region of a droplet changes from maximum to zero throughout the evaporation as shown in figure 2.6.

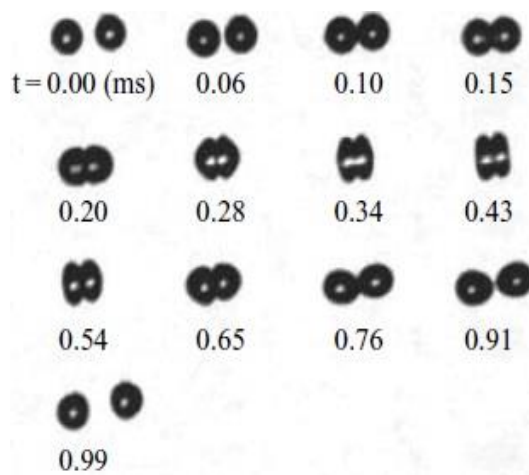


Figure 2.4. Collision and separation
of droplets (Head on)

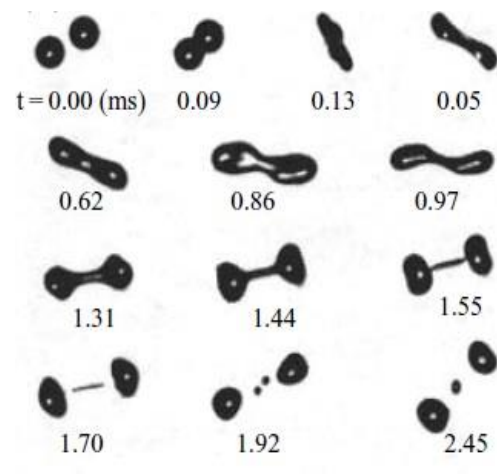


Figure 2.5. Collision and separation
of droplets (off-center)

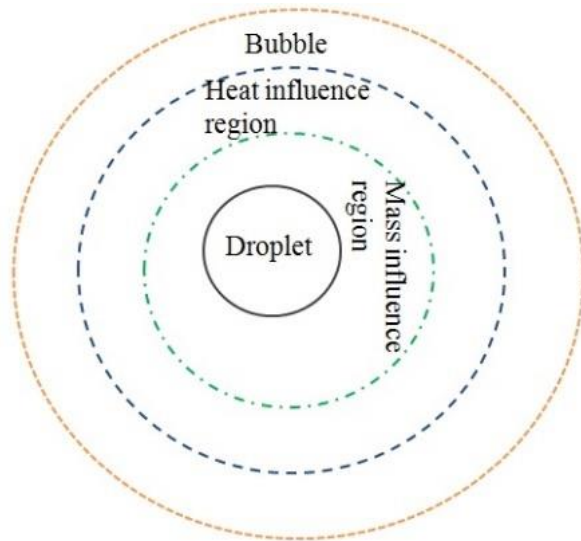


Figure 2.6. Evaporative region of droplet

2.2. Nozzle geometry

As per previous studies, Reynolds number, Ohnesorge number and Weber number have major influence on liquid breakup of flow characteristics and various experiments have been performed at high and fixed Reynolds number. Furthermore, some non-circular nozzle geometries have analyzed to examine their impact on spray characteristics. Most of the non-circular studies agreed that quality of spray characteristics and air-fuel mixing could be improved using non-circular fuel injector (Amini and Dolatabadi, 2011; Payri et al., 2017; Taskiran, O. O, 2018; Azad et al., 2012). These geometry shows the axis-switching phenomenon which generates an additional turbulence on spray and that results early primary and secondary breakup processes. Though, first switching happens at few equivalent diameters to injector tip, while second switching shows at outermost and others take place but they may or may not be visible.

2.2.1. Elliptical

The elliptical cross-section nozzle contains maximum numbers of axis-switching behavior than other non-circular injectors (Amini and Dolatabadi, 2011) as shown in Figure 2.7 and Figure 2.8. This process is basically interchange of major axis to minor axis at certain time interval. Where, initially it shows at very short interval and further becomes longer and finally diminishes. Thus, the spray cross-section changes from elliptical to circular and vice-versa. The instability generated from this oscillation growth continue till the jet disintegrate in downward spray. The spray characteristics through injector shows similar to spring-mass system, and where the similar competition is shown by inertia force and surface tension. Here, inertia force pushes to convert the cross-section into elliptical shape while surface tension work as a restoring force for resisting circular cross-section. Kashyap et al., 2009 investigated on elliptical nozzle and found that elliptical cross-section generated more wobbly behavior and shorter primary breakup length due to axis-interchanging process than circular jet and the instability in spray jet varied proportionally with limited ellipticity range.

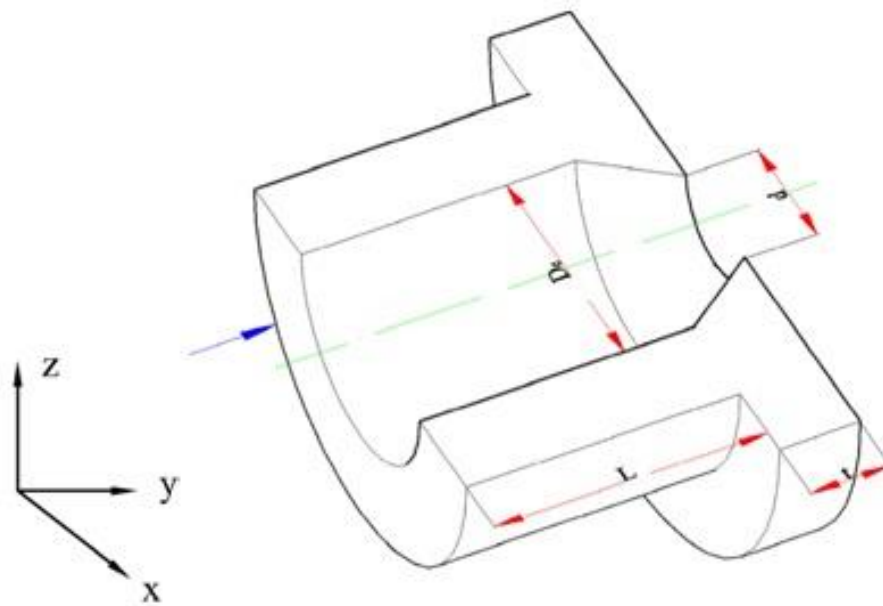


Figure 2.7. Nozzle with sharp contraction at exit (Ho and Gutmark, 1987)

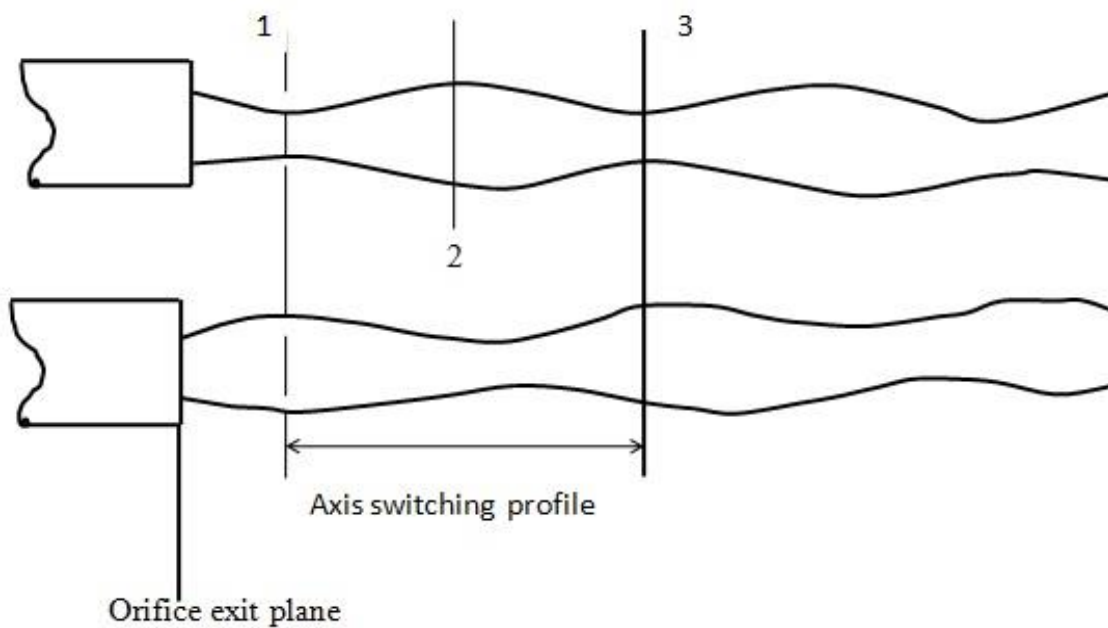


Figure 2.8. Axis switching of spray jet (Kasyap et al., 2009)

(Amini and Dolatabadi, 2011) examined on viscous liquid jet through capillary instability and found that symmetric uneasiness is unstable while asymmetric disquiet is not unstable, therefore, ellipticity becomes proportional to instability. The rationale of this study is also

supported by (Kashyap et al., 2009). Further, researchers did a comparative study between elliptical and circular nozzle on spray characteristics of fuel and found that circular spray exhibited longer tip penetration than elliptical spray.

However, the cone angle of circular spray was lower than elliptical spray. Moreover, the elliptical jet exhibited smaller sauter mean diameter (SMD) than circular jet and the air entrainment was higher for elliptical than circular spray (Yunyi et al., 1998; Yadav et al., 2023). But the dominance of viscosity and surface tension in AFs, there is less inclination towards axis swapping in AFs as compared to diesel fuel. Also, non-circular nozzle consists of significant impact on cavitation initiation, rapid collapse of cavitation structure and also inception. Furthermore, circular nozzle contains larger cavitation length than elliptical nozzle for different hole ratio of elliptical nozzle at similar injection conditions. (Lešnik et al., 2018; Kim et al., 2010).

2.2.2. Triangular

(Aleyasin et al., 2018) showed the comparative mixing quality and turbulence structure of circular and triangular jet. The triangular jet exhibited high turbulence growth rate as well as smaller liquid core length. The axis-switching phenomenon is also exhibited by triangular jet and showed the similar behavior as elliptical nozzle (Hashiehbafe and Romano, 2013). Even, number of studies performed on different triangular jets such as isosceles, equilateral, found that isosceles jet containing less apex angle (the angle between the pointed end) accounted better air-fuel mixing than other triangular and circular jets (Azad et al., 2012). Now, (Schadow et al., 2004) did comparative examination of spray characteristics between isosceles, triangular and equilateral jet and concluded that flat side exhibited a highly coherent structure and corner side presented a distinct peak. This enhances in combustion characteristics, due to fuel-oxidizer mixing and better chemical

reaction from large- and small-scale mixing respectively. Furthermore, isosceles jet exhibited longer core length, less air entrainment, and slower mean pressure recovery than equilateral jet. However, the decay rate of isosceles triangular jet was faster than equilateral jet (Quinn W. R.,2005).

2.2.3. Conical

Another non-circular geometry, conical cross-section showed that momentum flux and mass flow rate exhibited lower than circular cross-section nozzle. Consequently, cylindrical nozzle possesses longer spray tip penetration than conical nozzle. The spray spreading angle varies inversely to spray tip penetration (Yadav and Gautam, 2022). However, the cone angle of spray is influenced by nozzle geometry as well as ambient condition. Thus, conical nozzle comprises higher spreading angle than circular nozzle (Payri et al., 2017).

2.2.4. Round inlet

Injector having round inlets consist of different discharge coefficient, shows respective spray characteristics as shown in Figure 2.9 and Figure 2.10. A comparative analysis on spray characteristics of sharp inlet nozzle and round inlet nozzle have performed and found that sharp inlet nozzle generated smaller droplets than round inlet nozzle. Therefore, round inlet nozzle passes through lower combustion efficiency, lower NO_x and exhaust gas temperature, also high soot formation than sharp inlet nozzle (Taskiran O. O.,2018).

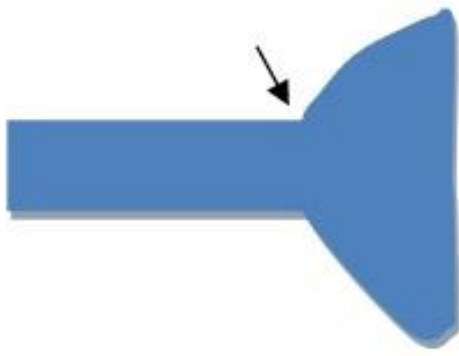


Figure 2.9. Nozzle inlet without rounding (Taskiran O. O.,2018)

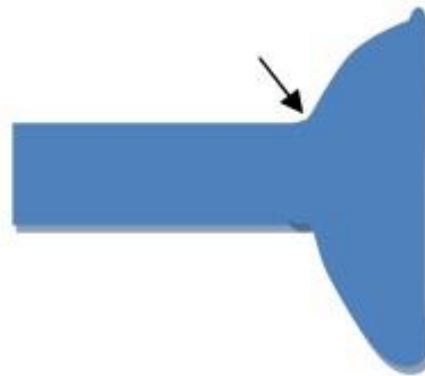


Figure 2.10. Nozzle inlet with rounding

2.2.5. Square and Rectangular orifice

The spray characteristics of non-circular geometry are also depicted by the rectangular and square orifice. The transformation of either rectangular or square jet to circular jet varies with injection pressure. The range of transformation shifts away from the nozzle tip and the axis-switching wavelength further improves with the rise in injection pressure. The above effect is observed owing to rivalry actions between inertia force and surface tension as debated earlier (Sharma and Fang, 2014).

Since, there is a very limited study available on square cross-section orifice. (Sharma and Fang, 2015) performed the study on a square cross-section orifice for (0-1000 bar) range of injection pressure and inferred that below 600 bar of injection pressure, the spray jet exhibited square jet structure, axis-switching characteristics while above the jet structure became nearly circular and the axis-switching phenomenon disappeared. This happened due to high inertia, turbulence and the significant influence of aerodynamic conditions, which confined the axis-shifting phenomenon. Thus, square orifice constituted wider spray

than circular orifice. Further, brief details of spray behavior of square and rectangular orifice are shown in 1 2.1.

2.2.6. Swirl Injector:

The atomization characteristics exhibit a crucial role in air-fuel mixing followed by combustion characteristics, the jet breakup process was further improved utilizing pressure swirl atomizer. However, this technology is earlier applied in DISI engines, aircraft air combustors and industrial furnaces. The excellent disintegration of fuel droplets and controlled fuel distribution in the combustion chamber promotes flame stability, augmented performance and slackened exhaust emissions (Fan et al., 2020; Laurila et al., 2020). Swirl atomizer contains the spray device which processes the spray jet to fine droplets from heavier droplets. Further, spray jet in gaseous medium forms higher surface area to volume ratio. The energy is gained from pressure drop and the fuel droplets attain high momentum than ambient gases. The device generates a centrifugal action on spray jet, which enables swirling and forms a conical sheet by spreading liquid jet at the orifice outlet (Rajamanickam and Basu, 2017; Jedelský et al., 2021). (Yadav and Gautam, 2021,2022) have investigated from their previous work that high injection pressure and swirl atomizer were able to improve the spray characteristics of fuel consequently it increases the combustion efficiency, decreases CO, HC emission. Further, researchers reported on spray characteristics of swirl atomizer in constant volume chamber that increase in injection pressure improves the cone angle. However, cone angle became persistent for the consistent rise of injection pressure. Subsequently, the axial velocity decreased using sloped grooves in the swirl. At high ambient temperature, Sauter mean diameter (SMD) at the outer periphery was more than spray axis. Spray axis contained higher vapor concentration than spray periphery.

Table 2.1. spray characteristics, performance and emission characteristics of various nozzle geometry

Nozzle geometry	Condition	Spray characteristics				Performance			References
		STP	Spray area	SCA	SMD	BSFC	BTE		
Elliptical	P_{inj} (50-90MPa), amb. Pr 1MPa Fuel: Diesel	(3.41- 3.66%) ↓	(11.59- 19.69%) ↑ along major axis	(15.90-21%) ↑ along major axis	↓	-	-	(Yu et al., 2018)	
Traingle(E quilateral)	P_{inj} (120- 160MPa), P_{back} 1 MPa Fuel : Biodiesel	(10.36- 17.64%) ↑	(22- 45%) along ↑ major axis	(21.11- 30.28%) ↑ along major axis	↓	-	-	(Yu et al., 2019)	
Conical compared with rectangular	P_{inj} 90MPa, amb. Density 22.8kg/m ³	3.13% ↑		51.51% ↓		-	-	(Payri et al., 2017)	
Round inlet	P_{inj} 50MPa, P_{back} 0.1 MPa Fuel: diesel		17.61% ↓ compared to sharp inlet		↓	-	-	(Taskiran O. O. 2018)	
Rectangul ar orifice	P_{inj} (40- 100MPa), P_{back} 1 MPa	(1.23-2.04) ↓		(6.86-8.94) ↑		-	-	(Sharma and Fang, 2015)	
Square shaped orifice	P_{inj} (40- 100MPa), P_{back} 1 MPa	(1.04-2.14) ↓		(5.89-8.34) ↑		-	-	(Sharma and Fang, 2015)	

They also suggested that spray quality with swirl atomizer can be boosted significantly by increase in injection pressure, Weber number and temperature. The increase in these parameters causes decrease in SMD, and it enhances the air-fuel mixing (Zhang et al., 2017; Li et al., 2011; Najafi et al., 2020).

2.3. Influence of spray's thermodynamics parameters

The injection parameter and thermodynamic parameters have major role in homogenous fuel-air mixing. Since, they contain injection pressure, injection timing, injection angle, injection quantity, fuel and air temperature. The fuel's spray experiences various nature of forces such as drag, inertia, viscosity, and surface tension, and these all act in deformation and ultimately breakup (Pickett et al., 2009; Genzale et al., 2010; Kostas et al., 2009). Even though, AFs show different physicochemical properties than mineral diesel still they are also influenced by injection as well as thermodynamic parameters.

2.3.1. Injection pressure

Numerous studies (Agarwal et al., 2014; Agarwal et al., 2013; Zhang et al., 2018; Chen et al., 2013) on injection pressure have been performed, and the conclusion was made that injection delay and spray tip penetration got increases with rise in injection pressure. Initially, the cone angle increased then it became constant for further increase in injection pressure. Biodiesel with higher density and viscosity than diesel fuel, showed longer tip penetration and smaller cone angle at the same injection pressure than diesel. Further, the higher compressibility of biodiesel promotes longer injection delay. Biodiesel exhibits larger SMD than diesel due to the indecent atomization characteristics of biodiesel. Several engine scientists investigated that fuel consumption and smoke were increased at low injection pressure through modification in the injection rate of the fuel pump along with nozzle area. Despite several advantages of ultra-high injection pressure, there are some

disadvantages such as wall-impingement which forms a fuel film leading to the generation of soot, HC and carbon deposits in the combustion chamber. Consequently, there is reduction in efficiency of diesel engine (Peraza et al., 2022; Agarwal et al., 2015). Droplet velocity, cone angle and Sauter mean diameter are the main parameters that are responsible for the cited problem. Hence, by optimizing these parameters, there would be an improvement in combustion efficiency and reduction in emissions (Zheng et al., 2020).

2.3.2. Ambient density

The ambient condition in the combustion chamber also influences the spray characteristics, like high ambient pressure leads to an increase in cone angle and decrease in spray tip penetration, SMD and that results in improved combustion efficiency. However, the effect of ambient conditions diminishes as the injection pressure reaches to ultra-high injection pressure (Hawi et al., 2019; Chauhan et al., 2010)

2.3.3. Injection timing

This parameter controls combustion characteristics. Numerous engine scientists observed that there was decrease in HC emissions and rise in NO levels by advancing pilot injection under lean conditions. Therefore, compensation occurs between these two groups of species (Lakshmanan and Nagarajan, 2009). The reason for this is the additional mixing of pilot fuel with the premixed mixture causes an enhancement in combustion efficiency. Though, this pattern cannot exist to nearly stoichiometric mixture. The unburned hydrocarbon stuck to the crevices of the cylinder receives at the early expansion stroke. As the lean mixture is not a limiting factor for combustion efficiency, thus HC emissions increase with relative crevices effect and the combustion phase is retarded. Eventually, the oxidation of fuel generates HC and releases crevices (Basha et al., 2016). However, further advancing in pilot injection timing promotes longer ignition delay, and that worsens combustion efficiency

(Behera et al., 2014). Hence, early injection timing with narrow-angle injection direction improves fuel atomization before entering the cylinder and the wall-wetting problem reduces as the distance between the cylinder wall and nozzle tip increases noteworthy. (Hoang, A. T, 2020; Boot et al., 2009).

2.4 Review of AFs Properties

2.4.1. Density

Biodiesel contains heavy molecules in their molecular structure and that causes biodiesel exhibits 10% denser than diesel as shown in Table 2.2. The density (g/cm³ or kg/m³) of fuel provides the information between injection delay (ignition quality) and combustion of fuel in CI engine (Gautam et al., 2013). Fuel density acts as the predecessor for breakup, viscosity and heating value. Hence, for the same volume of diesel and power output, the injection quantity of biodiesel is more than diesel fuel in the combustion chamber to compensate for the loss of power from biodiesel. Furthermore, biodiesels consisting of heavier molecules result in indecent atomization in the constant volume chamber. This is due to higher momentum and longer break-up time (Yoon et al., 2008). Consequently, there is soot generation as well as carbon deposits in the combustion chamber.

2.4.2. Kinematic Viscosity

The resistance offered between layers in the flow of liquid is known as kinematic viscosity. Biodiesel is more viscous than diesel as shown in Table 2.2. The fuel containing higher kinematic viscosity possesses through larger droplet generation leading to poor spray characteristics such as larger droplets, small cone angle, and higher spray tip penetration. Also, these add degradation in combustion characteristics (Knothe and Steidley, 2005). Moreover, injector choking, long-term durability and carbon deposits, filter plugging

also occurs for high viscous fuel, which leads to engine damage. However, there are certain ways to reduce viscosity of biodiesel like blending, preheating of fuel, blending with nano-additives etc. (Agrawal and Gautam, 2019, bhan et al., 2022).

2.4.3. Surface Tension

The theoretical definition of droplet formation suggests that the minimum energy required for atomization should be derived from surface tension energy multiplied by the surface area of the droplet. Spray atomization is majorly influenced by viscosity and surface tension, whereas droplet formation is by surface tension followed by viscosity, and inertia (Davanlou et al., 2015). However, the surface tension of biodiesel is accounted for by molecular structure like the number of unsaturated bonds, and length of the fatty acid hydrocarbon chain. Fatty acid hydrocarbon in molecular structure with a long chain exhibits higher surface tension (Phankosol et al., 2014). However, the variation of surface tension is similar to viscosity such as blending, pre-heating, and addition of nano-additives.

2.4.4. Flash point

It is the minimum temperature at which fuel gets combustible mixture as it contacts with spark or flame. Many studies concluded that biodiesel exhibits higher flash points than conventional diesel. However, the flash point decreases with the increase in residual alcohol in fuel (Carareto et al., 2012; Singh et al., 2012). This is the parameter where fuel disintegrates like storage based, transport based on hazard level. Thus, the least flash point is needed for safety, safe storage and acute handling of biodiesel

2.4.5. Cetane No

Cetane number (C_N) is vital physicochemical property of alternative fuel that influence combustion quality and ignition delay and is shown by dimensionless number. Fuel having high cetane no results in higher power output, better cold starting and a decrease in

emission. While lower C_N exhibits knocking, higher exhaust emission and quantitative unburnt hydrocarbon accumulated inside the cylinder (Gautam & Kumar., 2015). Biodiesel possesses major benefits than diesel fuel with fatty acid saturation and chain length. The oxygen content in biodiesel imparts higher C_N and that results in an improvement in combustion efficiency. Vegetable oil and non-edible vegetable oil show lower C_N than waste cooking oil and biodiesel. Diesel fuel presents lower C_N than biodiesel as shown in Table 2.2.

2.4.6. Heating Value

It is the energy liberated for the unit mass of fuel combusted in the combustion cylinder. The higher value is favourable for optimizing the injection system. Biodiesel contains lower heating value nearly 10-15% of diesel (Capuano et al., 2017; Singh et al., 2021). Thus, for the same power generation through biodiesel, additional biodiesel is injected due to the lower heating value of biodiesel. However, this value becomes more significant for high-power generation.

Biodiesel is an alkyl ester of long-chain fatty acid generated from various non-edible, edible and waste cooking oil feedstocks (Singh et al., 2020). Biodiesel with nearly similar physicochemical properties to conventional diesel which is used in the diesel engine. The special characteristics such as high cetane number, non-toxic, high flash point, no sulphur content, and renewable and sustainable nature make it more efficient choice in the energy sector (Marwaha et al., 2018). Most importantly, the unavailability of sulfur content in biodiesel improves the engine's life (Agrawal et al., 2020). While, the storage ability of biodiesel is exhibited due to higher flash point as compared to diesel fuel (Farooq et al., 2013). Biodiesel contaminates less to the environment than diesel because

Table 2.2.

Properties of diesel and alternative fuel used in CI engine, (An, H et al., 2012; Bousbaa et al., 2012; Kalam and Masjuki, 2002; Körbitz W, 1999; Gautam et al., 2019; Yaakob et al., 2013)

Prop ertie s	Measur ement appara tus	Sta nda rd Test met hod	Diesel	AFs			
				Biod iesel	VO	No n- edi ble Oil	WC O
Dens ity [kg/L]	hydrom eter	D94 1	0.815 – 0.867	0.87– 0.9	0.902 6– 0.946	0.9 16– 0.9 34	0.39 – 0.93 7
Kine matic visco sity @ 25– 40 °C [mm 2/s]	Red wood Viscom eter	D44 5	1.9– 5.7	3.5– 11.3	27.2– 72.6	27. 84– 79. 21	27.4 2– 201. 3
Heati ng value [MJ/ kg]	Bomb calorim eter	D24 0	41.87 – 45.34 3	32.9– 42.65	37– 40.5	34– 39. 87	37.2 7– 40.7 2
Ceta ne num ber	Ignition quality tester	D61 3	40–59	45– 70	37.1– 48.1	38. 1– 46	55.7 2– 61
Flash point [°C]	Penkys martins apparat us	D93	42–86	135– 250	150– 290	99– 257	243 – 290

Table 2.3. Effect of rheological property, injection parameter on spray, combustion, performance and emission characteristics

	STP	SCA	SMD	Wall impin oe	A/F	ID	C			P			References
							BSF	BTE	IME	CO	HC		
Density ↑	↓	↓	↑	-	↓	↓	↑	↓	↓	↓	↓	(Lin et al., 2009; Imdadul et al.	
Viscosity ↑	↓	↓	↑	-	↓	↓	↑	↓	↓	↓	↓	(Bhan et al., 2022); Sathivel et al. 2018)	
Surface tension ↑	↓	↓	↑	-	↓	↓	↑	↓	↓	↓	↓	(Lingfa et al. 2014; Suh and Lee 2016)	
Injection pressure ↑	↑	-	↓	↑	-	-	↓	-	↑	↓	↓	(Kumar et al., 2022; Zhang et al., 2018)	
Ambient pressure ↑	↓	↑	↑ ↓	-	-	-	-	-	-	-	↓	Kim et al. 2010	
Fuel Temperature ↑	↓	↑	↓	↑	-	-	↑	↑	-	-	↓	(Yadav et al., 2023; Raheman and phadatre, 2013	
Nozzle diameter ↓	↑	↓	-	-	-	-	-	-	-	-	↓	(shu et al. 2008; Ejim et al., 2007)	
Cavitation ↑	↑	↑	-	-	↑	-	-	-	-	-	↓	(Qiu et al. 2016; Payri et al. 2012)	
Biodiesel blends(D and	↑	↓	↑	-	↓	-	-	-	-	-	↓	Aboelazayem et al. 2018	

literature on impact of rheological properties, injection parameter and engine characteristics are shown in Table 2.3.

2.5. Production of biodiesel

Thereafter pretreatment, the production of biodiesel from WCO is similar to vegetable oils. However, the factors such as high FFA content, viscosity, water content, and density prevent it from the direct uses in CI engines. As, high viscosity is responsible for injector choking and carbon deposits on the combustion chamber, water content for engine wear, and high acidity of fuel are responsible for degradation of engine life (de Araújo et al., 2013). Therefore, it is mandated to reduce the FFA to permissible limit to use in diesel engine. There are several methods to lower these parameters for the generation of biodiesel from WCO. All methods include:

- Thermal cracking (pyrolysis)
- Dilution (Blending)
- Transesterification
- Micro-emulsification

2.5.1. Transesterification

Transesterification is considered a mostly used process due to high yields, low cost and simplicity (Enweremadu and Mbarawa, 2009; Wang et al., 2006; Gautam and Kumar., 2016,2018). Alcoholysis or transesterification constitutes the chemical reaction of vegetable oils with alcohol. The short-chain alcohol of three moles reacts with one mole of fat with the addition of a catalyst generates three moles of alkyl esters and one-mole glycerin (Patil et al., 2010). Further, triglycerides break into diglycerides, monoglycerides and followed by glycerol step by step. Then, it is easily separated into two layers through gravity as biodiesel and glycerol. Even, glycerol, the by-product is also used in cosmetic

industry. The light alcohols primarily used in the reaction are methanol and ethanol which constitute low-cost. Besides, higher alcohols like n-butanol, iso-propanol, tert-butanol, propanol, octanol and branched alcohols could be utilized but not due to higher price. Commonly, the transesterification process incorporates catalytic and non-catalytic processes where the catalyst improves the reaction rate as well as the solubility of alcohol and the catalytic transesterification method normally used is shown in Figure 2.11. The alkaline catalytic method is more economical and faster than acid catalysts with an equal amount of acid catalyst (Demirbas, 2009; Agarwal et al., 2012). This process of biodiesel production incorporates higher yield with considerable purity and shorter time (30-50 min). Numerous studies accepted alkaline catalyst which contains KOH, NaOH, KOCH₃ and NaOCH₃ and also suggested that hydroxide of sodium and potassium executed the experiment equally well. Further, the FFA of processed oil should be in the range of (0.5% < FFA < 3%) by use of an alkaline catalyst. Beyond this range, there is either soap formation or little yield of biodiesel (Wan Omar et al., 2009).

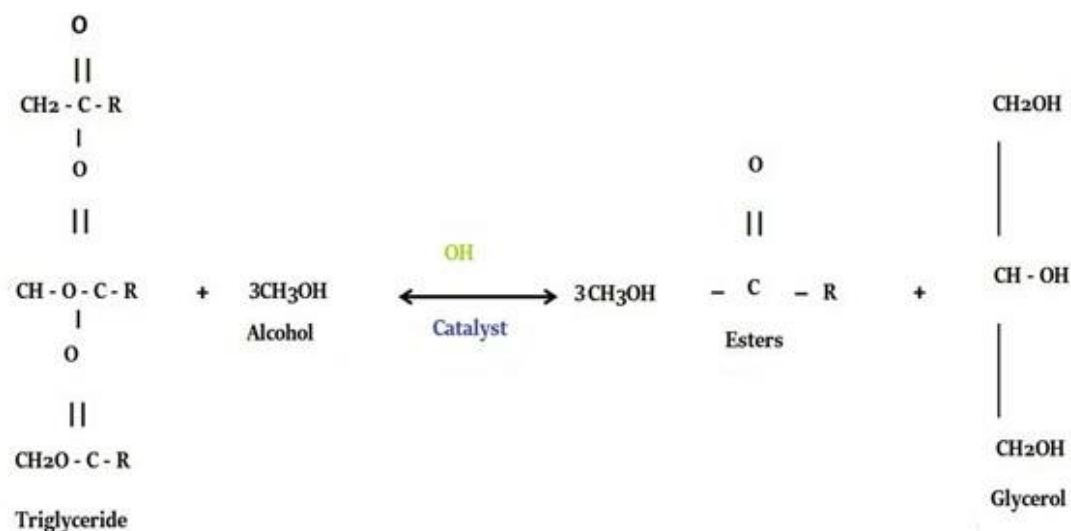


Fig. 2.11 chemical reaction associated with production of biodiesel

Likewise, acid catalyst incorporates hydrochloric acid, sulphuric acid, ferric sulphate acid, para toluene sulfonic acid (PTSA), Lewis acids (AlCl₃ or ZnCl₂) and phosphoric acid.

The different studies concluded that acid catalysts are more prone towards vegetable oil having high water and FFA content than alkaline catalysts. Hence, the acid catalyzed process is employed to decrease FFA content to sufficient level for base transesterification from where alkaline transesterification could perform. Moreover, in the absence of catalysts in further process, recovery of glycerol and purification of biodiesel becomes trouble-free, easier (Singh et al., 2019; Gautam et al., 2020; Guan et al., 2009). The transesterification process is mainly influenced by parameters such as reaction temperature, molar ratio, stirring speed, reaction time and catalyst concentration. Either yield reduction or incomplete reaction depends on the parameter to be optimized. Since, each parameter of the reaction affects the yield of biodiesel (Ouanji et al., 2016; Degfie et al., 2019).

2.6. Outcome of Literature Review

A different area of literature has studied spray characteristics followed by combustion performance and emissions characteristics. It was concluded that high injection pressure along with modification in the fuel injector is the best technique to improve spray characteristics, reduce emissions, enhance the combustion and performance of diesel engines. The following conclusions have been drawn from an exhaustive literature review.

1. Most of the literature recommended that the collective effect of the micro-hole nozzle diameter and higher injection pressure improved atomization strongly. This led to a drastic soot decrement in the flames produced by the fuels.
2. Literature survey shows that biodiesel exhibits lower volatility, slower mixing and larger fuel droplets with ambient air because of high surface tension and high viscosity. However, the SMD of biodiesel could be reduced through blending, preheating, and the addition of nano additives due to a decrease in viscosity and surface tension.

3. Some researchers found that an increase in injection pressure and ambient pressure caused a reduction in larger size particulates in the exhaust for all test fuel. Further, the concentration of lower particulate numbers could reduce by advancing SOI timings for all test fuels.
4. Various literature reported that the spray cone angle was initially increased and then became constant for further increase in injection pressure. However, SCA increased significantly with the rise of ambient pressure for all test fuels.
5. Literature indicates that the spray break-up, and spray disintegration process is positively influenced by cavitation generated inside the fuel injector. This phenomenon rapidly occurs at an ultra-high injection pressure and helps to improve spray characteristics.
6. Most of the literature agreed on the common denominator that at low injection pressure, the injection rate of diesel is slightly higher than biodiesel due to delay in needle lift for biodiesel or faster opening and closing of the needle. However, biodiesel exhibited a higher injection rate at high injection pressure. Biodiesel and its blend showed slower spray evolution as compared to diesel fuel. This is due to the higher viscosity of biodiesel compared to diesel.
7. Many engine specialists concluded that biodiesel with low fuel injection pressure and advanced injection timing showed lower NO_x emissions. This was due to incomplete combustion and lower in-cylinder temperature but there was an increasing trend of CO, HC and smoke emissions.
8. NO_x generation with increasing load showed the highest in castor oil followed by waste cooking oil and coconut biodiesel.
9. Among waste cooking oil, jatropha and Karanja, the emissions such as smoke, HC, and CO from waste cooking oil are significantly reduced than other biodiesel at high fuel

injection pressure and it is due to improved atomization results in the air-fuel mixing process.

10. Some researchers found that the theoretical model gives good agreement with experimental results of the macroscopic and microscopic behaviour of alternate fuel at low injection pressure. The theoretical results showed more deviation from experimental results at high injection pressure.

11. Different studies incorporated that an increase in injection pressure was an effective way to enhance fuel-air mixing in the combustion chamber of the CI engine, however, there was wall wetting problem for ultra-high injection pressure. Further, modification in the fuel injector causes an axis-switching phenomenon that improves the spray characteristics.

12. Some of the literature suggested that preheating of biodiesel could be an effective way to enhance spray behaviour due to the decrease in density, viscosity and surface tension and resulting into improvement in combustion efficiency.

2.7. Research Gap Analysis

After an exhaustive literature review, the following gaps are identified.

1. A very little quantum of work has been carried out on spray evolution, spray tip penetration, and fuel distribution at high injection pressure to enhance the spray characteristics of alternate fuel.
2. It has been observed that injection pressure and ambient pressure have a crucial role in spray breakup and atomization characteristics to improve combustion efficiency. Therefore, there is a need to investigate various ambient pressures.
3. Major contribution of surface tension and viscosity causes larger sauter mean diameter. It causes adverse effects on combustion and performance which need to study.

4. NO_x emissions are lower for biodiesels especially in the case of advanced injection timings and low Fuel Injection Pressures and higher HC, CO, and smoke emissions. It is yet to explore the emission characteristics at higher injection pressure.
5. It is worth noting the effect of different injection and ambient pressure on the performance and combustion of alternate fuel.
6. Cavitations occur in the nozzle which helps in spray evolution and atomization and injection parameters affect cavitations, which is yet too explored.
7. Due to limitations on experimentation, it is complex to visualize the spray pattern in detail. Therefore, it is mandatory to visualize a two-phase flow simulation to analyze the flow phenomenon that occurred inside the nozzle and outside the nozzle exit.
8. Most of the models explore the atomization characteristics considering the spherical shape of droplets. While the droplet shape varies with engineering applications, different environments include the combustion chamber of the IC engine.
9. As discussed in various research papers, the tandem effect of moving droplets during evaporation and heating cannot be ignored. When the ratio of distance between droplets and their diameter is less than about 10 micrometre.

2.8. Problem statement

From the comprehensive literature review, the research gap is identified. It was observed that an increase in injection pressure along with modification in the fuel injector is a promising way to improve spray combustion and emission characteristics of conventional diesel engine. This approach has major advantages since there could be use of different alternative fuel. The waste cooking oil is used for the production of biodiesel. Computational fluid dynamics has been used to visualize the spray characteristics of oil. Very little quantum of work has been explored and stipulated on the swirl nozzle which is

utilized for fuel injector. Further, to get the atomization behaviour of full cone structure, the new atomization model was explored with different blends of diesel to evaluate the spray and atomization characteristics. Then, the surface tension of different biodiesels is evaluated at elevated temperatures theoretically. The current research work focuses to show the effect of high injection pressure using waste cooking oil compared to diesel fuel from the swirl injector on spray characteristics.

2.9. Research Objectives

The objectives of the existing research were envisaged as follow.

1. Production of biodiesel from selected waste cooking oil
2. To determine the various physico-chemical properties of different test fuel in accordance with relevant standards
3. To determine the rheological property of fuel.
4. To study the spray characteristics by varying injection pressure of biodiesel using spraytec.
5. Modelling and Simulation of spray characteristics of fuels using Computational fluid Dynamics.
6. Comparative assessment of analytical and experimental results of spray characteristics
7. Performance, emission and combustion analysis of biodiesel in CI Engine and compare with baseline diesel

METHODOLOGY AND SYSTEM DEVELOPMENT

Overview

This chapter starts with selection of primary source and preparation of biodiesel from primary source. Moreover, the estimation of physico-chemical properties of all tested fuel is also described. Then, the system development for spray visualization, measurement of surface tension, and engine trails is explained with the range, accuracy and uncertainty of instruments. Further computational measurement of spray, combustion characteristics are performed using biodiesel, biodiesel- diesel and diesel

3.1. Introduction

This chapter includes the implementation of the steps used to carry out the research in this project. Figure 3.1 incorporates the summary of the flow chart of the problem statement. This contains biodiesel production from waste cooking oil and its physico-chemical as well as rheological properties (viscosity, density and surface tension). Then, the fuel possesses spray characteristics through experimental set-up as well as computational fluid dynamics from swirl injector along with uncertainty, accuracy and range of instruments. Further, the calculation of heat release rate and soot generation were described using computational fluid dynamics.

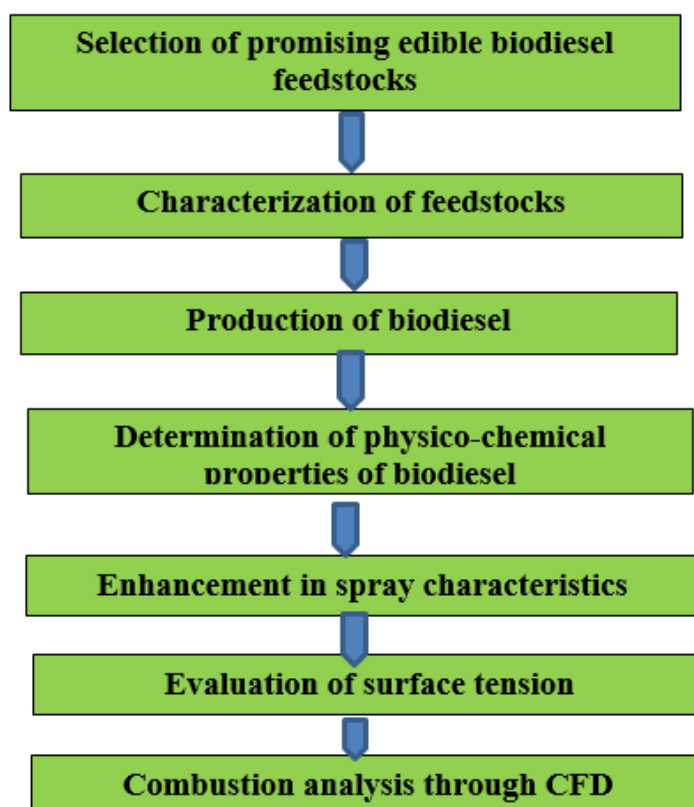


Figure 3.1: Flow chart of research methodology

3.2. Waste cooking as feedstock

Even though biodiesel production is used in every country, it has become a challenge to maintain economic viability. Therefore, manufacturers focus to make effort easily available feedstock like waste oils (Singh et al., 2020). Waste oils dispose of massively in all countries and it contributes to water pollution if no proper channel is implemented (Gui et al., 2008). These are derived from household, non-food sectors, restaurant and food sectors. However, waste plastic oil, waste tyre oil etc. are feedstock with the non-food sector and can generate biodiesel. However, the pyrolysis method is commonly used for the production of biodiesel from these stocks. The waste produced from various edible oils is known as waste cooking oil (WCO). This is also utilized for the generation of biodiesel. The edible oil global consumption in the year 2019-20 was found as 191.71 MMT (Shahbandeh, 2020). The edible oil constitutes soybean, sunflower, cottonseed,

olive, palm, peanut oil etc. The global consumption of edible oil is shown in Figure 3.2. Since, the assessment of WCO from edible oil is very difficult (Loizides et al., 2019) still, (Jiang and Zhang 2016) provided the production data of WCO from Equation 3.1

$$\text{WCO production} = [\text{population} \times \text{edible oil consumption per capita}] \times 30 / 100 \quad (3.1)$$

The above equation shows that worldwide production of WCO in the year 2019-20 was 57.51 MMT. Subsequently, the major issue of the availability of feedstock is resolved by utilizing WCO to produce biodiesel. WCO constitutes more amount of water as compared to fresh oil. Since, there is the use of water-containing food during the frying operation so the heat and mass transfer takes place between oil and food that's why the free fatty acid FFA content is high (Marmesat et al., 2007). Triglycerides possess through hydrolysis and that accelerates due to high water content and that leads to high FFA. Further, high FFA and water content result in saponification during biodiesel generation. Saponification reduces the biodiesel's yield and the amount of catalyst increases. So, the pre-treatment is required which is followed by transesterification process which produces higher biodiesel yield at viable cost (Buffi et al., 2017). The composition of fatty acid of WCO is given in Table. 3.1

Table 3.1. Fatty acid composition of waste cooking oil (Mittelbach, 1996; Ma and Hanna, 1999; Moazeni et al., 2019; Lam et al., 2010; Bautista et al., 2009)

Fatty acid	Chemical structure	Mol. weight (g/mol)	Chemical Name	Amount (%)
Lauric acid (C12:0)	C ₁₂ H ₂₄ O ₂	200.31	Dodecanoic acid	-
Palmitic acid (C16:0)	C ₁₆ H ₃₂ O ₂	256.43	Hexadecanoic acid	8.80
Oleic acid (C18:1)	C ₁₈ H ₃₄ O ₂	283.07	Cis-9-Octadecanoic acid	45.15

Stearic acid (C18:0)	$C_{18}H_{38}O_2$	284.48	Octadecanoic acid	4.20
Linoleic acid (C18:2)	$C_{18}H_{32}O_2$	280.44	Cis-9-cis-12- Octadecadeneoic acid	39.74
Myristic acid (C14:0)	$C_{14}H_{28}O_2$	228.37	Tetra decanoic acid	0.13
Linolenic acid (C18:3)	$C_{18}H_{30}O_2$	278.43	Cis-6-cis-9-cis- 12- octadecatrienoic acid	0.20
Arachidic acid (C20:0)	$C_{20}H_{40}O_2$	304.46	Eicosanoic acid	0.43
Gadoleic acid (C20:1)	$C_{20}H_{38}O_2$	310.51	Cis-9-Eicosenoic acid	-
Behenic acid (C22:0)	$C_{22}H_{44}O_2$	340.58	Docosanoic acid	0.75
Erucic acid (C22:1)	$C_{22}H_{42}O_2$	338.57	Docos-13-enoic acid	0.30

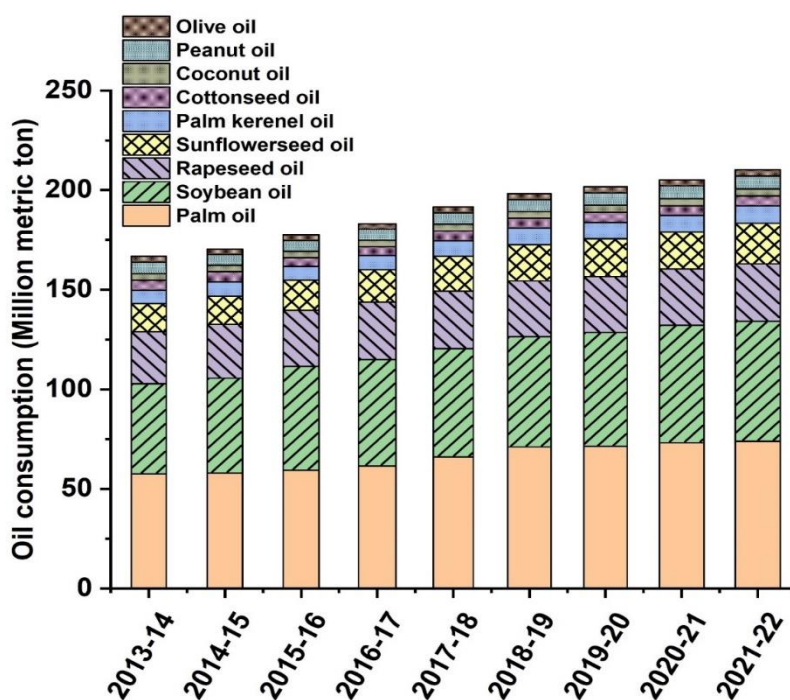


Figure 3.2. Vegetable oil consumption worldwide

3.2.1. Evaluation of Free Fatty Acid (FFA) content and Acid number

The amount of potassium or sodium hydroxide (in milligrams) essential to neutralize the FFA available in 1 gram of oil is known as the acid number. This is an ancillary estimation of the FFA content available in the sample of oil.

Firstly, methanol with a volume of 10 ml and 1 gm filtered waste cooking oil was mixed to prepare the solution in the burette and further 2 drops of phenolphthalein are added as an indicator in the solution. Further, potassium hydroxide (KOH), 0.1N drop by drop was poured into the burette. This process was carried out until the solution turned into pale pink colour and it was remained intact for the next 30 seconds or more than that. Finally, the volume of KOH consumed was measured through burette reading.

Thus, the fatty acid along with acid number was calculated using given equation 3.2.

$$\text{Acid number} = \frac{\text{Mol.wt(Alkali)} * V * N}{W} \quad (3.2)$$

Here, mol. weight (Alkali) = mol. weight of KOH. V, N and W are volume of KOH utilized in milligrams, KOH solution's normality, weight of test oil (in grams) respectively.

Further, the FFA was calculated using equation 3.3.

$$\text{FFA} = \frac{\text{Mol.wt(oleic acid)} * V * N}{W} \quad (3.3)$$

Where, mol. weight (oleic acid) = mol. weight of oleic acid in 1 ml N/10 KOH, and N, V and W represents normality of potassium hydroxide, volume of potassium hydroxide and weight of oil (grams) respectively.

3.3. Preparation of waste cooking oil biodiesel

The initial step of biodiesel making incorporates to effectuate the most acute estimation of free fatty acid availability in the oil. Upon subsequent proceeding of esterification reaction ($2 \text{ wt}\% \leq \text{FFA}$) or transesterification process ($2 \text{ wt}\% \geq \text{FFA}$) it's discerned WCO consists of more than 2% of FFA. As a matter of conjecture, an esterification reaction is a requisite to avert saponification before it proceeds to the transesterification process. Two major steps for production were accomplished:

- i) Esterification, then
- ii) Transesterification, along with an alkaline catalyst.

The rationale cited above is also done by (Gautam and Kumar, 2020) for biofuel generation from *Calophyllum inophyllum*, and *Jatropha curcas* oil with substantial FFA.

3.3.1. Acid-Catalyzed esterification

This incorporates the reaction of alcohol (methanol) with glyceride (WCO oil). Here, alcohol works as a reactant with the presence of p-toluenesulfonic acid (PTSA) an acid catalyst to restrict the surplus free fatty acid (FFA) content. To reduce reaction time and enhance the reaction rate, water content removal from filtered oil is implemented.

Initially, heating of the oil is performed up to 120°C for 30-40 min and consequently intended for cooling down to 60°C . This was crucial to remove the water content from filtered oil and that improves the reaction time and processing speed. Then, the prior solution of catalyst and methanol was mixed with oil. The oil mixture was stirred for about 2 h thoroughly with the assistance of a magnetic stirrer which rotates at around 400 rpm. The catalyst concentration and alcohol to oil ratio and catalyst concentration were taken at 0.5 (% w/w) and 6M:1 respectively. The end products extracted from the reaction were the catalyst, excess methanol, impurities and the mixture of esterified oil. Subsequently, the mixtures were separated by placing the mixtures at about 5 hr in a separate funnel.

Further, the water and alcohol present in the oil were treated by heating to 100°C for 1hr with a rotary evaporator in vacuum environment. Again, free fatty acid was computed and found to be 1.85% for esterified oil, and that was in theoretical condition range. Lastly this confirmed for further transesterification.

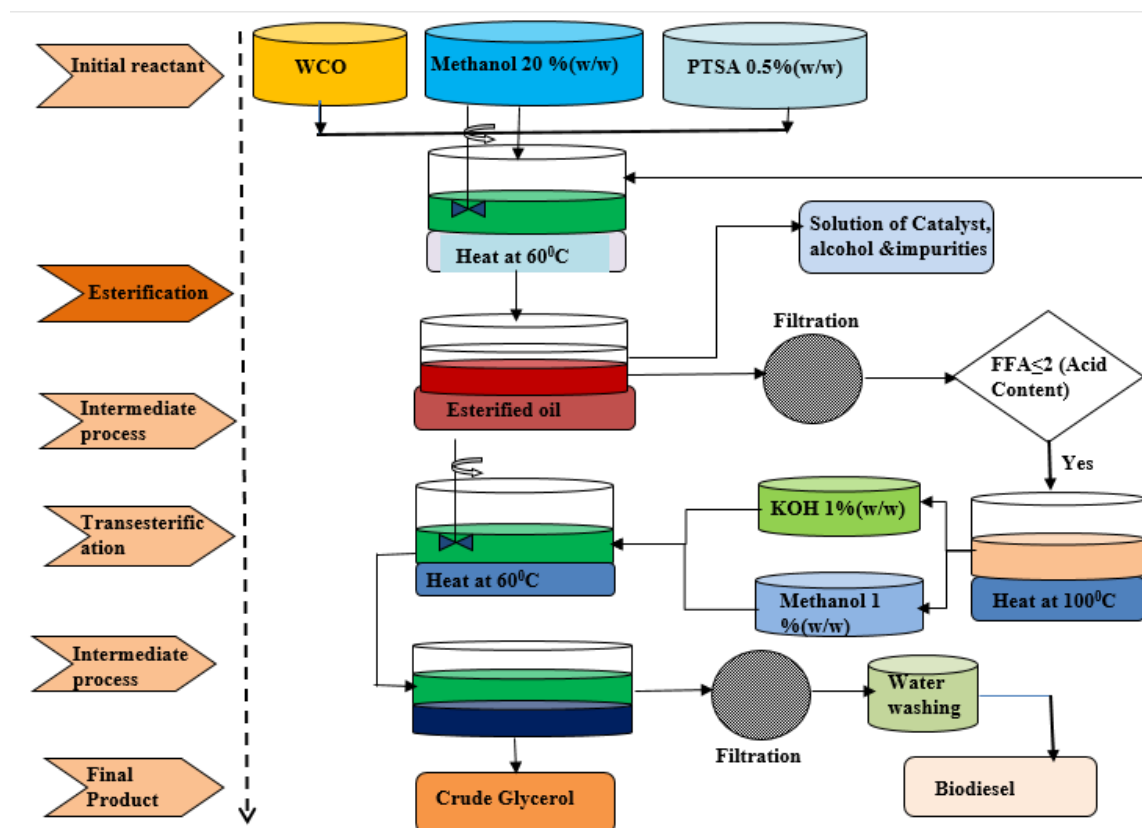


Figure 3.3. Process to produce biodiesel from WCO

3.3.2. Base-catalyzed Esterification

The conclusive stage was the base-catalyzed transesterification process in the generation of biodiesel. The reaction was less complicated to perform as methanol was already utilized to reduce FFA. The oil accumulated through various esterification processes was blended with KOH pellets (1% w/w) as well as (20% w/w). The methanol solution, catalyst to waste cooking oil ratio was considered to be 1:6M. Further, the mixture was heated for 120 min at 1000 rpm and transferred in a funnel for 12 hrs. The inferential step

included the final product of the process is making waste cooking oil methyl ester (WCOME) along with raw glycerol. Possessing the higher weight of crude glycerol than oil, it is settled down at the base and then sieved out. Thus, the residuals (esters) were gone through cleaning from hot water to obtain clean biodiesel. The schema of biodiesel production is illustrated in Figure 3.3

3.4. Determination of physico-chemical properties

The research contributes to important physico-chemical properties of waste frying oil and its methyl ester was assessed as per ASTM D 6751 standards. The properties consist of density, viscosity, distillation point, cold filter plugging point (CFPP), calorific value, moisture content, oxidation stability, carbon residue, flash point, copper strip corrosion etc. Some of the properties are discussed along with the equipment utilized for calculation as per their manufacturer.

3.4.1. Density

The density of fuel was measured by the equipment “Antan Par Density Meter”, Model DMA 4500 as shown in plate 3.1. The current investigation contains the measurement of the specific gravity of the test fuel sample at a temperature of 15⁰C as per standards ASTM D-4052. This instrument works on the U-tube oscillation principle. This method is generally used to measure liquid and gaseous density by measuring the frequency of oscillation. The measurement of frequency is done by the spring-mass system. To clean the test fuel pipeline, toluene with 10 ml was injected into the port. Then, the sample of 10 ml was injected into the port of the instrument. Five times replication was done through one pilot fuel and the final value was taken as the average of these values.

3.4.2. Kinematic viscosity

The kinematic viscosity was measured through viscometer as shown in plate 3.2. The measurement of viscosity and its variation with range of temperature can deliver a better

thoughtful waste cooking oil biodiesel as fuel lubricant. The viscosity was measured of various biodiesels at different ranges of temperature. The viscosity of fuels were measured through a “Petrotest Viscometer” as per standards ASTM D-445 at 40⁰C. The sample with the calculated entity flowed through the capillary tube. Further, the levelling time of fuel from the lower level to the upper-level mark in the capillary tube was noted. Subsequently, the multiplication of time duration to capillary constant calculates the kinematic viscosity as shown in equation 3.4.

$$v = k * t \quad (3.4)$$

where, v, k, and t represents kinematic viscosity (mm²/s); capillary constant (mm²/s²); (k= 0.005565 mm²/s²) and time (in second) respectively.

3.4.3. Calorific Value

This is defined as the amount of heat generated by burning unit mass of fuel under specific conditions in calorimeter. The high heating value is the total amount of heat generated in the combustion reaction of oxygen with carbon and hydrogen. It forms the oxide of carbon and steam further steam gets condensed by releasing heat in kJ/kg. The calorific value was measured as per the ASTM D240.0 standard from an isothermal bulb calorimeter. The combustion of fuel takes place at constant volume with an adiabatic water tank in presence of oxygen. The ignition takes place in fuel sample and combustion occurs in the bomb calorimeter. The rise in temperature in the thermocouple is measured and further the calorific value of the test sample is calculated. The equipment model, “Parr Model 6100EF” was used to measure the calorific value in the laboratory for biodiesel and its blends. Plate 3.3 represents the measuring device used in the laboratory.

3.4.4. Flash Point

The flash point is the minimum temperature upon which an ignitable mixture is formed by oil vapours as the air combines with oil droplets and generates a flash (Sinha et al 2007). This is measured by Pensky- Martens flash point apparatus by which the flash point is calculated as per ASTM D93 standards of the test fuel as shown in plate 3.4. The fuel sample was heated to the tiny pilot flame in a test cup through the upper cover at steady time durations. The lowest flash point observed were 130⁰C, 120⁰C measured by ASTM D-6751 and EN-14214 respectively.



Plate 3.1: Density meter

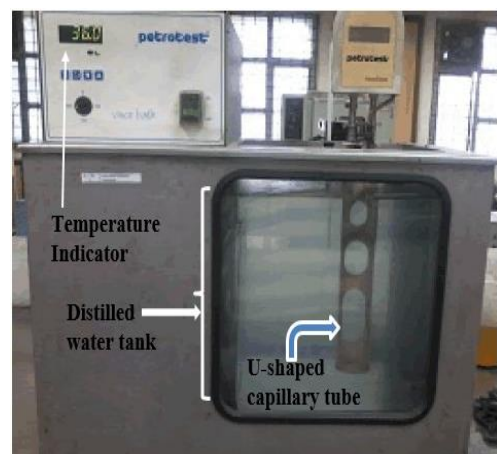


Plate 3.2: Viscometer

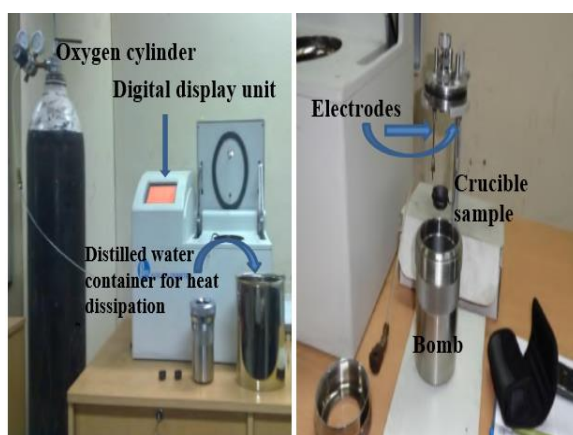


Plate 3.3: Bomb calorimeter



Plate 3.4: Flash point tester

3.4.5. Cetane Number

Cetane number (CN) is the evaluation of the ignition quality of diesel engine's fuel. It is the property of petroleum diesel or diesel type fuels which defines the quality of ignitibility in CI engines. The present study calculates the cetane index by the ASTM D4737 standard. Therefore, the cetane index was measured through distillation along with the density curve of various samples of fuel (Aleme and Barbeira, 2012). The equipment used to obtain the distillation temperature is given in plate 3.5. The autoignition value of various biodiesel and its blends is given by the below correlation (3.5).

$$ECI = 45.2 + [0.131 + (0.901)(X)][BT645] + (0.0892)(BT345) + [(BT345)8 - (BT745)8](107X + 60X8) + [0.0523 - (0.420)(X)][BT745] + [0.00049] \quad (3.5)$$

Here, D stands for density, and BT10, 50 and 90 for Boiling/ Recovery temperature to get 10%, 50% and 90% distilled fuel respectively. $Z = D - 0.85$

3.4.6. Carbon Residue:

This is the amount of carbon left over/deposited in the combustion chamber through the combustion of liquid/gaseous fuel. Micro Carbon Residue Tester (MCRT160) is used to determine the carbon residual as per ASTM D4530 measurement standards. This is usually seen through photographic view as shown in plate 3.6. Initially, the weighted fuel sample of 5gm is placed inside the crucible airtight of MCRT160. Further, the combustion was promoted steadily to 500°C with 10°C/min of interval then the combustion continued for 15 min. Finally, the cooling involves residual combustion products by eradicating nitrogen gases from the inside of system. When the temperature of the test- tube falls to 30°C, the traces or residue remains in it, which is weighted.

3.4.7. Distillation

The test sample of 100ml was processed through distillation as per the ASTM D-86 standards method. Plate 3.5 shows the instrument utilized for distillation. Firstly, the sample is kept in distillation flask where this process is carried out at given conditions. The temperature at which the condensed drop starts falling from the condenser at the lower end. Further, at certain intervals of time, the condensate volume is estimated against condensate temperature. Moreover, the highest temperature, all the fuel condensed is measured.

3.4.8. Oxygen Content (wt%)

The availability of oxygen in fuel has a major impact on governing combustion and emission species of CI engine. Higher extent of availability leads to more prone complete combustion and decrease in hazardous UHC and CO emissions. The major contributions of biodiesel are less soot emission than conventional diesel because of the factors like nil sulfur content, fuel bounded oxygen, unsaturated fatty acid, and less aromatic content. Therefore, the reduction in soot formation may lower the radiative heat transfer from combustible particles. EA3000 series CHNS/O elemental analyzer was utilized to measure the oxygen wt% as per ASTM D5373 standards and illustrated in plate 3.7. The process of measuring oxygen is a little bit different compared to the setup of hydrogen carbon, sulphur and nitrogen elements. This process is similar to a combustion reactor which utilizes oxygen for burning, 5% hydrogen with a pyrolysis reactor dissolved in helium and determine the oxygen gas. The whole setup exhibits acidic gas trapping mechanism, a gas chromatograph column to extract gas mixture and a pyrolysis reactor fortified with nickelized carbon wool. Further, the pyrolyzed product was carried out through circulating helium gas in the setup. Firstly, the fuel sample is placed into the reactor for heating upto 1080°C and resulting into the breakup of the sample and oxygen

gas releases. Then, nickel carbon wool reacts with oxygen to form nitrogen and carbon monoxide.



Plate 3.5. Distillation setup



Plate 3.6. Carbon residue tester

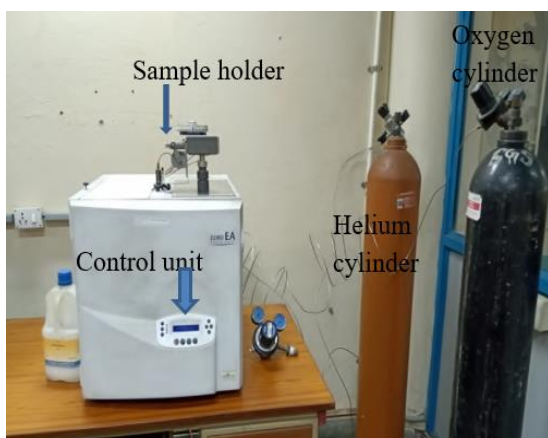


Plate 3.7. CHNS/O Elemental Analyzer



Plate 3.8. Copper strip corrosion tester

The generated pyrolyzed product is separated by passing to the GC separation column from where gases are detected and distinguished consequently by a thermal conductivity detector (TCD). TCD works as a medium that distinguishes the gases and further proceed into

elemental peaks. Therefore, specific signals are decoded by software and it relates the peak for every corresponding element available in the sample.

3.4.9. Copper strip Corrosion

The engine parts as well as engine linings pass through corrosion due to the availability of various kinds of sulphur and acids present in the fuel. Thus, various fuel samples are exposed through copper strip corrosion tests. Plate 3.8 shows the photographic view of the setup and test following the ASTM D130 standard. This parameter was evaluated by putting the copper strip for a time duration of 3 hrs in the fuel bath. The fuel temperature of the bath was maintained at 50⁰C. Further, the copper strip was removed after a specified time duration from the fuel bath. Then, the extracted strip was compared with the standard colour code which varies from 1 to 4.

3.5. Cold Flow Properties

The properties responsible for low temperatures in running diesel engines create difficulty like starting the engine, emitting white smoke, filter plugging and choking of the injector. The cold weather performance of fuel is bad and can be discretized as cold point (CP), pour point (PP) and cold filter plugging point (CFPP).

3.5.1. Cold Point & Pour Point

A cold point is the lowest possible temperature at which the wax in the fuel is first seen to crystallize and form a cloudy appearance. Moreover, the pour point of the liquid fuel is the least temperature at which fuel losses its flow characteristics. The estimation of the pour point and cloud point was conducted as per ASTM D97 and D2500 standards respectively. The instruments were used to measure the pour point and cloud point is shown in plate 3.9. The test tube with rubber cork filled with test fuel is kept inside the hole placed above the refrigerator. The cork consists of an opening at the centrally placed RTD temperature sensor that provides the temperature of the sample. Further, the test tube

is removed which is followed by visualizing at every temperature drop of 30°C to envisage pour point measurement as well as cloud point creation.

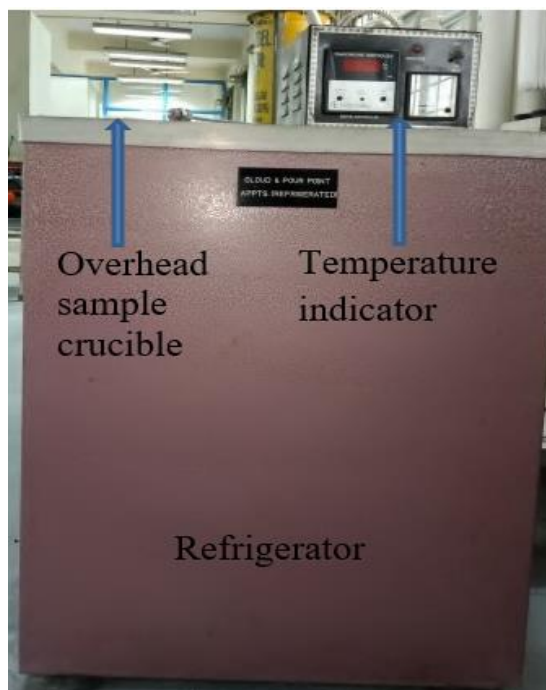


Plate 3.9. Cloud point and Pour point apparatus

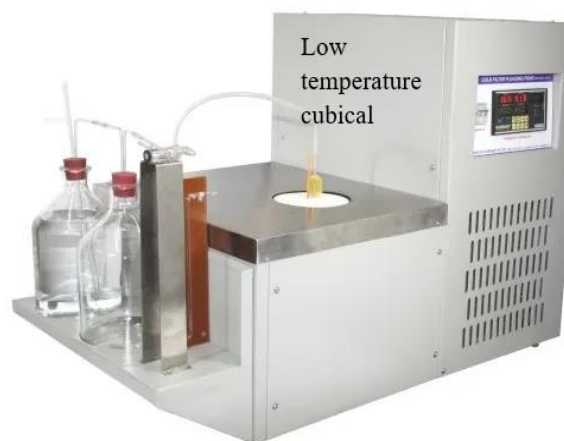


Plate 3.10. Cold filter plugging point apparatus

3.5.2. Cold Filter Plugging Point (CFPP)

The cold filter plugging point of fuel exists between the pour point and the cloud point. It is the point at which test fuel initiates gelling up in such a way that it can flow in a standard fuel filter for a certain duration. This property of fuel is measured using Linetronic Technologies as shown in plate 3.10. It works as per ASTM D6371 standards for the estimation of cold filter plugging points of biodiesel and their blends of diesel. Primarily, the first step consists of lowering the bath temperature to -34°C . As the temperature reached the specified range, the weighted quantity of fuel is drawn through vacuum supported mechanism into a capillary tube. Then, the temperature of the fuel sample is allowed to lower down in bath. The duration of 1 minute in which fuel column becomes

nearly steady from fluctuations in the standardized filter of 10 microns is taken as CFPP of fuel.

3.6. Experimental set-up to measure spray characteristics

The jet spray exit from the nozzle especially spray tip penetration, cone angle, and volume can be measured from the visualization of the spray. The setup consists of the common rail injection system which is the current demand of engine manufacturer. The visual pressure vessel made of stainless steel has been used to control ambient pressure. The optical window of diameter 85 mm from both sides is implemented for visual inspection as shown in Figure 3.4. Spray characteristics of fuel along with combustion characteristics could study similarly to diesel engine conditions. The ambient pressure is regulated through the intake valve whereas injection pressure is controlled through a common rail system (CRI 3-18). The first-generation common rail system was manufactured to maintain and control injector pressure up to 1350 bar. The ambient temperature is measured using thermocouple. The experimental setup exhibits single hole, electronically driven fuel injector where common rail includes a pulse width of 700 ms, frequency of 1.5 Hz and diameter of 0.18 mm. The spray visualization of fuel has been done through the Schlieren method. Two steps were involved in image processing. Initially, the pre-processing of the image was performed in MATLAB through custom-written code at the initial step and secondly the spray image was computed by ImageJ code. The fuel injection's activation was regulated through a delay/pulse generator, which can control the width of injection duration as well as signal to the injector driver and regulate the closing and opening of the injector valve. Here, the experiment exhibited the injection pressure in the range of (0- 2000 bar).

The image capturing of fuel spray was performed through the high-speed digital camera (Phantom v2640). The study exploited the camera which can produce 11,000

frames per second with a resolution of 512 x 512 pixels with 7 μm of exposure time. The light lamp of intensity 1000W was incorporated volumetrically to lighten the spray. Further, the injector is also coordinated with a high-speed camera through the same trigger pulse. To capture full-volume spray, the spray images were captured for 15 ms. Thus, the spray cone angle and spray tip penetration data were evaluated according to spray images.

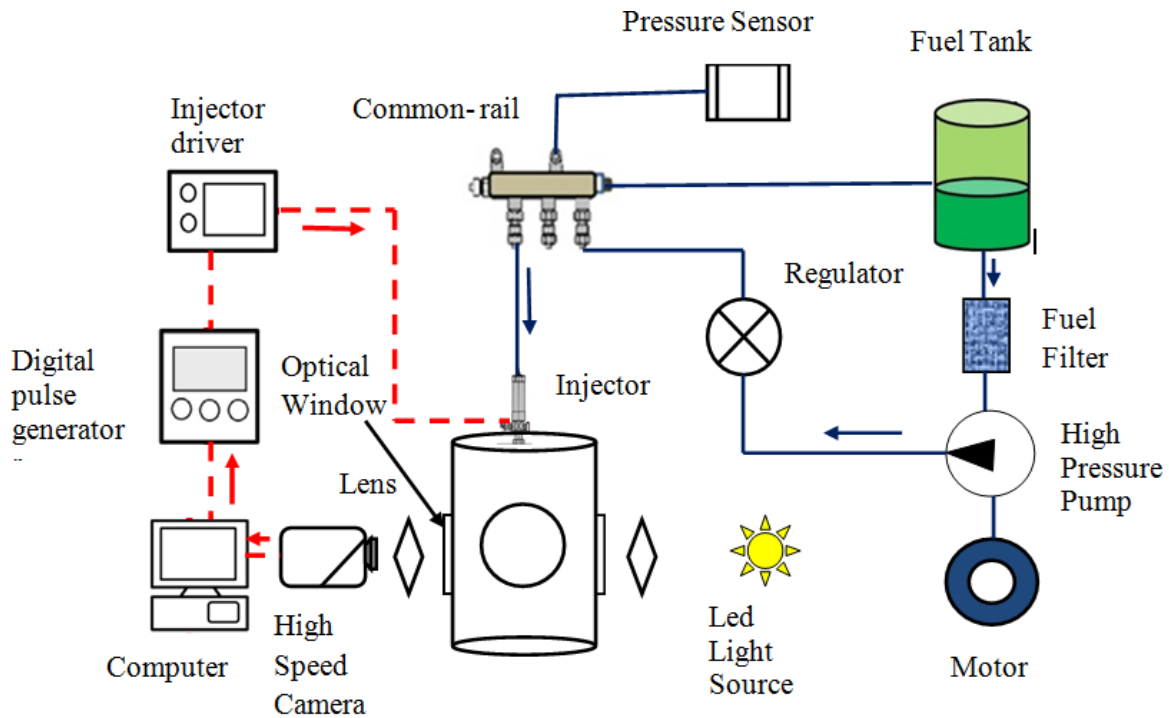


Figure 3.4. Experimental set up of visualization of spray characteristics of fuel

3.6.1. Experimental error and Uncertainties analysis

All experimentation consists of a little degree of uncertainty due to physical measurement and the vague measurement is known as error analysis. The root cause of the above can be human interference, calibration, device selection, random errors such as environmental conditions and the designing of experiments. Hence, the uncertainty analysis was done to state the correctness of current investigations. Each experiment was performed six-times and then the average was taken for the uncertainty value of various instruments and accuracy along with their range are shown in Table 3.2.

Table 3.2. Uncertainty analysis of experimental setup.

S. No	Device parameter s/specification	Range	Accuracy	Percentage uncertainties	Model
1	Pressure sensor	0-200,000psi	$\pm 0.35\%$	± 0.45	PXP0-200KS5T
2	Motor	0-5hp		± 0.20	MMG132-2-3-38FF-265-E
3	Pulse generator	1 mHz to 1.0 MHz	$\pm 1\%$	± 0.01	DG535
4	High speed camera	0-12,500 fps	$\pm 10\text{fps}$	± 0.4	Phantom v2640
5	Injector driver		$\pm 0.15\%$	± 0.17	TEMS, TDA-3200H
6	Light source				PAR64 1000W lamp
7	lens	512x512 pixel		± 0.26	
8	Injector	0.18mm		± 0.036	
9	Fuel Filter	0-6.5 microns	± 0.1	± 0.25	77066 WS
10	Fuel pump	0-200MPa	$\pm 10\text{Pa}$	± 0.15	CRS2-20-OHW
11	Thermocouple	95-9000c	0.75%	± 0.25	Constantan
12	Injection system	0-220 MPa	$\pm 12\text{Pa}$	± 0.30	CRI 3-18(CR DI)
13	Kinematic viscosity	0.2-20,000 mm ² /s		± 0.35	
14	Pressure gauge	0-100MPa	1%	± 0.45	SKF 107758 7/2

15	Sauter mean diameter	±0.01 %	±0.30
----	----------------------------	------------	-------

The uncertainty analysis of the engine trail parameter was measured through equation 3.6.

$$U_E = \left\{ \left[\left(\frac{\partial E}{\partial X_1} \right) u_1 \right]^2 + \left(\frac{\partial E}{\partial X_2} \right) u_2 \right]^2 + \left(\frac{\partial E}{\partial X_3} \right) u_3 \right]^2 + \dots + \left(\frac{\partial E}{\partial X_n} \right) u_n \right]^2 \}^{1/2} \quad (3.6)$$

where E shows the basic factor which depends on other factors X_1, \dots, X_n . X represents the amount in the experiments.

where, $u_1 \dots u_n$ is the uncertainty of obtained results. Finally, the overall uncertainty of experimentation was presented as:

$$\begin{aligned} \text{Overall Uncertainty} &= \sqrt{(\text{Uncertainty (\%)} \text{ of (SMD}^2 + \text{kinematic viscosity}^2 + \text{pressure} \\ &\text{sensor}^2 + \text{ambient pressure}^2 + \text{ambient temperature}^2 + \text{injection system}^2 + \text{Fuel Pump}^2))} \\ &= \pm 1.4566\% \end{aligned}$$

The overall uncertainty value is $\pm 1.4566\%$, which appear in the limit reported by studies (Raju et al., 2020; Venu et al., 2020).

3.7. Swirl Injector

Swirl injector contains three components like a widget, transparent nozzles and a main body. The three tangential slots machined with square cross-section are the main body mounted in the atomizer to supply fuel where the depth, length and width of slots are shown in Figures 3.5, 3.6 and 3.7 respectively. The inclination imparted for each groove is 45° in the downward direction. This ensures the injector that the jet consists of a tangential flow along with the axial flow. As the jet exited from the swirl injector, a thick liquid sheet is generated having cone structure move towards an increasing radius in a downward direction. Further, the thickness of the sheet got reduced due to the conservation of mass when the jet moves away from the injector (Baumgarten C, 2006).

The turbulence created in the inner nozzle disturbs the liquid surface of the jet. Thereby,

the growth of these perturbations is due to aerodynamics interaction. Finally, sheet break up occurs in ligaments at the time of critical amplitude. Now, the ligament passes under stimulation of gaseous forces and surface tension leading to break up into droplets. The secondary atomization phenomenon is the same as discussed in the section. 2.2.6. The instabilities created in the liquid sheet are administered by injection pressure followed by turbulence (Goodwin and Wigley, 2003).

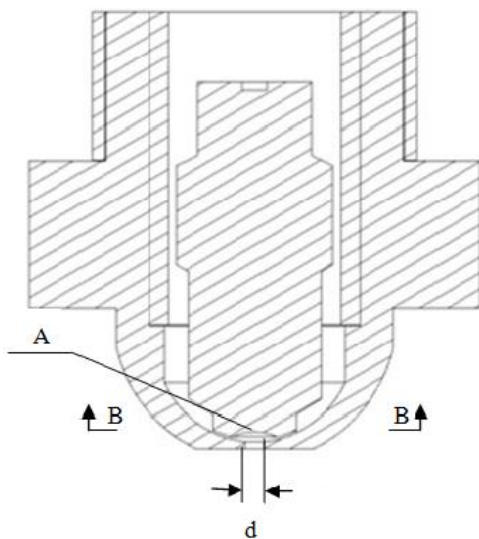


Figure 3.5. Cross-sectional view
of the pressure swirl nozzle

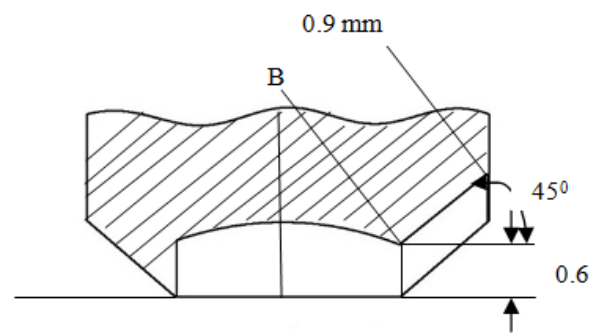


Figure 3.6. Geometrical specification of
slot in pressure swirl nozzle

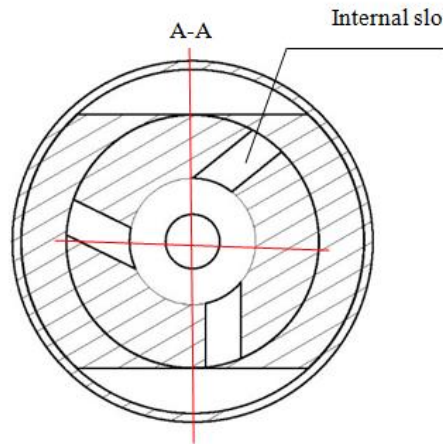


Figure 3.7. No of slots in the cross-section

3.8. Experimental set-up to measure surface tension of biodiesels

The equipment, the nima dynamic surface tensiometer has been used to measure the surface tension of biodiesel. This is regulated through a computer which examines and which applies the forces. Further, the counteract external force is exerted by biodiesel which is induced during the engagement of du Nouy ring in biodiesel evaluated as shown in Figures 3.8 and 3.9. This method is recognized as the pull-force method.

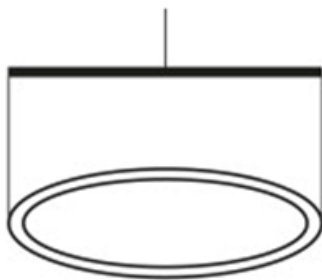


Figure 3.8. Ring of the Du Nouy
ring tensiometer



Figure 3.9. Du Nuoy ring tensiometer

This is measured through the given equation (3.7), (3.8)

$$P_t = P_r + \gamma_{\text{ideal}} * 4 \Pi r \quad (3.7)$$

$$\gamma = f * \gamma_{ideal} \quad (3.8)$$

here, R, Pt and Pr shows radius of ring, total force and weight of ring respectively. Due to differences in size, shape at inner and outer surface being not equal therefore surface tension should be measured by multiplying the factor f with the ideal value. Thus, the actual value of surface tension exhibits lower value than ideal surface tension.

3.9. Engine trial setup

The experimental trial was effectuated on a 4-stroke, 1-cylinder, stationary engine. These sorts of engines are extensively employed for decent power generation as well as in the Indian agricultural sector. Its working incepts by a water-cooled dynamometer possessing a 7.5 kW rating and an eddy current (or Foucault's current) which are engaged to the shaft to drive loading. The rated power and engine speed are 5.9 kW and 1500 rpm respectively of the engine. Furthermore, the setup with a control panel is compiled with a controlled data acquisition system to observe and evaluate fuel flow rate, load, ambient pressure, and temperature at various locations in the combustion chamber, as shown in Figure 3.10. The dynamometer was connected to a strain gauge-type load cell, providing precise engine load information to the control unit. The differential pressure transmitter (Model no: EJA110-EMV-5A-93NN) measured the flow rate with an accuracy of 0.046%, an adjustment range of 0-500mm of water. A piezoelectric pressure transducer of Kistler (6613CA) was used to calculate the combustion chamber pressure. Now the data acquisition system accumulates the data from measurement and then processes the data to “Engine soft” software on the computer. Thus, the signal received from the software was transformed into a comprehensible form. Furthermore, the quantities of destructive emissions such as CO, NO, HC, and smoke of test fuels were assessed through the di-gas analyzer AVL-444 as well as smoke meter AVL-437.

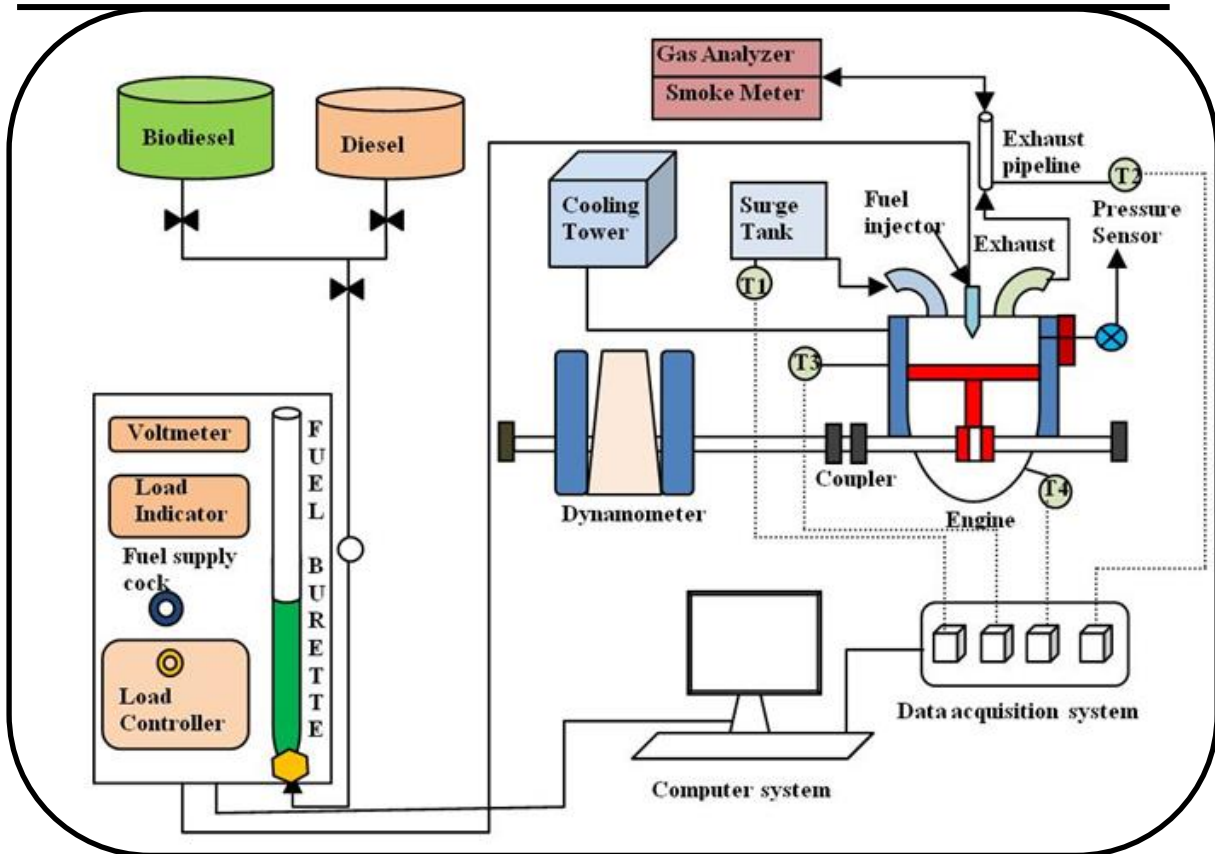


Figure 3.10. Engine trail setup

Subsequently, the engine trials were performed under various loading conditions as per the prescribed standards of BIS-10000. Where the corresponding value of brake mean effective pressure concerning loads varies from 0 bar to 6.3 bar. To get the robustness of data in the experiments, the engine requires to warm up till it reaches to steady state because it shows the point where the temperature of cooling water indicates stabilized. Preheated and unheated biodiesel along with neat diesel were tested and compared.

3.10. Computational Technique

The investigation of spray formation which is away from the nozzle is very intricate. This consists of unsteady, turbulent and complex behaviour. Since the phenomenon went through a continuous phase as well as discrete phase therefore, the Eulerian-Lagrangian method could be an effective process to examine this multiphase flow. The flow of gases

in constant volume mesh is described by Eulerian method, and the characteristics of droplets are tracked by langrangian approach as shown in Table 3.3.

Table 3.3. Eulerian- langrangian approach for multiphase flow.

Eulerian Method:	
Equation: Continuity equation, Energy, Momentum Equation	
Model: Turbulence, Cavitation	
Heat Exchange	Momentum Exchange
↑↓	↑↓
Mass Exchange	
Lagrangian Approach:	
Equation: Momentum, Energy	Model: Breakup (Primary & Secondary), aerodynamic drag, wall impingement, dispersion, collision and coalescence, Vaporization

The continuous phases along with discrete phases are modelled separately. Further, to get a distinct representation of the droplet disintegration, influence of spray characteristics, the gas-droplet coupling is considered. Moreover, the effect of the continuous phase and discrete phase on trajectory, and continuum are analysed respectively. Thus, the continuous phase as well as discrete phase couplings, are solved alternatively till the exchanging stopes. The Reynolds Averaged Navier Stroke (RANS) equations are applied for unsteady flow. Since they constitute multiphase flow like gas and liquid therefore transport equations are involved. Furthermore, the droplet exhibits turbulence behaviour that's why a stochastic model is employed. Since, the droplet experiences gravitational, drag and other forces, they all are determined through Newton's law of motion to obtain the droplet trajectory. The communication among drags forces, lift forces, mass transfer, specific transfer and heat transfer is implemented through the discrete and continuous phase.

3.10.1. Meshing of computational volume:

The present study consists of a 3D computational volume of dimension $1.5 \times 1.5 \text{ m}^2$ cross-section and 1.5 m length to get the computational solution. The fuel injector is implemented at the centre of a cross-section as shown in Figures 3.11a, 3.11b and 3.11c respectively. The computational volume was divided into millions of small volumes which is known as mesh grid. The discretization of computation volume is generally preferred to follow polyhedral control volumes or hexahedral mesh. These two provide advantages like higher accuracy and better convergence (Spiegel et al., 2011). Even if the generation of a tetrahedral grid is easier for complicated geometry such as small gaps, and long channels, still hexahedral mesh needs lower grid size as compared to tetrahedral for better accuracy. Further, tetrahedral mesh, having four neighbours create difficulties during the computation of the gradient. This is because of neighbour nodes which carry spatial positions. The tetrahedral mesh generates numerical diffusion larger as compared to hexahedral mesh. The computational accuracy reduces which leads to major deviation from actual results in tetrahedral mesh (Sosnowski et al., 2017). Thus, the computational volume was modelled by hexahedral cells despite of others as shown in Figure 6. It can impart faster convergence and better accuracy. The mesh size should be smaller than the minimum size of the droplet in the direct numerical study (DNS), while in the point source method, the mesh size should be larger than the droplet size. The current study constitutes a larger mesh size than droplet size hence point source method has been employed. The ANSYS FLUENT18.0 imparts extensive numerical methods to solve continuous phase equations a pressure solver is employed due to consideration of steady state.

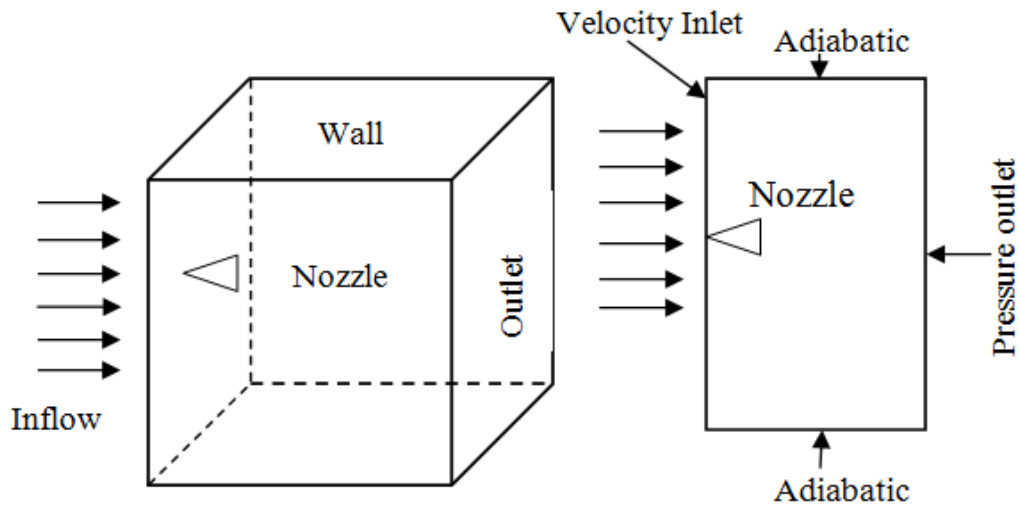


Figure 3.11(a) 3-D view of the computational volume ($1.5 \times 1.5 \times 1.5 \text{ m}^3$). (b) Side view of computational model with boundary conditions. In both Figure.(a), (b) Nozzle situated at the middle of Inflow wall

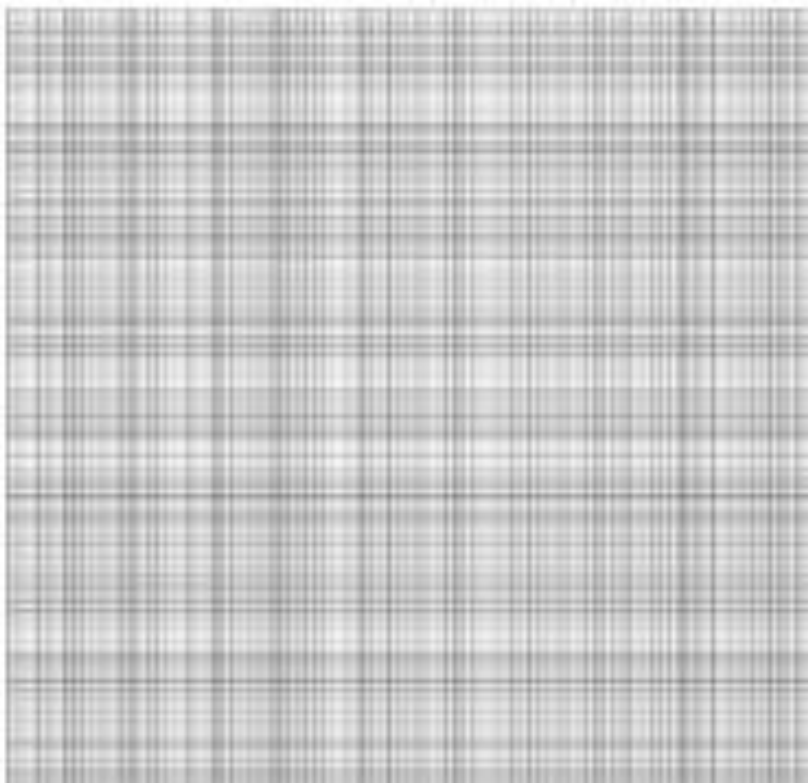


Figure 3.12. Meshing of computational volume

3.11. Numerical simulation

3.11.1. Continuous Phase Air

Continuity equation:

The continuous flow of gases is modelled through mass and momentum flow and was demonstrated through RANS conservation equations. This is placed in cartesian form as follow:

$$\frac{\partial(\rho u_i)}{\partial t} + \frac{\partial}{\partial x_i}(\rho u_i) = s_m \quad (3.9)$$

where ρ, u_i are density, and velocity in i^{th} direction

The incompressible and compressible flow is exhibited by equation 3.9.

s_m = mass inclusion to disperse phase from continuous phase

Momentum Equation:

The conservation of momentum can be stated in the form of partial differential equation

3.10. The equation in i^{th} direction as:

$$\frac{\partial(\rho u_i)}{\partial t} + \frac{\partial}{\partial x_j}(u_i u_j \rho) = -\frac{\partial p}{\partial x_j} + \frac{\partial T_{ij}}{\partial x_j} + g_i \rho + f_i \quad (3.10)$$

$$T_{ij} = [\mu(\frac{\partial u_i}{\partial x_j} + \frac{\partial u_j}{\partial x_i})] - 2/3(\mu \frac{\partial u_i}{\partial x_i} \delta_{ij}) \quad (3.11)$$

Furthermore, the equation of stress tensor is shown by equation 3.11, which is applied for Newtonian fluid: where, P static pressure, μ the molecular viscosity, $F_i, \rho g_i$, are external body force and gravitational body force, respectively.

The Energy equation.

The temperature distribution is expressed as:

$$\frac{\partial(\rho E)}{\partial t} + \frac{\partial}{\partial x_i}(\rho u_i H) = \frac{\partial}{\partial x_i} \left(k \frac{\partial T}{\partial x_i} \right) + \frac{\partial}{\partial x_i}(\tau_{ij} u_j) + \rho f_i u_i + q_H \quad (3.12)$$

where $u_i \rho f_i$ = Work done by body force, K and H are isotropic thermal conductivity, enthalpy respectively

E, q_H = Total specific energy, Energy exchange per unit volume caused by chemical reaction

The eddy viscosity method was applied to model the Reynolds stresses and for closure of transport equations the K- ϵ turbulence model was used (Sun et al., 2018). The solution was achieved through two assumptions, firstly the flow is fully turbulent and secondly considering negligible molecular viscosity. Thus, the standard K- ϵ turbulence model was utilized for developed turbulent flow as given in equations 3.13, 3.14.

$$\frac{\partial(\rho k)}{\partial t} + \frac{\partial}{\partial x_i}(\rho k u_i) = \frac{\partial}{\partial x_j} \left[\left(\mu + \frac{\mu_t}{\sigma_k} \right) \frac{\partial k}{\partial x_j} \right] + G_k + G_b - \rho \epsilon - Y_M + S_k \quad (3.13)$$

$$\frac{\partial(\rho \epsilon)}{\partial t} + \frac{\partial}{\partial x_i}(\rho \epsilon u_i) = \frac{\partial}{\partial x_j} \left[\left(\mu + \frac{\mu_t}{\sigma_k} \right) \frac{\partial \epsilon}{\partial x_j} \right] + C_{1\epsilon} \frac{\epsilon}{k} (G_k + C_{3\epsilon} G_b - C_{2\epsilon} \rho \frac{\epsilon^2}{k}) + S_\epsilon \quad (3.14)$$

where S_ϵ, S_k shows defined primary terms for dissipation rate, turbulent kinetic energy, respectively. the above equations contain the value of constants are

$C_{1\epsilon} = 1.44, \sigma_\epsilon = 1.3, C_{1\epsilon} = 1.92, \sigma_k = 1.00, C_\mu = 0.09$, the turbulent flow energy due to the average velocity gradient and buoyancy are indicated as G_k, G_b .

(Sun et. al., 2018) did an investigation on spray development along with their disintegration through numerical model in multiphase flow. The Eulerian- lagrangian approach was applied to formulate the continuous phase medium and the discrete phase medium is described through the langarangian approach. The spray behaviour, closure

and collision were modelled through standard k- ϵ turbulence model. The accuracy and less deviation from standard experimentation are attracted towards the implication (Asheim et al., 1988; Chang et al., 1993).

3.11.2. Discrete Phase

The droplet's motion in the flow field is explained by Newton's second law by considering negligible effect of gravitational force. However, the drag force is only responsible for retardation. The droplet motion is defined by the equation 3.15.

$$\frac{1}{6} \rho_p \pi d_p^3 \frac{du_p}{dt} = \frac{1}{2} (u_g - u_p) |u_g - u_p| \rho C_D \pi \frac{d_p^2}{4} + f \quad (3.15)$$

$$C_D = a_1 + \frac{a_2}{\text{Re}} + \frac{a_3}{\text{Re}^2} \quad (3.16)$$

where, u_p , u_g shows particle velocity and gas velocity respectively. Further, an additional force is working apart from drag force. The droplet coefficient (C_d) is calculated using equation 3.16.

where Re is Reynolds no, $a_1=0.1-3.67$, $a_2 = -1662.5$ to 148.62 and $a_3 = -4.74 \times 10^4$ to 5.416×10^6 are constants which are depends on Re mentioned by (Morsi and Alexander, 1972).

3.11.3. Break-up and atomization

The liquid jet from the pressure swirl atomizer is forced with an axial circulation motion. That makes the development of conical liquid film with a smaller thickness. After the exit from the nozzle, the jet with tangential motion convertes into rotational motion. Due to the above phenomenon, the liquid sheet experiences the aerodynamic disturbance in the sheet which further breaks into ligaments. The breakup into ligaments is caused by several reasons such as drag force, turbulence generation in a liquid state, and disposal of the cavitation bubble. However, the cause of the above mechanism is also gas and liquid

density. The relative velocity between gas and liquid, viscosity and surface tension are responsible for the breakup mechanism. Therefore, to model the above mechanism, a linear instability sheet atomization model is effectuated. Further, the axial and radial motion of the sheet creates an air core that is enfolded with liquid film. The thickness of the film (h_t) is achieved by equation 3.17.

$$h_t = 0.5(D_{inj} - \sqrt{D_{inj}^2 - \frac{4\dot{m}_{eff}}{\pi\rho_1 V_{axis}}}) \quad (3.17)$$

$$U = K_v \frac{\sqrt{2\Delta p}}{\sqrt{\rho_1}} \quad (3.18)$$

$$u_{axis} = U \cos \theta \quad (3.19)$$

where, $\theta, \dot{m}_{eff}, \rho_1, V_{axis}, D_{inj}$ shows half angle, mass flow rate, liquid density, axial velocity and injector diameter respectively. The axial velocity through injector and total velocity are calculated through equation 3.18, 3.19. where, K_v coefficient of discharge of nozzle, l_b breakup length is shown in equation 3.20 3.22.

$$K_v = \max\left[\frac{7}{10}, \frac{4\dot{m}_{eff}}{\pi d_{inj}^2 \rho_1 \cos \theta} \sqrt{\frac{\rho_1}{2\Delta p}}\right] \quad (3.20)$$

$$\eta_b = \eta_0 e^{i\lambda x + \omega x} \quad (3.21)$$

$$l_b = \frac{U}{\Omega} \ln\left(\frac{\eta_b}{\eta_0}\right) \quad (3.22)$$

η_0, η_b are wave amplitude and surface development as in equation 3.21. And λ, ω are wave number and growth rate respectively. Now the mass balance concept defines the ligament diameter at breakup point is shown in equation 3.23, 3.25.

$$D_0 = 1.88d_L(1 + 3Oh)^{1/6} \quad (3.23)$$

$$h_b = \frac{(d_{inj} - h_0)h_0}{(d_{inj} - h_0 + 2L_b \sin(\frac{\theta}{2}))}, \quad (3.24)$$

$$d_l = \sqrt{\frac{fh_b}{\lambda_b}} \quad (3.25)$$

h_b shows the sheet thickness as a function of diameter that affects breakup length and λ_b the wave number. Where, $(d_{inj}-h_0)$ is the evaporated film thickness as shown in equation 3.24. The weber's approach of capillary instability (Asheim et al., 1988) has been considered for ligament to droplet breakup which is Weber number We , Oh Ohnesorge number 3.26, 3.27

$$We = \frac{\rho u_{rel}^2 d_p}{\sigma} \quad (3.26)$$

$$Oh = \frac{\mu_p}{\sqrt{\rho_p \sigma d_p}} = \sqrt{We} / Re \quad (3.27)$$

Where surface tension and droplet diameter are indicated as d_p , σ respectively. Further, secondary breakup of cone-shaped sheet was modelled through Taylor analogy breakup model. This model describes the natural vibration system in oscillation with distorted droplet. It focuses especially on excretion of aerodynamic force on droplets system. The damping force on the mass is derived through liquid viscosity force while surface tension force is derived through spring force (Belhadeh et al., 2012).

$$\frac{f}{m} = c_f \frac{\rho u_{rel}^2}{\rho_l r} \quad (3.28)$$

$$f - kx - d \frac{dx}{dt} = m \frac{d^2x}{dt^2} \quad (3.29)$$

X, shows movement of droplet. To get the equation of coefficient, Taylor's approach is used in equations 3.28, 3.29,3.30,3.31.

$$\frac{d}{m} = c_d \frac{\mu_1}{\rho_1 r^2} \quad (3.30)$$

$$\frac{k}{m} = c_k \frac{\sigma}{\rho_1 r^3} \quad (3.31)$$

Where, μ_1 , t and r are liquid viscosity, time and drop radius respectively.

$$\frac{r_1}{r_2} = \frac{7}{3} + \frac{\rho_1 r_1^3}{8\sigma} \left(\frac{dy}{dt}\right)^2 \quad (3.32)$$

$$\frac{d^2 y}{dt^2} + 5 \frac{\mu_1}{\rho_1 r^2} \frac{dy}{dt} + \frac{8\sigma}{\rho_1 r^3} y - \frac{2}{3} \frac{\rho u_{rel}^2}{\rho_1 r} = 0 \quad (3.33)$$

The droplet breakup is assumed to be, $y > 1$ (Belhadeh et al., 2012), where r_1 and r_2 , are bigger and smaller diameter of droplet which is shown in relation 3.32, 3.33

3.11.4. Droplet Evaporation

The evaporation in air-fuel droplet is induced through heat and mass transfer where, both heat and mass transfer are influenced by Reynolds number, which shows the dominance of inertial force over viscous force. h_c , Re and convective mass transfer are calculated through equations 3.34, 3.35 (Elbadawy et al., 2015). The equations indicate that lowering the Reynolds no affect Nusselt no and Sherwood no.

$$Sh = \frac{h_c m d}{D} = 2 + 0.6 Re_d^{1/2} Sc^{1/3} \quad (3.34)$$

$$Nu = \frac{h_c d}{k_\infty} = 2 + 0.6 Re_d^{1/2} Pr^{1/3} \quad (3.35)$$

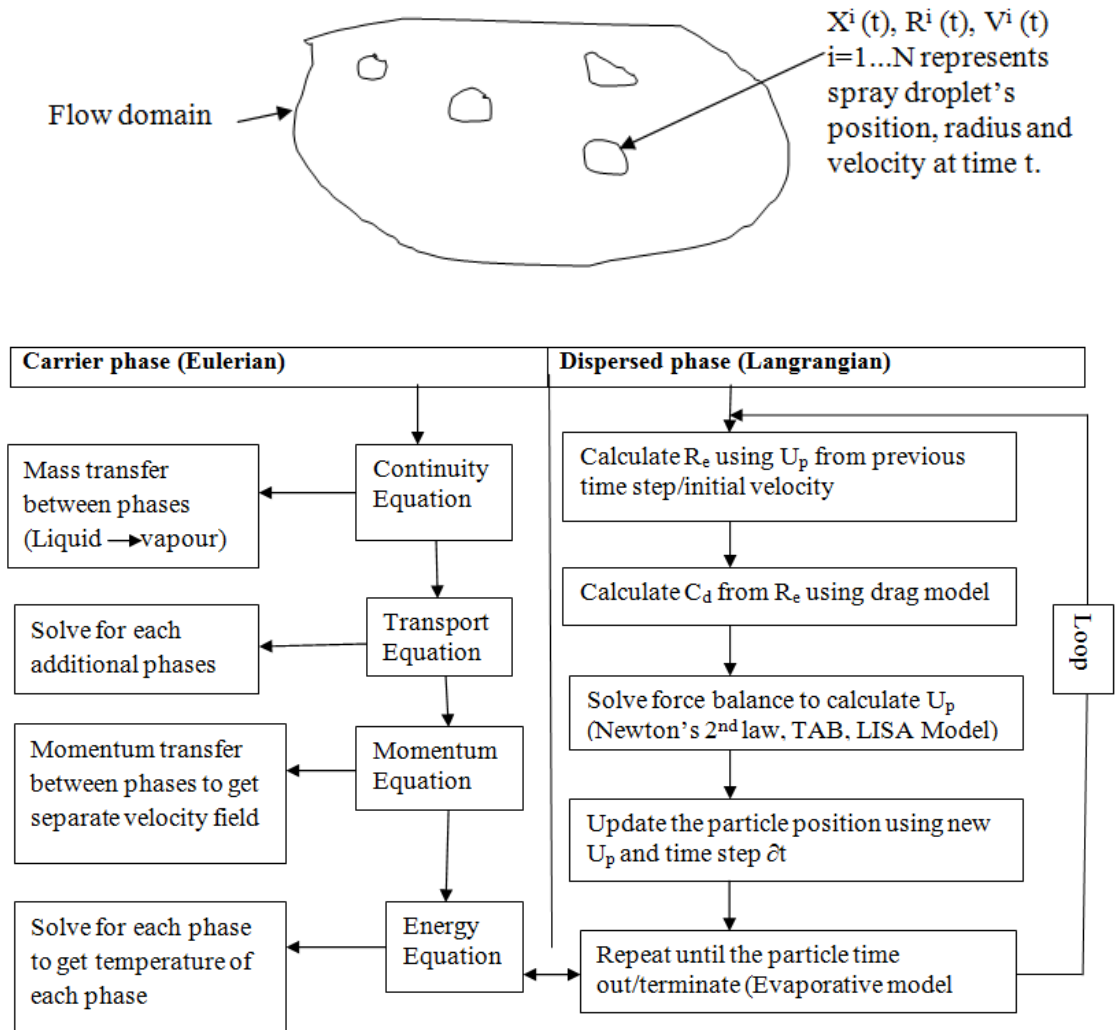


Figure 3.13. Flow chart depicting the spray characteristics

3.11.5. Cavitation Modelling

The cavitation generated at high injection pressure influence the spray characteristics. Homogeneous equilibrium model [HEM] has been implemented which showed better agreement with experimental results in terms of mass and momentum flux measurement as well as injection velocity as per previous studies (Payri et al., 2015).

$$\left(\frac{\partial \rho(t, p(\vec{x}, t))}{\partial P}\right)_t = \Psi \quad (3.36)$$

$$\Psi = \frac{1}{c^2} \quad (3.37)$$

The vapor amount in the fluid is evaluated through void fraction ξ as shown in equation 3.36, which may 0 or 1 for non-cavitation and fully cavitation flow respectively.

$$\xi = \max\left(\min\left(\frac{\rho - \rho_{l,sat}}{\rho_{v,sat} - \rho_{l,sat}}, 1\right), 0\right) \quad (3.38)$$

$$\Psi = \xi\psi_v + (1 - \xi)\psi_l \quad (3.39)$$

Where, Ψ_v , and Ψ_l are vapor and liquid compressibility respectively, and are calculated using linear model and that are more accurate and stabilized with respect to convergence (Chung T, J. 2002). The study assumes that speed of sound is constant, and if it is considered to be liquid and vapor then equation 3.38, 3.39 can be derived from equation 3.37 and found as in equations 3.40 and 3.41.

$$\rho_v = \psi_v p \quad (3.40)$$

$$\rho_l = \rho_l^0 + \psi_l p \quad (3.41)$$

Simulations concerning the combustion aspect, the chemical kinetic solver having SAGE details, were modelled through CHEMKIN-formatted input files. The couplings of gas phase calculations along with the SAGE with chemical kinetics solver have been utilized. To speed up the numerical solution, the SAGE detailed with chemical kinetics is solved by a multi-zone model such as a similar thermodynamics state of group cells. Now, the surrogates of WCO composition were five major biodiesel components such as methyl linoleate ($C_{19}H_{32}O_2$), methyl linoleate ($C_{19}H_{34}O_2$), methyl oleate ($C_{19}H_{36}O_2$), methyl

stearate ($C_{19}H_{38}O_2$) and methyl palmitate ($C_{17}H_{34}O_2$). Methyl decanoate ($C_{11}H_{22}O_2$), methyl-9-decenoate ($C_{11}H_{20}O_2$) with the single and double bond in hydrocarbon chain respectively and n-heptane for surrogates of WCO have been presented in the study (Han and Reitz, 1995) for biodiesel fuel in detailed reaction mechanism (3034, 8580 species and reactions). (Luo et al., 2012) did reduction to 115 species and 460 reactions of detailed mechanism that was given by the study (Herbinet et al., 2010). Further, OH^* (hydroxyl radical) was added to the biodiesel and diesel mechanism to capture the flame structure and ignition. The soot formation, of carbonaceous agglomerates from HC fuel molecules, is a very intricate process. This is the transition process of gaseous –solid phase where the solid phase did not contain physical and chemical structures. Subsequently, the transition is exhibited by different physical and chemical steps (Omidvarborna et al., 2015). Therefore, to produce more practical results along with less computational time and also most desirable for emission control and diesel engine design, soot simulation in computational volume was found from oxidation rates and formation of C_2H_2 species by the Hiroyasu model paired with Strickland and Nagle constable models (Hiroyasu and Kadota, 1976; Nagle J, 1962). A cubical geometry of cross-section $1.5 \times 1.5 m^2$ and length of 1.5m was used for combustion simulation as shown in Figure 3.12. The formulation and composition of waste cooking oil surrogates derived from five major components of biodiesel are presented in Table 3.4. Where major components of biodiesel are devised by the appropriate proportion of surrogate mixing and also to the number of molecules. Either saturated or unsaturated type hydrocarbon chain has been considered to get formulation.

Table 3.4. Breakdown of surrogates of WCO with devising from main components of biodiesel

Main components of biodiesel		Major mass fraction component of biodiesel	Estimated resulting mixtures based on the surrogates	Mass fraction of Tri-surrogate		
Name	Formula			nC7H16 (n-heptane)	C11H22O2 (methyl decanoate)	C11H20O2 (methyl 1-9-decenoate)
Methyl Palmitate	C ₁₇ H ₃₄ O ₂	0.085	0.8C ₇ H ₁₆ ₆ + C ₁₁ H ₂₂ O ₂	0.8*0.085 / 1.8	1 *0.085/ 1.8	
Methyl Oleate	C ₁₉ H ₃₆ O ₂	0.428	1.1C ₇ H ₁₆ ₆ + C ₁₁ H ₂₀ O ₂	1.1 *0.428 / 2.1		1 *0.428 / 2.
Methyl Stearate	C ₁₉ H ₃₈ O ₂	0.029	1.2C ₇ H ₁₆ ₆ + C ₁₁ H ₂₂ O ₂	1.2 *0.029 / 2.2	1 *0.029/ 2.2	
Methyl Linoleate	C ₁₉ H ₃₄ O ₂	0.103	C ₇ H ₁₆ ₆ + C ₁₁ H ₂₀ O ₂	1*0.103 / 12		1*0.103 / 3/2
Methyl Linoleate	C ₁₉ H ₃₄ O ₂	0.355	1.05C ₇ H ₁₆ ₆ + C ₁₁ H ₂₀ O ₂	1.05 *0.355 / 2.05		1*0.355 / 2.05

Each surrogate component mass fraction from the relation= Mole of surrogate in resulting mixture*mass fraction of major biodiesel component/Total mole of resulting surrogate mixture

3.12. MODEL DESCRIPTION OF SURFACE TENSION OF BIODIESELS

The atomization characteristics of fuel in diesel engine are majorly influenced by physical properties especially surface tension followed by viscosity. This property directly hits the combustion efficiency and emission like it could be enhanced by increasing the higher surface area to volume ratio of droplets and vice-versa. Different biodiesel consists of variations in rheological properties such as viscosity, surface tension, bulk modulus, density etc. Therefore, each biodiesel shows different spray and atomization characteristics. As per the literature review, the droplet's generation is easier for the biodiesel having low surface tension and that causes better atomization characteristics and air-fuel mixing. The surface tension of fuel is measured differently like theoretically as well as experimentally and they have their limitations of measurement at heated fuel. The current study chose three mathematical models according to the literature and compare their results with experimental results, also did modifications in the existing model to get a more accurate model to the standard result using MATLAB. The parachor-based method known as "Macleod – Sudgen", averaged carbon atoms and a double bond in FAME, and the surface tension of each FAME are the models used to estimate the surfaced tension of biodiesels a range of temperatures. The modelling and coding of these models are performed on MATLAB.

3.12.1. THE PARACHOR BASED MACLEOD-SUDGEN MODEL

The Macleod- Sudgen model, a parachor-based method is used to estimate the surface tension of biodiesel. The FAME composition in mass fraction along with their parachor value of biodiesel was used to predict the surface tension of different biodiesel as shown in Table 3.5. Where, the group of atoms consisting of composition and their linkage are

assigned by the parachor values. The individual FAME containing parachor value are shown in Table 3.6.

Table 3.5. Parachor values by Knotts and Allen of each FAMES

S.No	FAMES	Parachor value by Knotts	Parachor value by Allen
1	C8:0	NA	NA
2	C12:0	574	567
3	C10:0	495	489
4	C16:0	737	723
5	C14:0	657	645
6	C18:0	817	801
7	C18:2	795	779
8	C16:0	737	723
9	C18:1	806	879
10	C18:3	782	768
11	C22:1	967	946

Suden suggested the estimation of parachor values of FAME using equation 3.42.

$$\sigma = [P(\rho_l - \rho_v)]^4 \quad (3.42)$$

where, σ , ρ_l , ρ_v indicate surface tension, liquid density and vapor density respectively and calculated through experimentally. These values were considered to be inclusive as atomic structural, ring and bond structural component as given in Table 3.6. Thus, the parachor value of biodiesels were calculated by applying above data. However, the knowledge of parachor value is necessary for estimation of surface tension. Thus, the available mass fractions (X_i) of FAME in biodiesels is needed to measure the parachor value of biodiesel. This is evaluated through equation 3.43.

$$P_{bdf} = X(i) * P_{ch}(i) \quad (3.43)$$

Here, P_{bdf} , $X(i)$ and P_{ch} shows parachor of biodiesel, mass fraction and parachor respectively.

Table 3.6. Increment to parachor/structural contribution

S. No	Group	Group	Increment in parachor value $\{[(mN/m)^{0.25}] * mol/cm^3\}$	Increment in parachor value $\{[(mN/m)^{0.25}] * mol/cm^3\}$
1	C	1-methylbutyl	9.0	211.7
	H (in OH)	1,1-dimethylpropyl	10.0	207.5
2	H	1-ethylpropyl	15.5	209.5
	H (in HN)	1,2-dimethylpropyl	12.5	207.
3	CH ₂ > 12 carbons	Triple bond	40.3	40.6
	CH ₂ < 12 carbons	1,1,2-trimethylpropyl	40.0	243.5
4	1-methylpropyl	Four-member ring	171.9	6.0
5	1-methylethyl	Three-member ring	133.3	12.5
	1,1-dimethylethyl	Six-member ring	170.4	0.8
6	2-methylpropyl	Five-member ring	173.3	3.0
7	C ₆ H ₅	Seven-member ring	189.6	4.0

Further, molecular weight and density play an important role in measurement of surface tension (γ) as shown in equation 3.44.

$$\gamma = [(P_{bdf} * \rho) / M_w]^{0.25} \quad (3.44)$$

where, ρ , P_{bdf} , M_w are density, parachor of biodiesel fuel and molecular weight respectively

3.12.2. THE GIBBS FREE ENERGY MODEL

Literature suggested parachor based model showed larger deviation than Gibbs free energy model in prediction of surface tension of biodiesel. The Gibbs free energy model states that a compound having molecular structure $\text{CH}_3\text{-(CH}_2\text{)}_z\text{-X}$ can be alienated into three groups X, $(\text{CH}_2)_z$ and $-\text{CH}_3$. Then, the Gibbs free energy transfer to gas form from liquid form was total sum of all component's free energy.

$$\Delta G = \Delta G_f + \Delta G_1 + \Delta G_2 + \dots + \Delta G_z \quad (3.45)$$

The free energies of methylene and methyl group are represented as $\Delta G_1 \dots \Delta G_z$ as given in equation 3.45. They constitute a little variation in groups. Further, Equation 3.45 can be simplifying to equation 3.46.

$$\Delta G = \Delta G_f + z\delta G \quad (3.46)$$

Where, ΔG_f , δG and z are free energy with functional group X, change of free energy per unit carbon atom and number of carbon atom respectively.

The summation of Gibbs free energy can be employed for various physical properties such as viscosity, vapor pressure of FAME. Hence, a relationship among free energy of liquid component with interface interaction, surface tension, pressure and composition are set up as given in equation 3.47.

$$\gamma = (\partial G / \partial A), T, P, X(i) \quad (3.47)$$

where, A shows surface area, then the standard Gibbs free energy equation is written as in equation 3.48.

$$\Delta G = \Delta H - T\Delta S \quad (3.48)$$

Further, the combining the equations 3.47 and 3.48, the equation 3.49 follow as:

$$\gamma = (\Delta H_f / \Delta A) - (T\Delta S_f / \Delta A) + (z\delta H / \Delta A) - (z\delta TS / \Delta A) \quad (3.49)$$

this can be also written as:

$$\gamma = a + bz + cT + dzT \quad (3.50)$$

the surface tension of saturated FAME can be measured through equation 3.50. But, the surface tension of unsaturated FAME is estimated by adding another parameter in equation 3.50 and that term is $-db$, double bond. Here, m indicates total no of double bonds in unsaturated FAME. Further, by combining equations 3.51, 3.47 and 3.48, the equation 3.52 is written as follow:

$$\Delta G = \Delta G_f + z\partial G + m\Delta G_{db} \quad (3.51)$$

$$\gamma = a + bz + cT + dzT + em + fmT \quad (3.52)$$

The coefficients a, b, c, d, e and f was estimated through the study (Freitas et al., 2012) and found to be 0.01, 0.12, 0.14, 0.17 and 0.19 respectively for the present study.

Finally, the equation 13 can be used to measure surface tension of biodiesel.

There are two modifications needed: firstly, consider the biodiesel constitute a single FAME and secondly the average no of double bond available in FAME.

Thus, the calculation of double bonds and average no of carbon atoms in biodiesel could be found from equations 3.53 and 3.54 as follow:

$$Z_{avg} = \sum X(i) * z(i) \quad (3.53)$$

$$M_{avg} = \sum X(i) * m(i) \quad (3.54)$$

Therefore, the modified equation by considering above condition is given in equation 3.55:

$$\gamma = 60.211 - 0.4307 * Z_{avg} - 0.1125 * T + 0.00207 * Z_{avg} * T + 3.676 * M_{avg} - 0.00893 * M_{avg} * T \quad (3.55)$$

3.12.3. THE DALTON TYPE MASS AVERAGE MODEL

Dalton type mass average model is used to measure surface tension of biodiesel with their components and can be through equation 3.56.

$$\gamma = \sum X(i) \cdot \gamma(i) \quad (3.56)$$

where, $\gamma(i)$ and $X(i)$ represent the surface tension and mass fraction of each component.

Further, to measure the surface tension, the parachor based MacLeod -Sugden equation is applied as given in equation 3.57.

$$\gamma = \left(\frac{P\rho}{M} \right)^4 \quad (3.57)$$

Further, the parachor based MacLeod-Sugden equation are used to estimate surface tension value is shown in equation 3.58.

$$\rho = 1.069 + \frac{3.575}{M} + 0.0113N_d - 7.41 \times 10^{-4}T \quad (3.58)$$

Here, P, ρ and M show the parachor parameter, density and molecular weight respectively.

Moreover, Ramirez-Verduzco suggested an empirical correlation to obtain density of liquid as temperature, double bonds in fatty acid chain and molecular weight.

Finally, the conclusive equation 3.59 obtained by combining the equations are as follow:

$$\gamma = \sum_{i=1}^n X_i [P_i]^4 \left(\frac{1.069 + 0.113N_i - 7.41 \times 10^{-4}T}{M_i} + \frac{3.575}{M_i^2} \right)^4 \quad (3.59)$$

However, the literature suggested that this model generally over-predicts the desired value of surface tension. This could be corrected through addition in individual FAME to weight factor. However, modification in existing equation made more complexity to method, but is better than parachor based model.

RESULTS AND DISCUSSION

Overview

This chapter discussed the comprehensive investigation of the findings of the present research. The compositions of fatty acids available in waste cooking oil biodiesel, rheological properties of biodiesel, and estimation of spray characteristics through computation were elaborated meticulously. The argument is elaborated based on the findings from computational work and also comparing them with experimental results, and earlier findings from literature review. Furthermore, the identification of the model's strength has been explored through the validation of spray and combustion characteristics. Finally, spray and combustion characteristics are analyzed from a swirl injector using waste cooking oil biodiesel, biodiesel-diesel, diesel fuel.

4.1. Physico-chemical properties

This section exhibits the testing of waste cooking oil and its blend as well as blends of diethyl ether along with diesel fuel. the methods are described in the previous section.

The testing of fuels is performed using 1 litre waste cooking oil biodiesel from respective equipment as per ASTM standards.

4.1.1. Density

This is one of the important properties which imparts key information for usability in diesel engine. Even, heating value and cetane number are also related to the density of the fuel. thus, the power output of the engine is directly influenced by the density of the fuel (Lam et al., 2016). According to the EN 590 and ASTM D1298 standards for diesel fuel,

the density should vary from 820- 845 kg/m³ and 820-860 kg/m³ respectively. The density of fuel is measured through Anton par density meter. The density of test fuels such as WCO biodiesel and its blend, blend of diethyl carbonate and diesel are shown in Figure 4.1. this is observed that DEC 20 showed the highest density while diesel lowest. The density of DEC20, B100, B25 and D were 0.903, 0.876. 0.84 and 0.83 respectively. Further, it was seen that as the blending of diesel fuel increased, the density decreases still higher than diesel fuel.

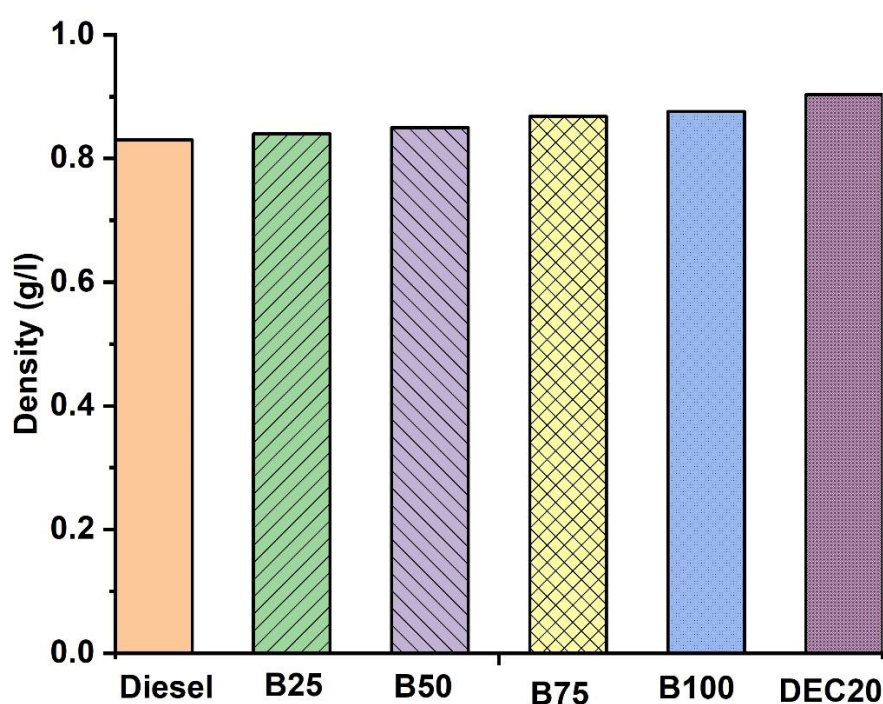


Figure 4.1. Density Vs test fuel samples

4.1.2. Kinematic viscosity

Kinematic viscosity is the key parameter in spray atomization and fuel injection systems and that affects combustion, performance and emissions directly or indirectly. However, this property is influenced by temperature variation. Moreover, carbon deposits and soot formation in diesel engines also increase because of poor atomization of spray jet. As per the EN 590 and ASTM D445 standards to use as diesel fuel in CI engine, the range of kinematic viscosity should be 2 – 4.5cSt. the kinematic viscosity of test fuel samples is

shown in Figure 4.2. The kinematic viscosity of DEC20, B100, B25 and D are respectively 2.71, 4.65, 3.04 and 2.60 mm²/s. The data show that the blending of diesel can decrease the kinematic viscosity due to oxygen content. The study (Manchanda et al., 2018) showed that kinematic viscosity is also influenced by the presence of oxygen, i.e increase of oxygen in fuel causes higher viscosity.

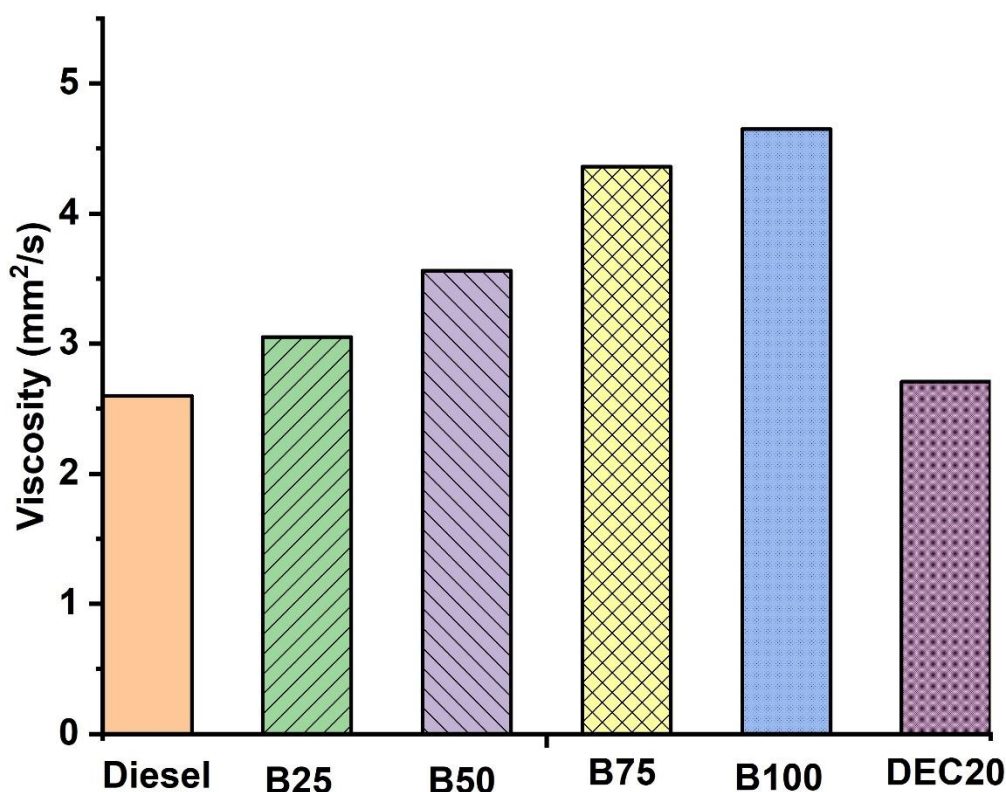


Figure 4.2. Kinematic viscosity Vs test fuel samples

4.1.3. Distillation Data

The fuel sample's distillation was done through the equipment and procedure described in section 3.4.7. The distillation temperature was measured at 10%, 50% and 90% of test fuel was recovered. The temperature recorded at the time of 10% fraction of fuel is recovered directs the comfort at which vaporization occurs and shows higher volatility. Moreover, the temperature at which 90% fuel is recovered shows the difficulty of vaporization due to the heavier molecular weight of the compound and that results in

engine deposits and particular emissions (Lapuerta et al.,2011). The experimental results show that B25 exhibited lower distillation temperature as compared to B100 while higher than D. B25 recovered 10% of fuel fraction faster than B100 as shown in Table 4.1. Further, the highest temperature recovered is lower than ASTM D6751 limit.

Table 4.1. Properties of test fuel.

Properties /Fuel	Diesel (D)	B100	DEC 20	B25	B50	B75
Viscosity (mm ² /s)	2.60(at 40 ⁰ c)	4.65(at 40 ⁰ c)	2.71(at 25 ⁰ c)	3.04(at 40 ⁰ c)	3.56	4.36
Density (g/l)	0.83(at 40 ⁰ c)	0.876(at 40 ⁰ c)	0.903(at 20 ⁰ c)	0.84(at 40 ⁰ c)	0.85	0.868
Distillation temperature (°C)	320	360		345	351	357
Surface Tension (mN/m)	30.3	34.7	26.2	27.7	30.7	32.3

4.2. Model Validation

The computational study of spray is based on the model which supports the standard experimental results or previous results. Thus, to validate the computational model applied in the simulation, an experimental study on STP and SCA was performed. The spray tip penetration was measured as per the description in the previous section while the spray cone angle was evaluated from an empirical study of (Reitz R D,1978) as presented in equation 4.1.

$$\tan\left(\frac{\theta}{2}\right) = A\left(\frac{\rho_l}{\rho_g}\right)^{0.5} \quad (4.1)$$

The test fuel taken for both experimentation as well as computation is blend of di-ethyl carbonate in diesel (DEC20). The working condition and main properties of test fuel is given in Table 4.1. Here, the injection duration for both investigations is 1.5 ms. The quantitative comparison of the experimental study to the computational study at injection pressure 100MPa and ambient pressure 2.4MPa have performed using the previously described model. The tip penetration of the computational study showed consistent with the experimental study and exhibited an error within 5% of standard results. While the cone angle initially rises and after 0.3ms the angle becomes constant trends. Similar trends of the cone were also seen from computational study and come under 3% of error.

Further, to robust the modelling of spray, characteristics the validation of the computational model was performed from the study (Zhang et al., 2017). It was seen that the cone angle initially increased and after a lapse of time it became constant and which shows better agreement with the theoretical study.

4.3. Grid Independence Test

The computation results in change as per the types of grids and mesh size in the computational volume. The grid size variation was performed on spray tip penetration such as coarse to fine mesh. Initially, the coarse mesh size 1 million was employed which showed a larger deviation from the experimental result, further, the mesh sizes vary such as 1.5, 1.75, 1.95, 2.32, 2.56 million and found that there was a little deviation observed from 1.95 million to 2.56 million. Therefore, the grid size of 1.95 million has been taken in this study for better accuracy of simulation as shown in Figure 4.3. Further, the deviation from experimental results possesses more in-cell reduction. The normalized residual level of 10^{-6} was used to converge the solution because an increase in level makes it difficult in converging. Thus, the present study accepts the level of grid refinement and grid independence and the simulation results have been performed.

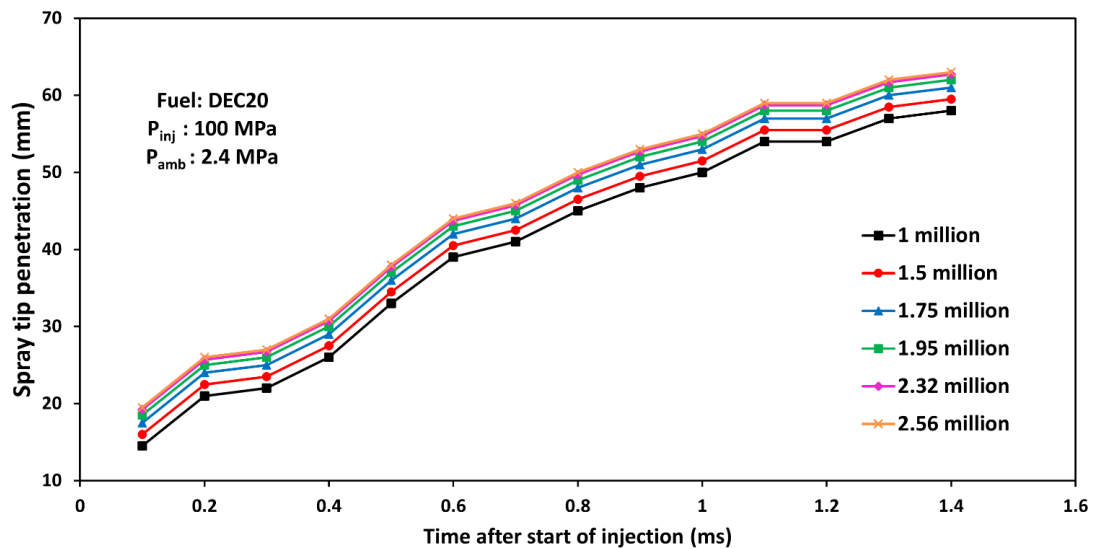


Figure 4.3. Grid Independence test summary

4.4. Results and Discussion

4.4.1. Spray Tip Penetration and Cone angle

The spray tip penetration of fuels B100, B75, B50, B25, and D are computed at 1100 bar and 1600 bar of injection pressure as shown in Figures 4.4, and 4.5 respectively. It is seen that as the injection pressure increases the penetration length of all test fuels increases in injection duration. However, B100 showed the highest tip penetration followed by B25 and D at 1100 bar of injection pressure. A similar trend of tip penetration was also observed at 1600 bar as shown in Figure 4.5. This phenomenon occurred due to higher density and viscosity, which imparted higher momentum and that leads to an increase in primary breakup length. The trend of longer tip penetration at high injection pressure is also supported by previous studies (Kuti et al., 2020; Gautam and Kumar, 2020). Moreover, the increment rate of tip penetration became lower at 1600 bar as compared to 1100 bar due to the influence of ambient pressure, which generated higher air resistance to spray formation. Thus, the tip penetration is also reduced at higher ambient pressure

(Bhikuning et al., 2020). This was also seen that B25 showed nearly the same or longer tip penetration than diesel fuel. This might be caused by the viscosity of the fuel which creates frictional resistance between the injector and fuel. The spray cone angle of test fuels is shown in Figures 4.6 and 4.7. The cone angles of all fuels are computed at 1100 bar and 1600 bar having ambient pressure of 2.8 MPa at an injection duration of 1.5 ms. Since, the droplets present on the boundary converts to smaller one and also, they diffuse easily. Due to this, the spray cone angle showed a decreasing trend. Further, this was also observed that a drastic reduction after a shorter duration of time and further became constant for all the fuels at all injection pressure.

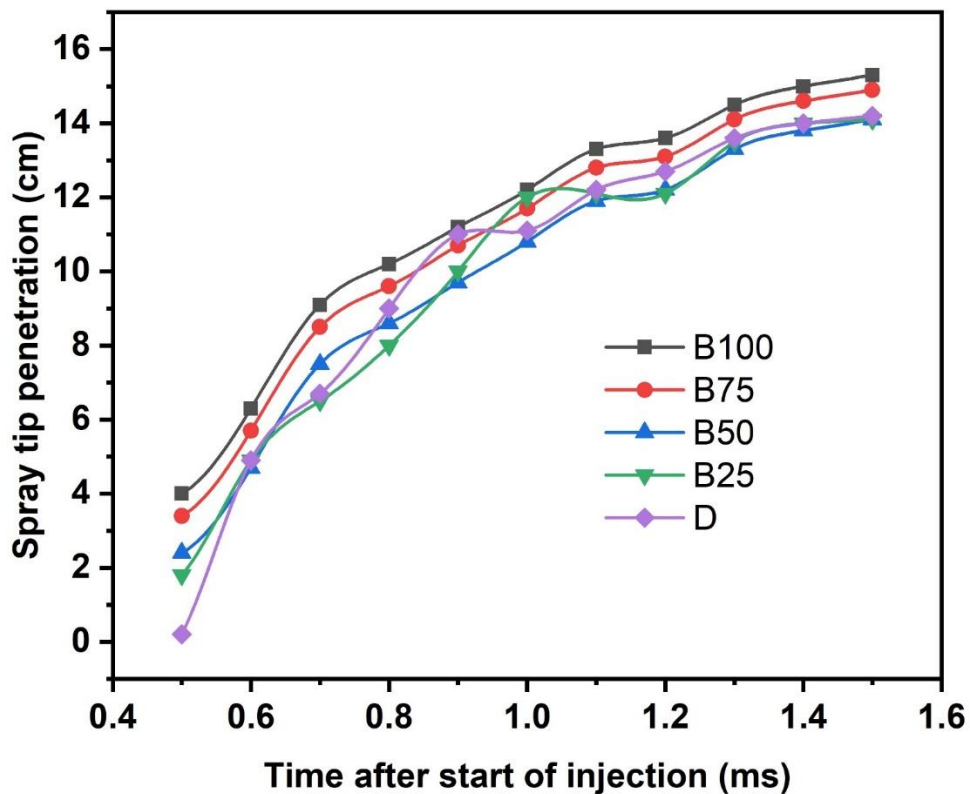


Figure 4.4 STP vs STOI at 110 MPa

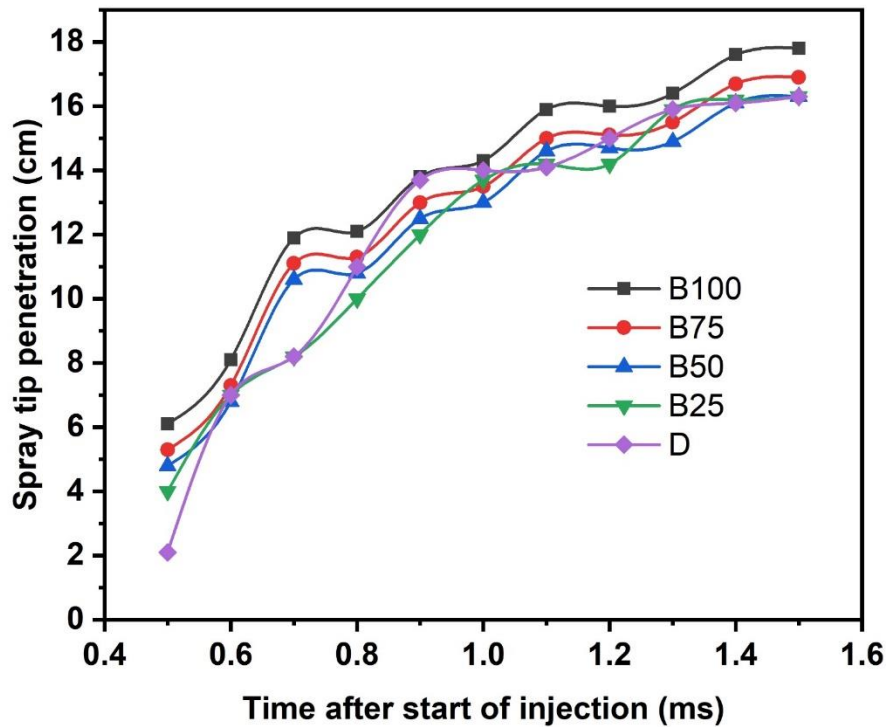


Figure 4.5 STP vs ASOI at 160 MPa

Biodiesel consists lower cone angle at the initiation of injection. The aerodynamics of WCO's is not stronger and this is because of high viscosity followed by density. This makes it very difficult for air to enter into spray volume. The above statement is also justified through equation 4.1, which states that an increase in the kinematic viscosity of gas is due to a rise in the density of the gas. Thus, the reason behind the narrow spray cone angle could be the higher viscosity of gas in the constant volume cylinder (Li et al., 2017; Hawi et al., 2019). Therefore, the B25 contained a smaller cone angle than diesel fuel due to the higher viscosity of the fuel.

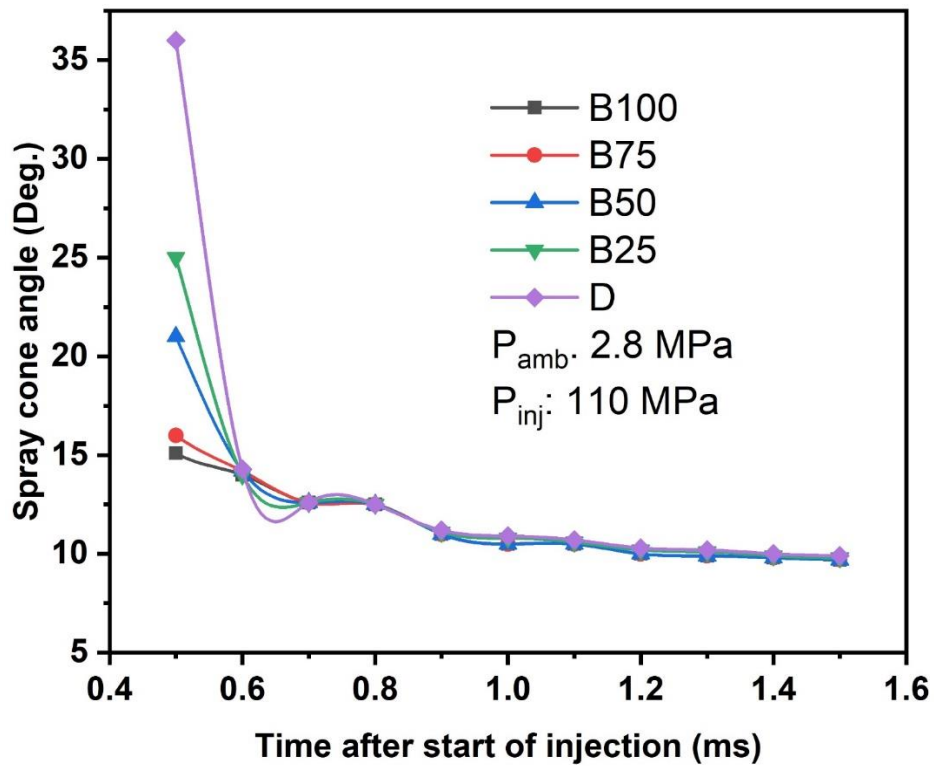


Figure 4.6 SCA vs ASOI at 110 MPa

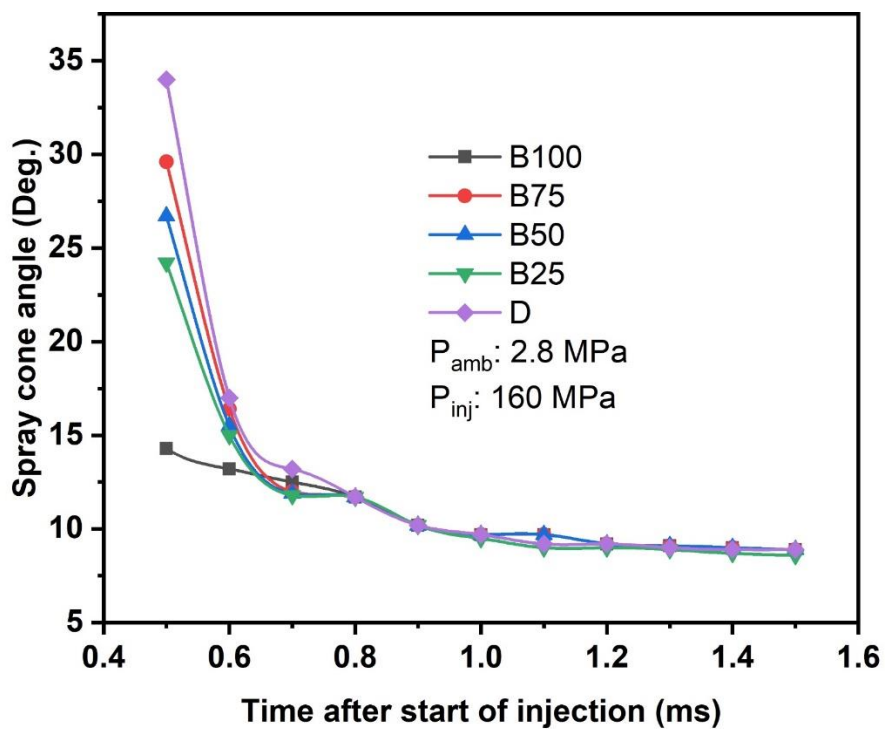


Figure 4.7. SCA vs ASOI at 160 MPa

4.4.2. Sauter Mean Diameter

The sauter mean diameter of diesel, B25, B50, B75 and B100 fuel at injection pressures of 1100bar, 1600 bar is shown in Figure 4.8. Where, the injection duration is considered as 1.5ms. firstly, it was seen that SMD showed a decreasing trend from 1100 bar to 1600bar. Secondly, B100 showed the highest SMD followed by B75, B50, B25, D at all injection pressure, the earlier one is due to faster secondary disintegration with increase in injection pressure and the later is cause of higher rheological properties of B100, where, surface tension is higher than drag force and that resist the further breakup in to smaller droplets from larger droplets. However, B25 showed the near rheological property to diesel, because blending of diesel made reduction in viscosity and surface tension. Still, B25 showed larger SMD than diesel fuel. This study is also supported by (Agarwal et al., 2013).

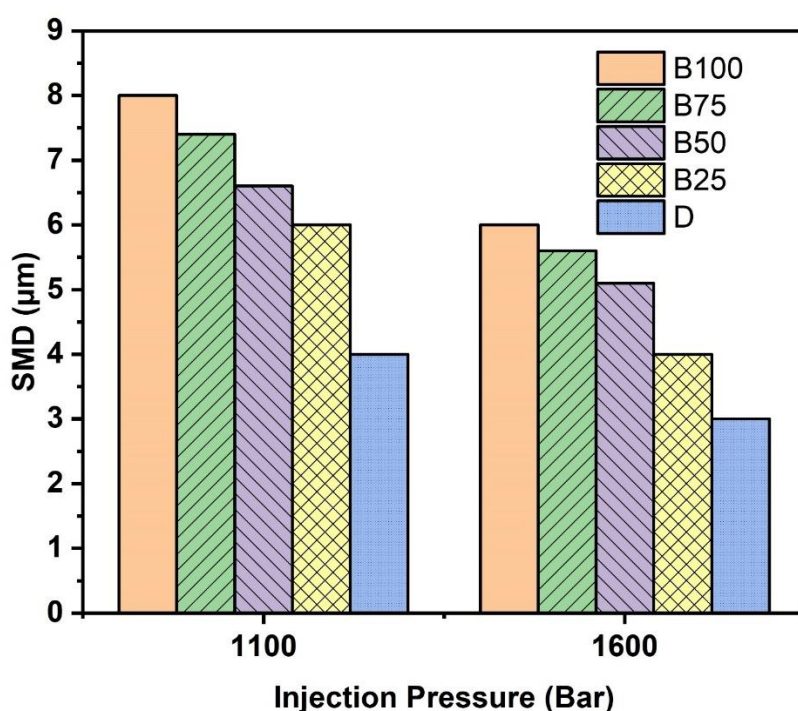


Figure 4.8. SMD vs Injection Pressure at 110 MPa, 160 MPa
for test fuels

4.4.3. Parachor Based model

The prediction of surface tension from parachor-based model needs three properties namely: molecular weight, density and parachor value of biodiesel. The comparison of density, molecular weight and parachor value (as per Allen and Knott) has been performed on six biodiesels as mentioned in Table 4.2. These parameters imparted the effect on the surface tension of mentioned six biodiesels. Here, Allen and Knott values of parachor different FAMES were evaluated and found that both showed different characteristics. Figure 4.9 depicts that the biodiesels exhibited nearly similar values of surface tension and that reveals a very close value evaluated through parachor-based model. However, the Knott value is lower than Allen for every mass fraction of fatty acid methyl esters. This happened as a result of the corresponding FAMES molecular weight at the time of generation. The variation in mass fraction of FAME causes, rapeseed and jatropha represented the largest variation in Allen and Knott values.

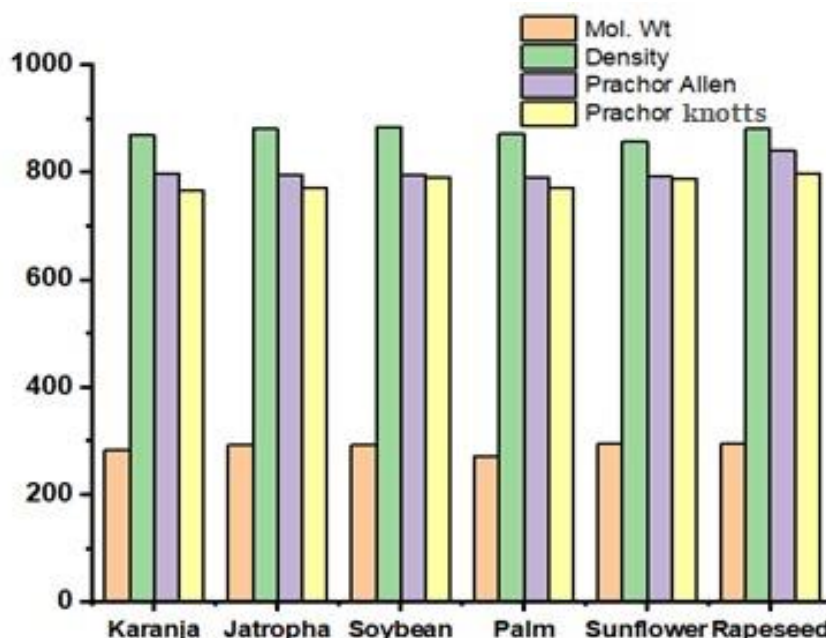


Figure 4.9: Mol.wt, density, Prachor (Allen and knotts)

vs test fuels

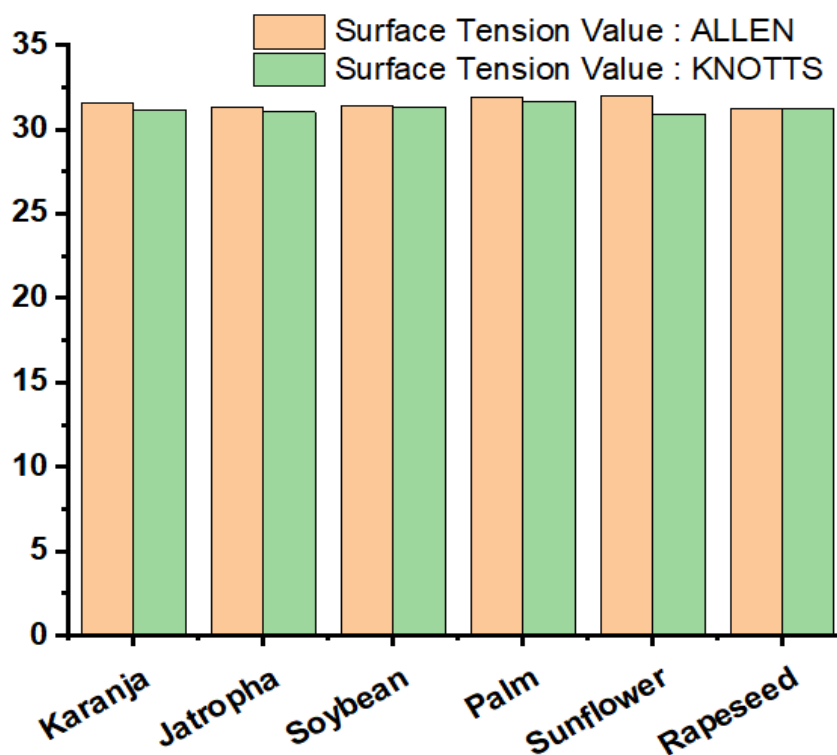


Figure 4.10: Surface tension (Allen and Knotts) vs test fuels

The surface tension of biodiesel varies with molecular weight and density as per equation 3.44. Further, it was found that rapeseed consisted the lowest surface tension through Allen and sunflower exhibited the highest surface tension by Allen. The measured value of surface tension using parachor-based model is shown in Figure 4.10. Further, to validate the parachor based model (as per Knott's and Allen's parachors), the Allen and Knott process was validated through experimentation as shown in Figure 4.11. It was found that the Allen method is more distant from the measured value than the Knott value, this is because of less sampling characteristics of the Allen method. Furthermore, the error analysis along with the percentage error of experimental value and predicted value was estimated as shown in Table 4.2.

Table 4.2. Error study for the parachor based model (Knotts parachors') and Allen parachors' with calculated surface tension

Biodiesel	Measured surface Tension (mN/m)	Knotts parachors' base model(mN/m)	Allen parachors' base model(mN/m)	% Error (Knotts Parachors)	% Error (Allen Parachors)
Karanja	28.62	31.18	31.60	8.9	10.41
Soybean	28.20	31.33	31.38	11.09	11.27
Jatropha	30.10	31.04	31.36	3.12	4.18
Sunflower	28.37	30.92	31.99	8.98	9.23
Palm	28.50	31.66	31.91	11.08	12.01
Rapeseed	29.39	31.22	31.27	6.22	6.39

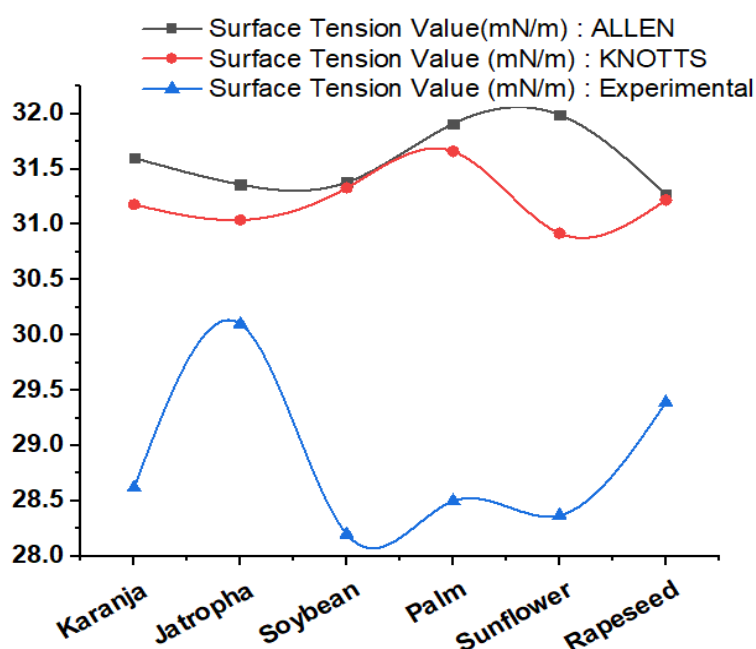


Figure 4.11. Experimental vs measured by Allen's and Knotts's

parachor

4.4.4. Prediction of surface tension using Gibbs free energy model

The estimation of surface tension through the Gibbs model needs especially information on double bonds along with the average no of carbon atoms in the biodiesel. Further, the composition of mass fraction as well as the working temperature range is required for the prediction of surface tension. The number of double bonds and averaged carbon atoms are presented in Table 4.3. The model can explore every biodiesel which exists as a single fatty acid methyl ester.

Here, the estimated value average no of carbon atoms, and average no of double bonds is considered as the value of carbon atoms and double bonds of fatty acid methyl ester in biodiesel. Thus, the complexity associated with FAMEs composition is resolved with this method and seems to be a more accurate model towards calculation. Moreover, the measurement of surface tension at 400C has been done for all biodiesels and also calculated with other ranges of temperatures. The comparative analysis was performed for experimental measurement and theoretical expression and found that in a wide range of temperatures, the theoretical values are close to the standard value evaluated from experimentation. The comparative measurement of surface tensions of jatropha, Karanja, sunflower, palm, rapeseed and soyabean oil is shown in Figure 4.12 and Figure 4.13.

Heating of biodiesel causes a reduction in surface tension and the decrement is not linear since the presence of fatty acids in biodiesels. It was observed that soyabean oil exhibited a faster decrement in surface tension among all biodiesels. Furthermore, the error related to Gibbs free model is lower than the parachor based model as given in Table 4.4 and the above observation is also made by the study (Cao et al., 2021).

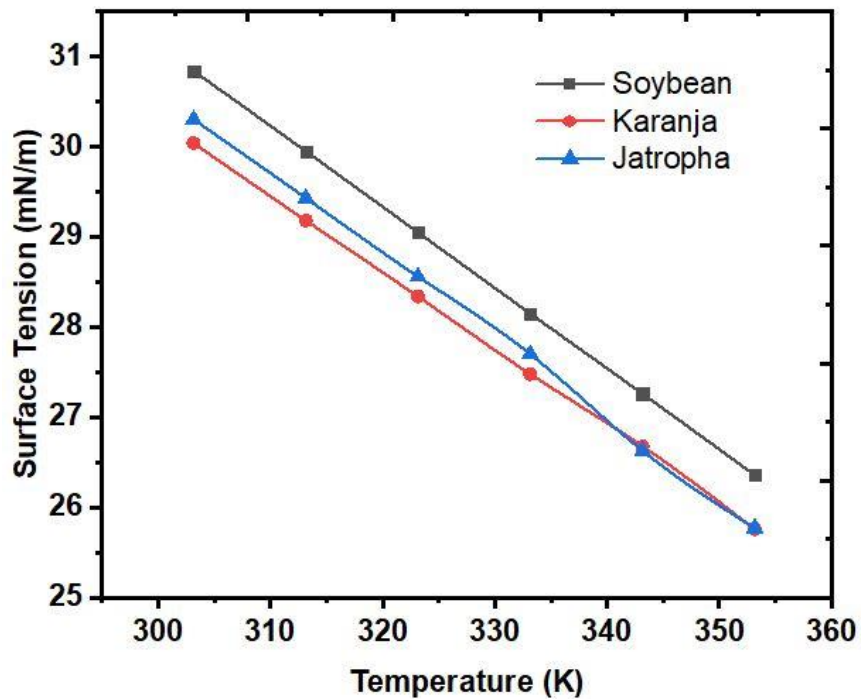


Figure 4.12. Surface tension (Jatropha, karanja, and soybean) vs temperature

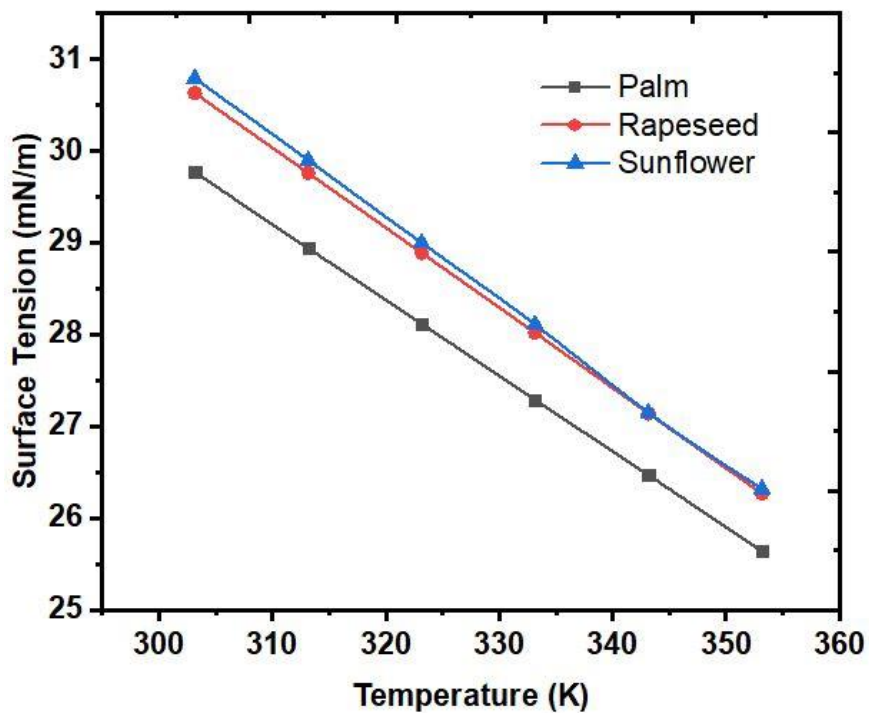


Figure 4.13 Surface tension (rapeseed, sunflower, palm) vs temperature

Table 4.3. Average number of double bonds, carbon atoms and surface tension using Gibbs model at 40°C

Biodiesel	Avg no of double bonds	Avg number of C atoms	γ_{calc}(mN/m)
Karanja	0.87	16.95	29.44
Soybean	1.56	17.80	30.22
Jatropha	1.1	17.20	29.69
Palm	0.59	17.12	29.19
Rapeseed	1.3	17.89	30.02
Sunflower	1.52	17.68	30.17

Table 4.4. Error estimation using Gibbs energy model (at 313K)

Biodiesel	$\gamma_{predicted}$ (mN/m)	Measured surface Tension (mN/m)	% Error	Error = $\gamma_{predicted} - \gamma_{experiment}$
Karanja	29.44	28.62	2.8	0.82
Soybean	30.22	28.20	7.1	2.02
Jatropha	29.69	30.10	1.3	-0.41
Palm	29.19	28.50	2.4	0.69
Rapeseed	30.02	29.39	1.8	0.63
Sunflower	30.17	28.37	6.3	1.8

4.4.5. Dalton type mass average model

The prediction of surface tension through Dalton type mass average model needs the parameters and are FAMES composition and surface tensions of FAMES individually. Further, the measurement of surface tension of all biodiesel was estimated separately and compared with the experimental investigation, there were larger deviations in surface

tension of biodiesels among all three previously discussed models. This, it is least suited for measurement of surface tension at wide range of temperature. The surface tension evaluated through Dalton type mass average model is shown in Figure 4.14 and the error analysis is presented in Table 4.5.

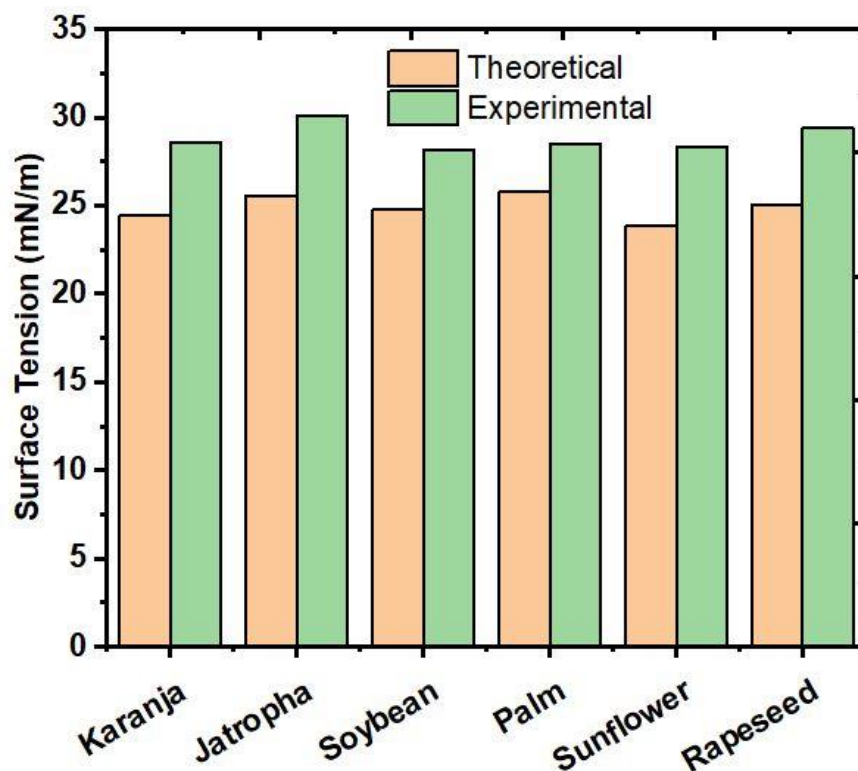


Figure 4.14. Surface tension through Dalton model

Table 4.5. Error estimation (Dalton type mass average model) at 313K

Biodiesel	$\gamma_{predicted}$ (mN/m)	Measured surface Tension (mN/m)	% Error	Error = $\gamma_{predicted}$ - $\gamma_{experiment}$
Karanja	24.48	28.62	14.46	-4.14
Soybean	24.77	28.20	12.16	-3.43
Jatropha	25.58	30.10	15.01	-4.52
Palm	25.79	28.50	9.52	-2.71
Rapeseed	25.05	29.39	14.76	-4.53
Sunflower	23.84	28.37	15.61	-4.34

4.5. Grid convergence study

The grid convergence study has been done for evaporative spray characteristics with the conventional nozzle to select minimum cell size. To get this, the chemistry solver was turned off. The mesh resolutions were obtained by equation 4.2. Furthermore, to select the cell size for better convergence, a comparative study has been incorporated between experimental and predicted spray length of waste cooking oil at injection pressure, ambient pressure and ambient temperature of 100 MPa, 2.4 MPa, and 600K respectively. The details of the simulation is given in Table 4.6.

Table 4.6. Simulation parameter

Break-up model	LISA-TAB
Droplet collision	No time Counter algorithm (NTC)
Droplet evaporation	Sherwood number, Schmidt number
Kinetic Modelling	SAGE chemical Kinetic solver
Mechanism	
Fuel	Surrogates
Waste Cooked oil Biodiesel	$C_{11}H_{22}O_2$ (6.04%), $C_{11}H_{20}O_2$ (42.9%), nC_7H_{16} (51.1%)
Soot formation model	Hiroyasu-NSC
Simulation period for spray	0-1.5ms
Simulation period for combustion	Upto 2.2 ms
Time step	$1*10^{-6}$ (highest), $1*10^{-11}$ (lowest)
Ambient condition	
Pressure (MPa)	4.0
Density (kg/m^3)	15
Temperature (K)	800
Injection conditions	
Nozzle Diameter (mm)	
Conventional nozzle	0.18 mm
(CN)	
Swirl Nozzle (SN)	0.18 mm, No of slots: 3 (120^0 apart), Inclination angle for each groove: 45^0 [16]
Fuel Injection Pressure (MPa)	300,200,100
Duration	1.5 ms

The spray images were recorded in high-speed camera during experiment and these images was processed through MATLAB to get spray pattern.

$$dx = dx_{base} * 2^{-(embedscale)} \quad (4.2)$$

Table 4.7. Embed scale with 1 reduced cell size from equation 4.2, where $dx_{base} = 2$ mm

Embedded Scale	Reduced Cell Size (mm)
4	0.125
3	0.25
2	0.5
1	1

Experimental work showed that spray length improved until a quasi-steady state was achieved. Nearly the same occurrence was obtained in predictive spray length at every mesh size. Now, it was seen from Table 4.7 and Figure 4.15 that spray tip penetration at a cell size of 0.5 and 1mm is over-predicted after injection timing of 0.74 ms as compared to 0.125 and 0.25mm minimum cell size. A very little difference was observed for both minimum cell sizes of 0.25 as well as 0.125 mm after the start of the timing of 0.70 ms for predicted tip penetration convergence. By considering the primary and secondary atomization period at the end of injection, spray tip penetration consisted of better accuracy to grid convergence at a mesh resolution of 0.25 mm. Based on these findings, 0.25 mm of minimum cell size and thrice embedded scale was recognized as suitable for the activity, and also able to resolve the flow field especially at the injector as shown in Figure 4.15. Further, to identify the robustness of the model again a comparative study of (Wang et. al.,2010) [Figure 9] with predicted liquid length has been done to select a minimum cell using swirl nozzle and again found that minimum cell size of 0.25 mm with the embedded scale of 3 was observed suitable for simulation process as shown in Figure 4.16.

4.6. Validation

Spray characteristics of fuel have a significant effect on air-fuel mixing and that create differences in combustion, performance and emissions in diesel engine. To ensure the robustness of the numerical model, evaporative spray tip penetration was compared against the data presented by (Bhikuning et al.,2020). The Quantitative comparison of simulated and experimental results was done at fixed injection pressure, ambient pressure, and temperature of 250MPa, 2.13 MPa, and 600K respectively using WCO. It was observed that initially liquid spray length was generated which was further changed into an evaporative state. These phenomena occurred due to better disintegration of droplets in secondary atomization, where droplets move in hot quiescent air, surface evaporation and better air entrainment in spray volume that enhancement leads to form shorter liquid penetration and longer vapour penetration. Initially, the tip penetration increased rapidly, however after 0.8 ms ASOI, the increment was reduced due to loss of momentum as shown in Figure 4.17.

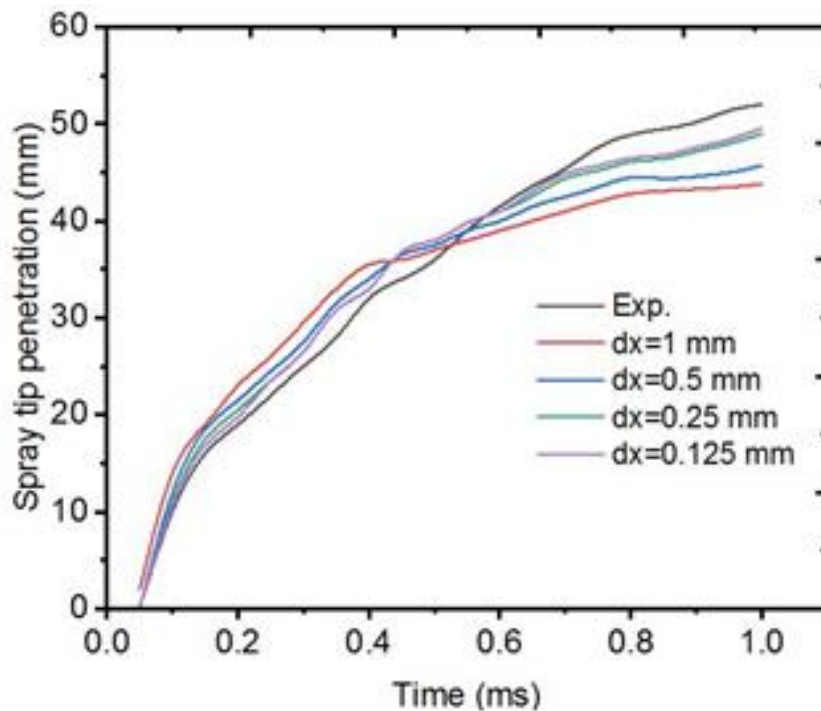


Figure 4.15. Grid independence test with the comparison of experimental and predictive spray characteristics

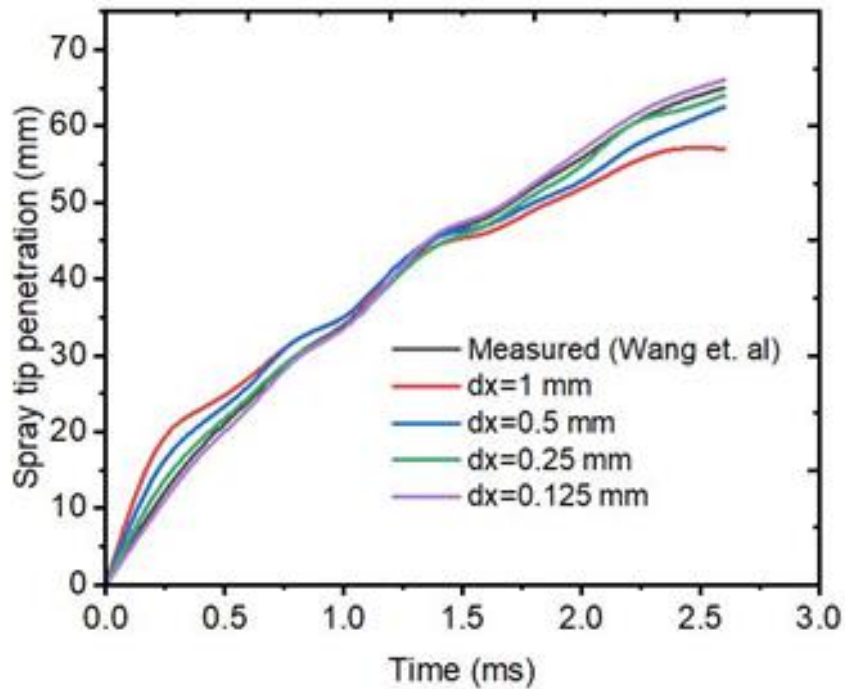


Figure 4.16. Computer model validation with study of (Wang et al.,2010)

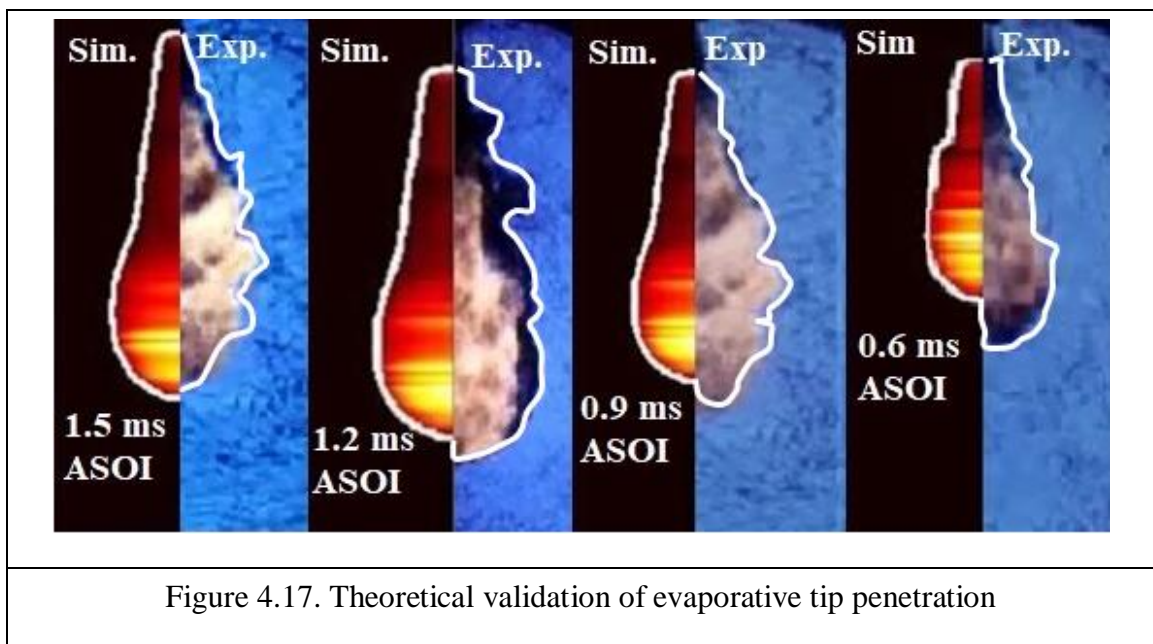


Figure 4.17. Theoretical validation of evaporative tip penetration

The comparative assessment of simulated study of spray tip penetration showed a better agreement with (Bhikuning et al.,2020) at mesh resolution of 2 mm and error was found to be less than 5%

4.7. Evaporative spray characteristics

Spray tip penetrations for the conventional nozzle at all injection pressures (100 MPa, 200 MPa, 300 MPa) are higher than the swirl nozzle. The difference in tip penetrations became an increasing trend at higher injection pressures (<200MPa). The spray momentum gets reduced in swirl nozzle more than conventional nozzle and the loss of momentum of the spray is due to an additional peripheral rotation of spray along the spray axis, which provides additional surface energy and that enhances early secondary atomization (Lin et al.,2010). Another, aspect which is responsible to reduce spray momentum in swirl nozzle is the additional friction force acting by the curved slots in the nozzle and there is a more viscous dissipation rate. However, as shown in Figure 4.18, the swirling impact is less at low injection pressure. Therefore, it shows nearly similar trends.

Further, the spray cone angle was also calculated through equation 4.1. It can be noted that the spray cone angle decreased with an increase in injection pressure from 100 to 300 MPa at constant ambient pressure as shown in Figure 4.19. This is due to high rheological properties and among these especially viscosity and higher momentum (Hoang A T, 2018). It was also observed that the cone angle is less sensitive towards injection pressure. While in the case of swirl nozzle, the spray angle is primarily influenced by swirl chamber, nozzle orifice diameter and length, ambient pressure and temperature, and surface tension of the liquid. Faster disintegration of fuel jets in swirl nozzle due to energy dissipation makes the sensitivity towards injection pressure (Zhang et al.,2017).

4.8. Air Entrainment

The quality of air-fuel mixing depends on air entrainment

within the spray and this is mainly influenced by cone angle, tip penetration, stoichiometric air-fuel ratio and ambient condition. Air entrainment analysis provides sufficient information for balancing nozzle diameter, injection pressure and timing, the geometry of the nozzle and so on. This is also an important parameter to govern soot formation. Hence, this should be analysed well for conventional and swirl nozzles. The mass of air entrained for both type of nozzles are shown in Figure 4.20 and it is calculated by the model proposed by (Rakopoulos et al., 2004) as shown in equation 4.3.

$$m_a(t) = \left(\frac{\pi}{3}\right) \left(\tan\left(\frac{\theta}{2}\right)\right)^2 S(t)^3 \rho_a \quad (4.3)$$

Where, $m_a(t)$ represents the air entrained mass within the spray at time t in kg, $S(t)$ shows the tip penetration at time t in m, θ is spray cone angle in radians and ρ_a shows the ambient density of air in kg/m^3 .

The increasing trend of averaged cone angle with injection pressure in swirl nozzle, while decreasing trend of averaged cone angle with injection pressure in conventional nozzle makes a significant difference in mass air entrainment as shown in figure 4.20. Another cause is due to liquid films breaking into liquid ligaments due to centrifugal and shear force, and secondary atomization which is the breaking of liquid ligaments into droplets (Fan et al., 2020). Further centrifugal force and shear force increase with an increase in injection pressure while rheological properties decrease with an increase in same. Hence the swirl nozzle can generate more air entrainment than the conventional nozzle.

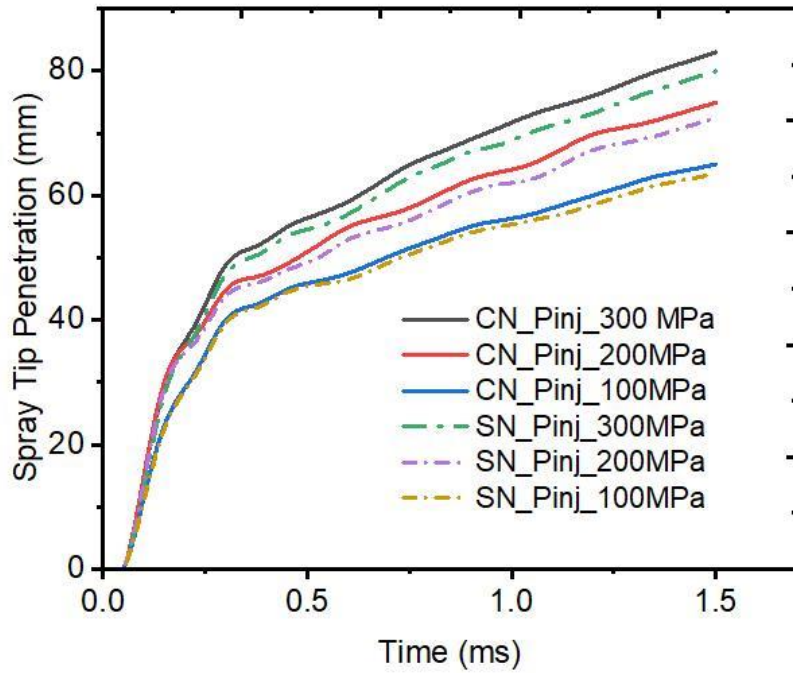


Figure 4.18. Evaporative STP vs ASOI at 100, 200, 300MPa with CN and SN heometry.

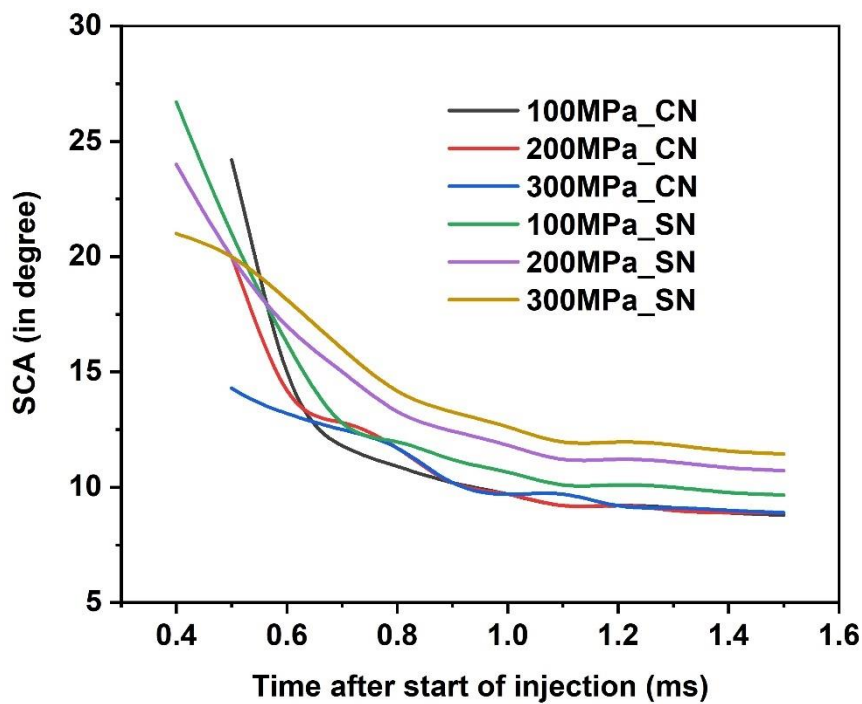


Figure 4.19. SCA vs ASOI for CN and SN at different injection pressures.

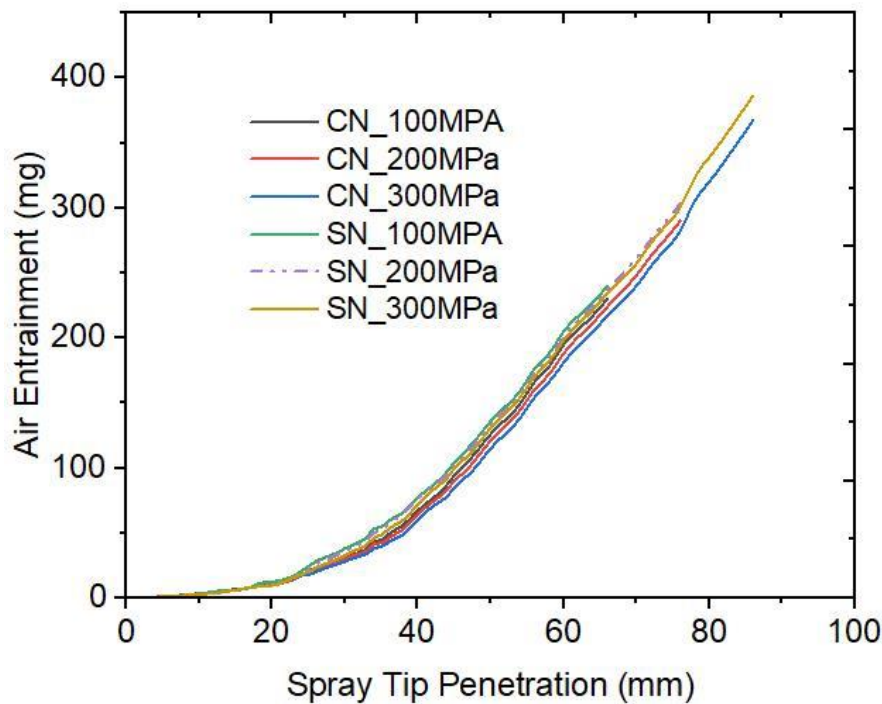


Figure 4.20. Mass of air entrained vs STP for CN and SN at different injection pressures

4.9. Ignition Delay

In the current work, Ignition delay (ID) was carried out through the period between the first appearance of OH* species to the start of injection in combustion phenomena. It was observed from Figure 4.21 that irrespective of nozzle geometry, ignition delay was shortened with the increase in injection pressure from 100MPa to 300MPa. Subsequently, the shortening of ignition delay was seen more for swirl nozzle as compared to the conventional nozzle at the corresponding injection pressure. The difference in ignition delay was significant at higher injection pressure (≤ 200 MPa). ID is majorly influenced by injection pressure, rheological properties of fuel and also from other parameters such

as nozzle diameter, cetane no. An increase in injection pressure leads to shorter breakup length, lower SMD, finer atomization and superior dispersion. Therefore, enhancement in atomization characteristics provides a shorter ID. The rationale of the study is also suggested by (Kannan and Anand, 2012; Agarwal et al., 2015). The above discussion showed that the atomization characteristics of swirl nozzle at higher injection pressure are better than conventional nozzle at higher injection pressure and that could be attributed to improved air-fuel mixing and that also promoting to faster air entrainment to reacting spray. Further, earlier results also showed that shorter IDs exhibited shorter lift-off length (Payri et al., 2016).

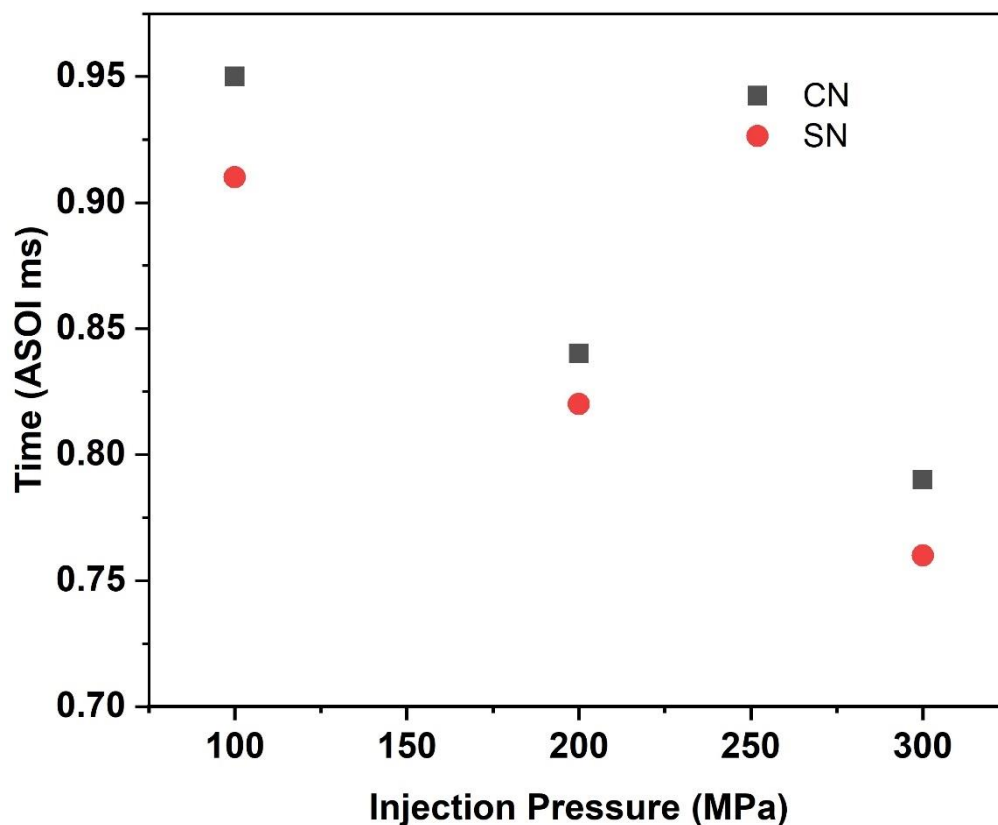


Fig. 4.21. Ignition delay vs Injection Pressure for CN and SN with injection pressure from 100MPa to 300 MPa.

4.10. Flame lift-off length

It was earlier got that flame lift-off is a good indicator of how well fuel-air mixed earlier to combustion. Previous results (Payri et al., 2016; Naber and Siebers, 1996; Hawi et al., 2019) showed that high injection pressure, ambient density and temperature, and oxygen concentration will reduce lift-off length. After the occurrence of ignition, the flame grows downstream and it becomes stable at a quasi-steady position considerably downstream of the injector tip. The distance from the injector tip to the location of the quasi-steady flame location is known as the flame-lift-off length. As shown in Figure 4.22, the downstream region of flame lift-off is distinguished by a zone of non-premixed, that relies on upstream air entrained, which is generally generated at the boundary of the diffusion zone (Dec J. E, 1997). However, flame lift-off length through simulation was defined as the initial axial location of OH* favre-averaged mass fraction which reaches 2% of its limit in computational volume (Wang et al., 2013). It was observed that as the injection pressure increased from 100MPa to 300MPa, spray momentum increased and that push the flame downstream at the lean side. Consequently, flame travelled upstream to rich mixture zone for stabilization for both injectors. However, a slight reduction in flame lift-off for swirl injector was observed as compared to the conventional nozzle. This reduction was only noticeable at high injection pressure (200MPa, 300MPa). The above reduction in lift-off is due to more concentration of OH* species on the edge of vaporized spray and that have more propinquity to the oxidant as shown in Figure 4.22. Since, the primary atomization length decreases more in swirl atomizer than conventional nozzle. therefore, more air (O₂ only) entrainment enhanced the air-fuel mixing.

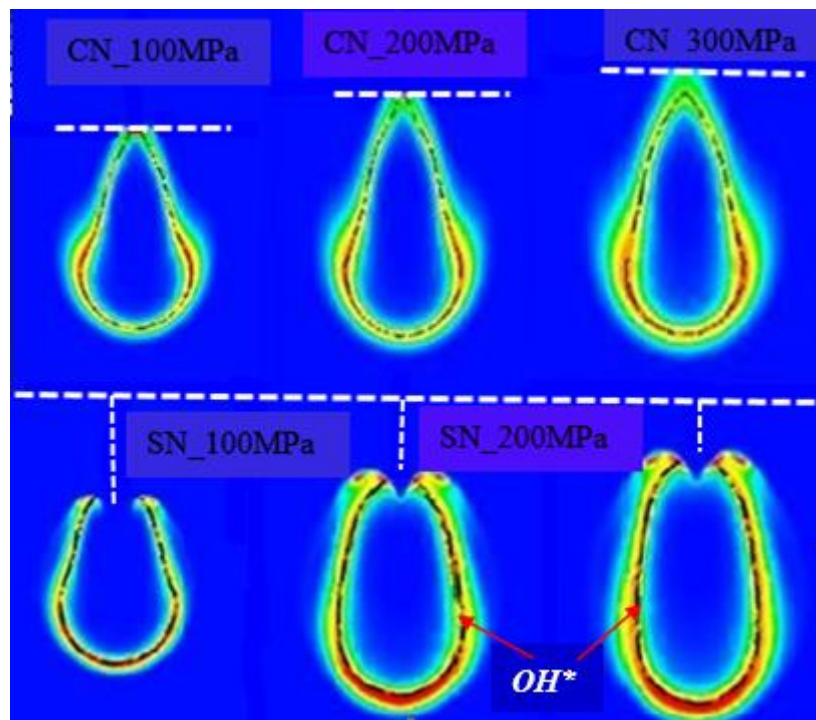


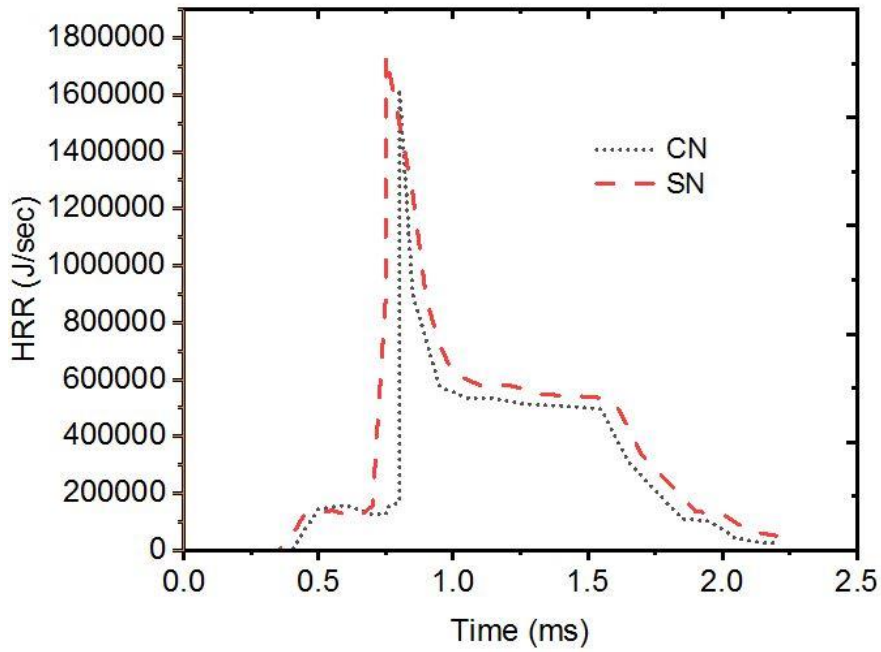
Figure 4.22. Variation of OH* flames of SN with injection pressure from 100MPa to 300 MPa.

4.11. Heat Release Rate and Maximum Temperature

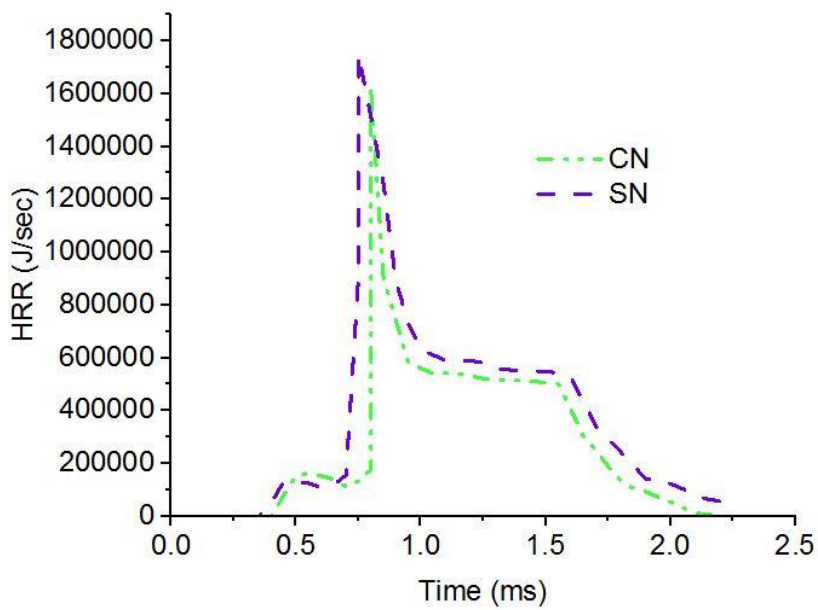
Maximum temperature and HRR are presented for both injectors at different injection pressures as shown in Figure 4.23 (a-c). Two peaks have been identified for both injectors, a sudden increase in HRR showed that ignition must have occurred. First and second-stage ignition can be controlled by chemical kinetics. Where the initial stage of ignition happens due to chain branching reactions which are more prone at lower temperatures and more oxygen concentrations (Bogin et al., 2013). On the other side, ignition at the second stage became leading due to chain propagation reaction when the temperature rises. Though, the first stage is also known as “cool flame” or LTHR (low-temperature heat release). This could be supposed that low-temperature flame distinguished by CH₂O species contained upstream, and OH* was characterized by high-temperature flame and

exhibited downstream. Due to the upstream location of CH₂O species, hot flames of WCO tend to move towards the injector location and additionally hot air is entrained upstream, which mixes with cool flame and that leads to happening of high-temperature ignition.

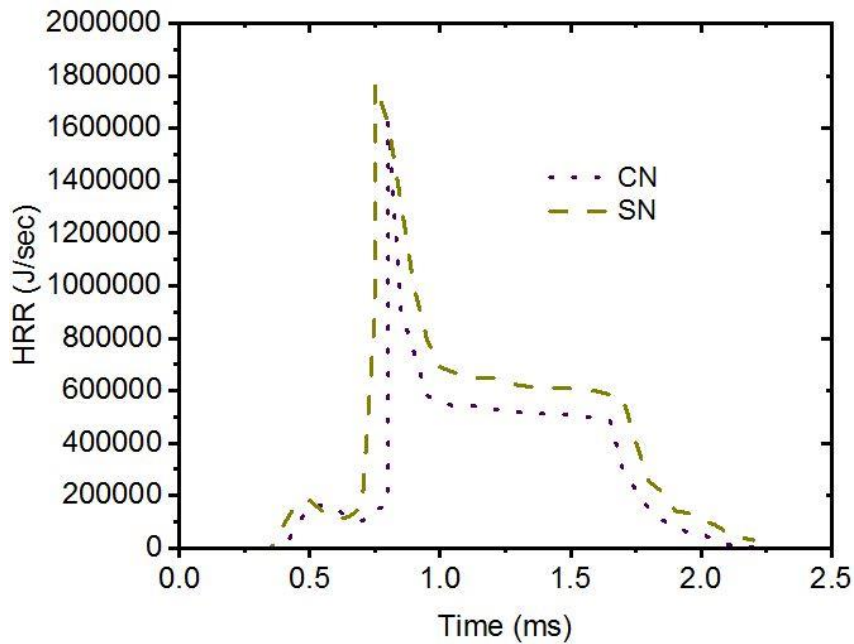
As the fuel is injected, the fuel droplet mixes with hot air and vaporization occurred. Consequently, a reduction in ambient temperature was observed for every injection pressure. Further, the sensible heat of air is reduced due to the vaporization of fuel, which decreases the injected spray's temperature. As the injection pressure increases from 100 MPa to 300MPa, fuel spray rotation and droplet rotation along their axis create more surface area to act as drag force and that enhanced faster disintegration and that causes enhanced air-fuel mixing in quiescent hot air. Entrainment of hot air was easier than conventional nozzles at high injection pressure (Agarwal et al., 2015; Zhang et al., 2017). Another aspect of disintegration into droplets is the varying nature of the rheological property of biodiesel with injection pressure. Rheological properties of biodiesel decrease with an increase in injection pressure and among all, lower surface tension makes the spray easier to break up into small droplets (Reitz and Diwakar,1986). Thus, better atomization causes faster vaporization and combustion and that leads to improvement in HRR. However, it was seen that at an injection pressure of 1000 MPa, the peaks of HRR are nearly the same with a little improvement in the second peak for swirl nozzle. Similarly, the temperature distribution showed the nearly same pattern up to 2.2 ms ASOI. When, the injection pressure reached 200MPa, and 300MPa, a significant difference was observed in HRR and Temperature distribution for swirl nozzle as compared to the conventional nozzle. Moreover, less improvement was seen in HRR and temperature distribution up to 0.8 ms ASOI at injection pressure of 200MPa and 300MPa as shown in Figure 4.24(a-c) and Figure 4.25(a-c).



(a) 100 MPa



(b) 200MPa



© 300MPa

Figure 4.23(a-c). HRR vs Time for CN and SN for injection pressure (100-300MPa) respectively

Afterwards improvement in HRR was noticeable for swirl nozzle. This is due to the reaction zone of CH_2O and OH^* being moved downstream for the increase in injection pressure. Downstream movement of the reaction zone occurred due to delay in the disintegration of droplets. The OH^* species was oriented downstream at the edge of vaporized spray particularly at the region of stoichiometry where there is close nearness of flame with oxidant. That confirms that generation of fine droplets are being more prone towards air (O_2 part) being entrained. This pushes the production of more OH^* species in the flame (Sarathy et al.,2011). Therefore, it was observed that an increase in injection pressure exhibited more conversion of CH_2O to OH^* species for swirl nozzle as compared to the conventional nozzle.

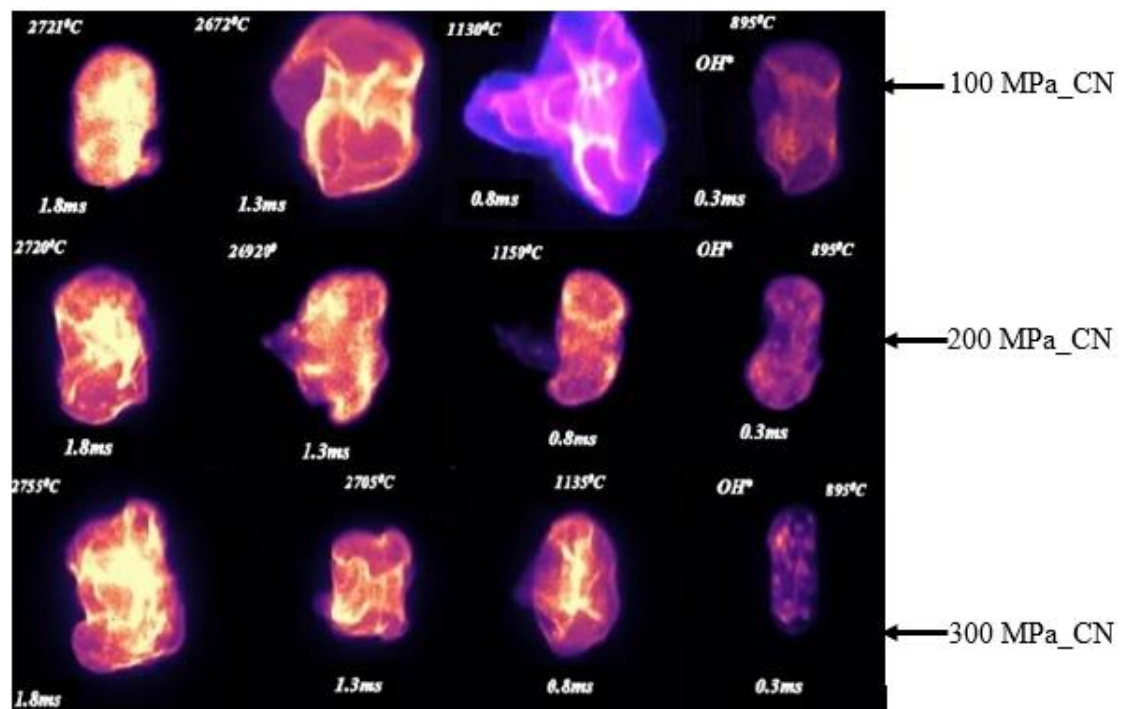


Figure 4.24. Temperature vs Time of spray through OH species of CN

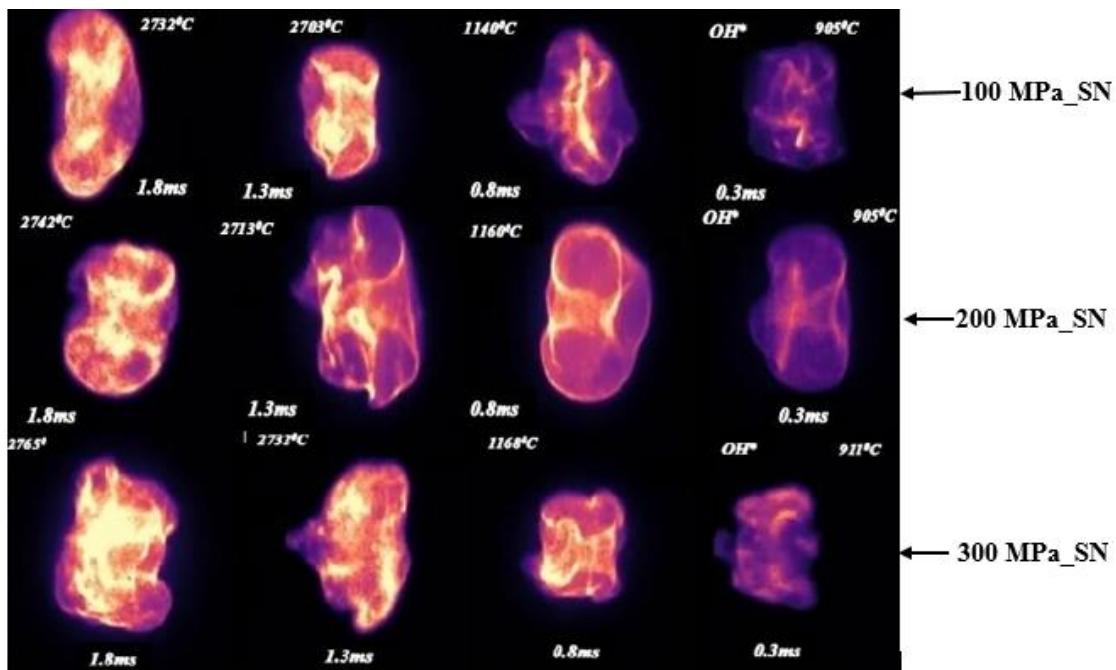


Figure 4.25. Temperature vs Time of spray through OH species of SN

4.12. Emission

The detail study of soot formation using six-step phenomenological soot model has been shown in Figure 4.26. Oxidation and soot formations are categorized into various parts

such as precursor formation through C_2H_2 , aromatic structures with four rings and three rings, the inception of particles from soot precursor, particle coagulation, surface growth by C_2H_2 , precursor oxidation, and particle surface oxidation through OH and O_2 . Here the carbon atoms of soot particles and soot precursor are denoted as C(S) and C(PR) respectively. The soot precursor formation (R(S3), R(S2), R(S1)), reaction rates, particle surface growth (R(S6), R(S5)), particle inception R(S4) soot precursor oxidation R(S10) are considered in the form of Arrhenius equation. C_2H_2 has been considered to be the pioneer for soot generation. This constitutes an important mechanism of soot formation building block of polycyclic aromatic hydrocarbon (PAH). (Wang et. al 2013) reported that C_2H_2 is the species which influences the PAH growth method through the mechanism of hydrogen abstraction carbon addition (HACA). This is the point to ponder that the difference between soot oxidized and gross soot formed is net soot formed. This confirms that whatever soot was generated in the flame, further, it went for oxidation through upstream air entrainment and hence net soot is remaining one. Figure 4.27 (a-c) shows that as the injection pressure increases from 100MPa to 300 MPa, overall net soot formation was reduced for both fuel injectors. This occurred due to enhancement in fuel-air mixing and leading to greater upstream air entrained of the combustion zone. Hence, an increase in injection pressure leading to OH* increase is due to improve in oxidation causing less soot to form. Initially, the mass concentration of soot particles increased from the start of combustion till the end of injection (1.5 ms ASOI). Subsequently, soot

decreased caused by improvement in oxidation.

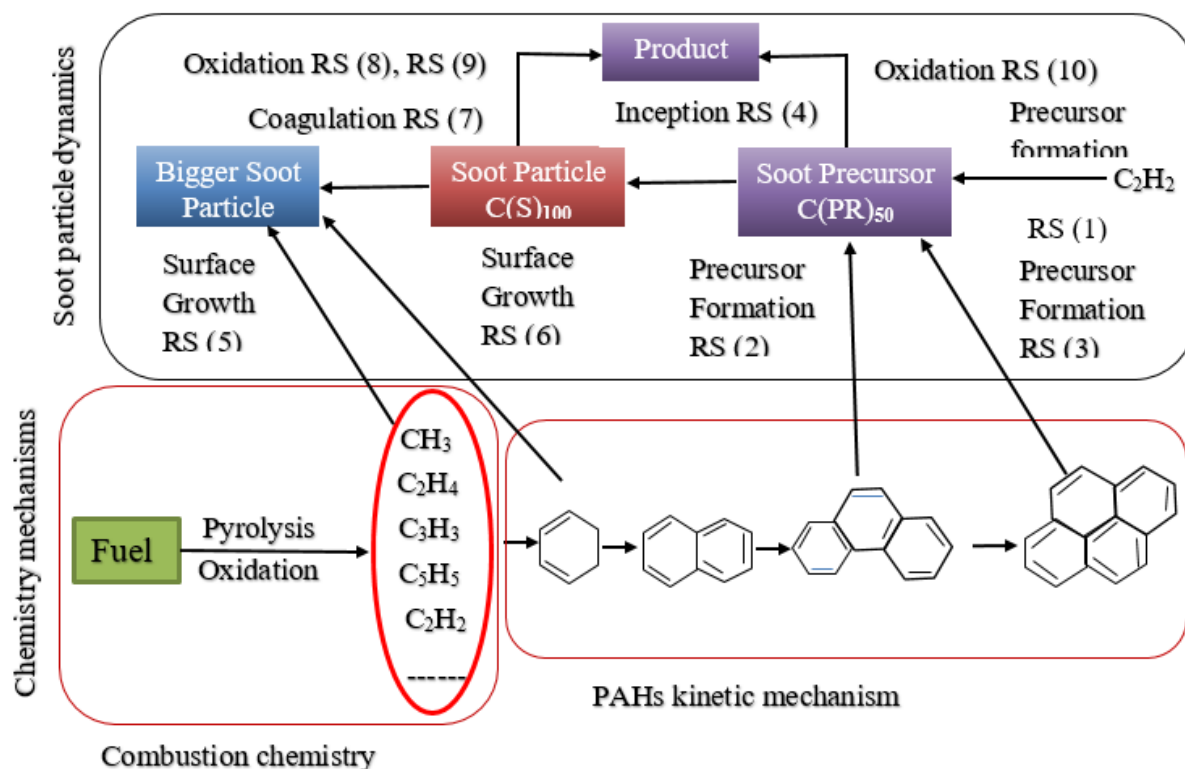
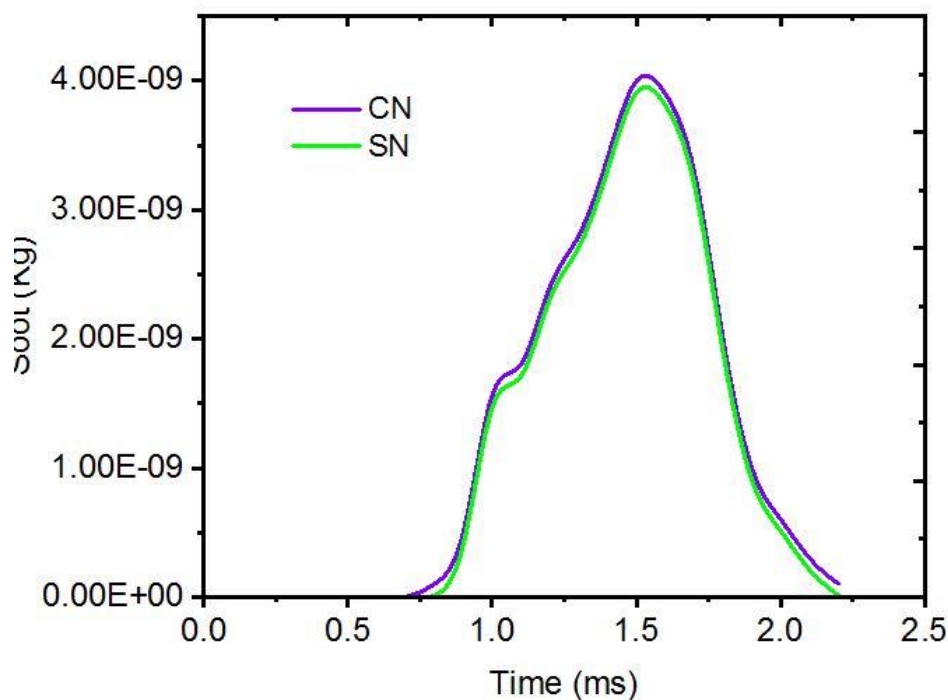
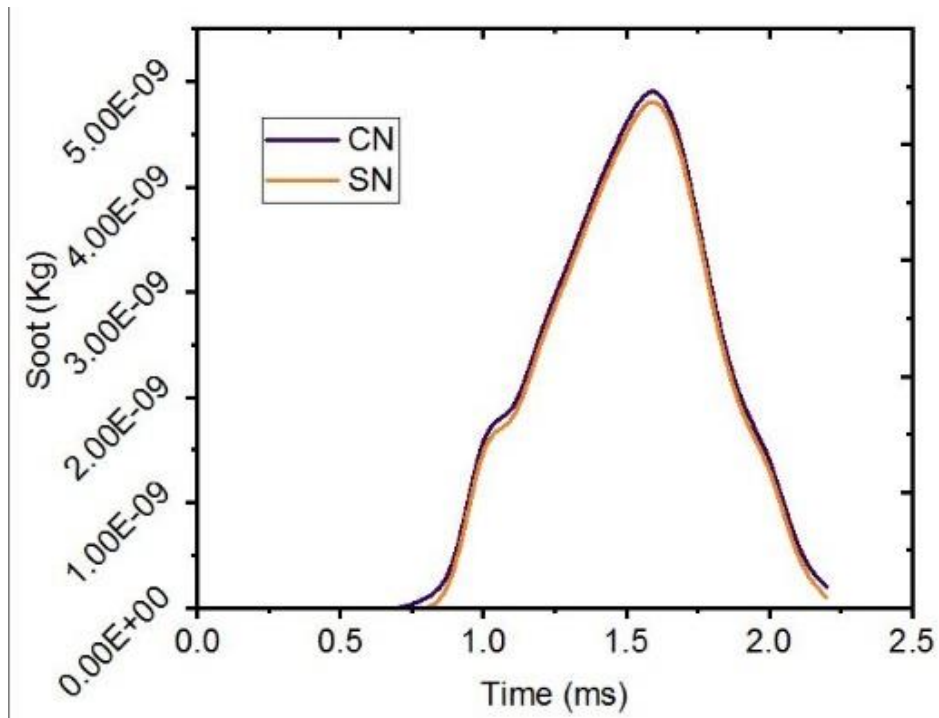


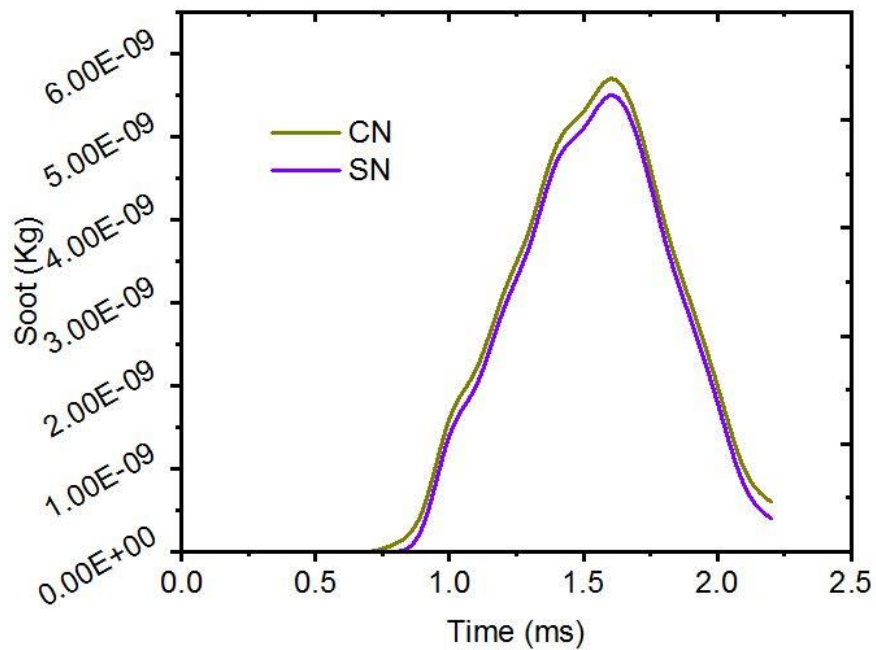
Figure 4.26. Graphic representation of the phenomenological soot model



(a) 300 MPa



(b) 200 MPa



© 100MPa

Figure 4.27(a-c). Soot vs time of CN and SN for injection pressure 100-300MPa

Since biodiesel has an affinity to offer oxygen during secondary atomization to spray molecules in combustion phenomena hence the oxygenated behaviour of biodiesel decreases soot formation and improves soot oxidation (Wang et al.,2016; Bandbafha et. al.,2018).

However, it was seen that soot formed through swirl atomizer is lower than conventional nozzle for all injection pressure. This happened due to swirl nozzle consist better atomization characteristics than the conventional nozzle and especially at higher injection pressure due to faster secondary atomization (Salvador et.al.,2021; Zhang et.al.,2017). Though, the difference between soot formations for both injectors at lower injection pressure is less due to the reduced impact of the centrifugal action of swirl injector.

CONCLUSION AND FUTURE SCOPE**Overview**

In the current work, the logical outcomes are drawn through computational study and experimentation using WCO biodiesel. Furthermore, the strength of the model is identified through standard data acquired from experimentation and also from previous literature. The evaluation of surface tension from the different model are carried out and found that Gibbs free model imparts closure results to standard data. Further, the recommendation for future work has been explored, and finally the references as well as appendices associated with the current research work have been enumerated

5.1. Conclusions

The current study explores the different techniques to improve spray characteristics of waste cooking oil biodiesel and also analyses their effects on combustion and emission. Initially, the physicochemical properties of tested fuel are examined according to ASTM standards. Subsequently, the surface tension of different biodiesel at a wide range of temperatures is measured through various theoretical models and compared their accuracy towards standard value. The modelling of spray generated from swirl nozzle was done and compared the spray characteristics and atomization characteristics among biodiesel-diesel blend, biodiesel and diesel. Moreover, spray combustion characteristics of waste cooking oil (WCO) were performed using swirl nozzle (SN) and conventional nozzle (CN) with the same cross-section area. Surrogates of WCO were used in the simulation such as n-heptane, methyl decanoate and methyl-9-decenoate. The computation consists Eulerian- Lagrangian approach to emphasize multiphase flow and linearized instability

sheet atomization model and Taylor analogy break up model to identify atomization, film formation and sheet breakup. Further, to identify the model's strength, validation of spray tip penetration s performed.

Following conclusions are obtained:

1. Waste cooking oil consists of a third generation of biodiesel and the waste is generated almost per capita 30% edible oil. The biodiesel produced from WCO lower the cost and reduces the burden on water purifier plants.
2. The physicochemical properties of biodiesel-diesel blends are near diesel fuel as per ASTM standards. Further, for all surrogates of waste cooking oil, the methyl oleate contains the highest mass fraction.
3. B100 showed longer spray tip penetration, and lower cone angle followed by B25 and Diesel fuel. Even, the increase in ambient pressure showed little decrement in penetration length and increment in cone angle.
4. The Sauter mean diameter of B100 was highest while diesel was lowest at every injection pressure. However, B25 showed lower than B100 and higher than diesel even at higher injection pressure.
5. There was an improvement in spray characteristics such as spray tip penetration, cone angle and Sauter mean diameter using swirl injectors in diesel engines as compared to conventional injectors.
6. The modelling of spray through linearized instability sheet atomization model and Taylor's analogy model imparted comprise of sheet breakup, atomization and film formation. The validation of the model with standard value showed better agreement and the deviations were below 5% to the standard data.

7. All biodiesel exhibited a reduction in surface tension of biodiesel decreased as the temperature of the fuel increases. However, the biodiesel consisting lower average no double bond possessed through faster reduction in surface tension of biodiesel.
8. The Gibbs free energy model is more accurate towards the standard measurement of surface tension at a wide range of temperatures as compared to Parachor Based model and Dalton-type mass average model.
9. Swirl nozzle depicted a decrease in spray tip penetration by 1.98%, 3.33% and 3.56% as compared to the conventional nozzle, while increase in cone angle by 4.35%, 6.11% and 6.88% for injection pressures of 100 MPa, 200 MPa and 300 MPa respectively
10. The mass of air entrained shows that an increase in injection pressures leads to better air-fuel mixing in SN due to an increasing trend of cone angle and little reduction in tip penetration while CN shows a reducing trend of cone angle.
11. The improved air-fuel mixing due to better atomization characteristics in SN leads to shorter ignition delay than CN, higher surface area to volume ratio of droplets generated through CN also makes the above.
12. Predicted flame-lift-off length for both injectors increased with an increase in injection pressure, but SN exhibited lower lift-off length than CN due to earlier atomization and more air entrainment.
13. Increase in spray volume makes more air interaction and that improves the vaporization characteristics with an increase in injection pressure. Since SN consist bigger spray volume than CN at higher injection pressure That causes higher HRR in SN and the above reason is also applicable for maximum temperature.
14. Swirl injector exhibited reduction in soot compared to CN at injection pressure of 100MPa, 200MPa and 300 MPa respectively. This is due to strongly enhanced atomization characteristics through SN.

5.2. Scope of Future Work

1. The current study examines the atomization characteristics of fuel assuming a circular droplet shape, however, in actuality it is spherical. Thus, further study can be performed by taking circular shape.
2. The present study, compared combustion characteristics of the swirl nozzle and conventional nozzle using waste cooking oil biodiesel as fuel. therefore, further examination is needed on the comparative assessment of biodiesel and its blends using swirl nozzle.
3. Even though the swirl nozzle exhibited better spray characteristics than conventional nozzle still efforts are required to study more about non-circular fuel injectors.
4. Efforts can also be deployed to implement an air swirl in the diesel engine to enhance air-fuel mixing in the combustion chamber.
5. The research on yield improvement can also be made without influencing the production cost of biodiesel. Further, the rise in photon-to-fuel conversion efficiency (PFCI) by the use of synthetic biology can be innovative research in future.

REFERENCES

- ❖ Aboelazayem, O., El-Gendy, N. S., Abdel-Rehim, A. A., Ashour, F., & Sadek, M. A. (2018). Biodiesel production from castor oil in Egypt: Process optimisation, kinetic study, diesel engine performance and exhaust emissions analysis. *Energy*, 157, 843-852. doi: 10.1016/j.energy.2018.05.202.
- ❖ Agarwal, A. K., Dhar, A., Gupta, J. G., Kim, W. I., Choi, K., Lee, C. S., & Park, S. (2015). Effect of fuel injection pressure and injection timing of Karanja biodiesel blends on fuel spray, engine performance, emissions and combustion characteristics. *Energy Conversion and Management*, 91, 302-314.
- ❖ Agarwal, A. K., Dhar, A., Gupta, J. G., Kim, W. I., Lee, C. S., & Park, S. (2014). Effect of fuel injection pressure and injection timing on spray characteristics and particulate size–number distribution in a biodiesel fuelled common rail direct injection diesel engine. *Applied energy*, 130, 212-221. Doi: 10.1016/j.apenergy.2014.05.041.
- ❖ Agarwal, A. K., Dhar, A., Srivastava, D. K., Maurya, R. K., & Singh, A. P. (2013). Effect of fuel injection pressure on diesel particulate size and number distribution in a CRDI single cylinder research engine. *Fuel*, 107, 84-89.
- ❖ Agrawal, S., & Gautam, R. (2019). Optimization of Engine Performance Parameters and Exhaust Emissions in CI Engine Fuelled with Soapnut Bio-Diesel Blend Using Artificial Neural Networks (No. 2019-01-1167). SAE Technical Paper. doi: 10.4271/2019-01-1167
- ❖ Agrawal, T., Gautam, R., Agrawal, S., Singh, V., Kumar, M., & Kumar, S. (2020). Optimization of engine performance parameters and exhaust emissions in compression ignition engine fueled with biodiesel-alcohol blends using taguchi method, multiple regression and artificial neural network. *Sustainable Futures*, 2, 100039. Doi: 10.1016/j.sftr.2020.100039
- ❖ Aleme, H. G., & Barbeira, P. J. (2012). Determination of flash point and cetane index in diesel using distillation curves and multivariate calibration. *Fuel*, 102, 129-134.
- ❖ Aleyasin, S. S., Fathi, N., Tachie, M. F., Vorobieff, P., & Koupriyanov, M. (2018). On the development of incompressible round and equilateral triangular jets due to Reynolds number variation. *Journal of Fluids Engineering*, 140(11), 111202.. Doi: 10.1115/1.4040031.
- ❖ Amini, G., & Dolatabadi, A. (2011). Capillary instability of elliptic liquid jets. *Physics of Fluids*, 23(8), 084109. Doi: 10.1063/1.3626550.

- ❖ An, H., Yang, W. M., Chou, S. K., & Chua, K. J. (2012). Combustion and emissions characteristics of diesel engine fueled by biodiesel at partial load conditions. *Applied Energy*, 99, 363-371. Doi: 10.1016/j.apenergy.2012.05.049
- ❖ Asheim, J. P., Kirwan, J. E., & Peters, J. E. (1988). Modeling of a hollow-cone liquid spray including droplet collisions. *Journal of Propulsion and Power*, 4(5), 391-398. Doi: <https://doi.org/10.2514/3.23079>
- ❖ Azad, M., Quinn, W. R., & Groulx, D. (2012). Mixing in turbulent free jets issuing from isosceles triangular orifices with different apex angles. *Experimental thermal and fluid science*, 39, 237-251. Doi: 10.1016/j.expthermflusci.2012.01.028.
- ❖ Basha, S., Rao, P., Rajagopal, K., & Kotturi, R. (2017). Design and analysis of swirl in acetylene aspirated diesel engine and its effects on performance & emissions. *International Journal of Latest Trends in Engineering and Technology*, 8(2), 390-399.
- ❖ Baumgarten, C. (2006). *Mixture formation in internal combustion engines*. Springer Science & Business Media.
- ❖ Bautista, L.F., Vicente, G., Rodríguez, R., Pacheco, M., 2009. Optimisation of FAME production from waste cooking oil for biodiesel use. *Biomass Bioenergy* 33 (5), 862–872. <https://doi.org/10.1016/j.biombioe.2009.01.009>
- ❖ Behera, P., Murugan, S., & Nagarajan, G. (2014). Dual fuel operation of used transformer oil with acetylene in a DI diesel engine. *Energy conversion and management*, 87, 840-847.
- ❖ Belhadef, A., Vallet, A., Amielh, M., & Anselmet, F. (2012). Pressure-swirl atomization: Modeling and experimental approaches. *International Journal of Multiphase Flow*, 39, 13-20. Doi: <https://doi.org/10.1016/j.ijmultiphaseflow.2011.09.009>.
- ❖ Bhan, S., Gautam, R., & Singh, P. (2022). An experimental assessment of combustion, emission, and performance behavior of a diesel engine fueled with newly developed biofuel blend of two distinct waste cooking oils and metallic nano-particle (Al₂O₃). *Scientia Iranica. Transaction B, Mechanical Engineering*, 29(4), 1853-1867.
- ❖ Bhan, S., Gautam, R., & Singh, P. (2022). Analyzing the impact of adding aluminum oxide and cerium oxide nanoparticles to waste cooking biodiesel on engine performance, combustion and emissions characteristics. *Petroleum Science and Technology*, 1-29. doi: 10.1080/10916466.2022.2136705
- ❖ Bhikuning, A., Sugawara, R., Matsumura, E., & Senda, J. (2020). Investigation of spray characteristics from waste cooking oil, bio-hydro fined diesel oil (BHD) and n-tridecane in

a constant volume chamber. *Case Studies in Thermal Engineering*, 21, 100661. Doi: <https://doi.org/10.1016/j.csite.2020.100661>.

- ❖ Boggavarapu, P., & Ravikrishna, R. V. (2013). A review on atomization and sprays of biofuels for IC engine applications. *International journal of spray and combustion dynamics*, 5(2), 85-121. doi: 10.1260/1756-8277.5.2.85
- ❖ Bogin Jr, G. E., Osecky, E., Ratcliff, M. A., Luecke, J., He, X., Zigler, B. T., & Dean, A. M. (2013). Ignition quality tester (IQT) investigation of the negative temperature coefficient region of alkane autoignition. *Energy & Fuels*, 27(3), 1632-1642.
- ❖ Boot, M. D., Luijten, C. C. M., Somers, L. M. T., Eguz, U., van Erp, D. D. T. M., Albrecht, A., & Baert, R. S. G. (2009). Uncooled EGR as a means of limiting wall-wetting under early direct injection conditions (No. 2009-01-0665). SAE Technical Paper. Doi: 10.4271/2009-01-0665.
- ❖ Bousbaa, H., Sary, A., Tazerout, M., & Liazid, A. (2012). Investigations on a compression ignition engine using animal fats and vegetable oil as fuels. *Journal of energy resources technology*, 134(2). Doi:
- ❖ BP Statistical Review of World Energy 2022, <https://www.bp.com/content/dam/bp/business-sites/en/global/corporate/pdfs/energy-economics/statistical-review/bp-stats-review-2020-full-report.pdf>.
- ❖ Buffi, M., Valera-Medina, A., Marsh, R., Pugh, D., Giles, A., Runyon, J., Chiaramonti, D., 2017. Emissions characterization tests for hydrotreated renewable jet fuel from used cooking oil and its blends. *Appl. Energy* 201, 84–93. <https://doi.org/10.1016/j.apenergy.2017.05.104>.
- ❖ Cao Y, Du J, Bai Y, Ghadiri M, Mohammadinia S. Towards estimating surface tension of biodiesels: Application to thermodynamic and intelligent modeling. *Fuel*. 2021 Jan 1;283:118797.
- ❖ Carareto, N. D., Kimura, C. Y., Oliveira, E. C., Costa, M. C., & Meirelles, A. J. (2012). Flash points of mixtures containing ethyl esters or ethylic biodiesel and ethanol. *Fuel*, 96, 319-326. Doi: 10.1016/j.fuel.2012.01.025
- ❖ Carus, M., 2019. Chart of the week 50, press release, 2019-12. UFOP chart (accessed 09/2020). <https://news.bio-based.eu/global-biodiesel-production-is-increasing/>.
- ❖ Chang, K. C., Wang, M. R., Wu, W. J., & Hong, C. H. (1993). Experimental and theoretical study on hollow-cone spray. *Journal of Propulsion and Power*, 9(1), 28-34. doi:10.2514/3.11481.

- ❖ Chauhan, B. S., Kumar, N., Du Jun, Y., & Lee, K. B. (2010). Performance and emission study of preheated Jatropa oil on medium capacity diesel engine. *Energy*, 35(6), 2484-2492. Doi: 10.1016/j.energy.2010.02.043.
- ❖ Chen, P. C., Wang, W. C., Roberts, W. L., & Fang, T. (2013). Spray and atomization of diesel fuel and its alternatives from a single-hole injector using a common rail fuel injection system. *Fuel*, 103, 850-861. Doi: 10.1016/j.fuel.2012.08.013.
- ❖ Chung, T. J. (2002). *Computational fluid dynamics*. Cambridge university press
- ❖ Czerwonatis, N., & Eggers, R. (2001). Disintegration of liquid jets and drop drag coefficients in pressurized nitrogen and carbon dioxide. *Chemical Engineering & Technology: Industrial Chemistry-Plant Equipment-Process Engineering-Biotechnology*, 24(6), 619-624.
- ❖ Davanlou, A., Lee, J. D., Basu, S., & Kumar, R. (2015). Effect of viscosity and surface tension on breakup and coalescence of bicomponent sprays. *Chemical Engineering Science*, 131, 243-255. Doi: 10.1016/j.ces.2015.03.057
- ❖ de Araújo, C.D.M., de Andrade, C.C., de Souza e Silva, E., Dupas, F.A., 2013. Biodiesel production from used cooking oil: a review. *Renew. Sustain. Energy Rev.* 27, 445–452. <https://doi.org/10.1016/j.rser.2013.06.014>.
- ❖ Dec, J. E. (1997). A conceptual model of DL diesel combustion based on laser-sheet imaging. *SAE transactions*, 1319-1348.
- ❖ Degfie, T.A., Mamo, T.T., Mekonnen, Y.S., 2019. Optimized biodiesel production from waste cooking oil (WCO) using calcium oxide (CaO) nanocatalyst. *Sci. Rep.* 9 <https://doi.org/10.1038/s41598-019-55403-4>, 18982.
- ❖ Diesel Technology Forum Annual Report 2019, <https://www.dieselforum>.
- ❖ Ejim, C. E., Fleck, B. A., & Amirfazli, A. (2007). Analytical study for atomization of biodiesels and their blends in a typical injector: surface tension and viscosity effects. *Fuel*, 86(10-11), 1534-1544. doi: 10.1016/j.fuel.2006.11.006.
- ❖ Elbadawy, I., Gaskell, P. H., Lawes, M., & Thompson, H. M. (2015). Numerical investigation of the effect of ambient turbulence on pressure swirl spray characteristics. *International Journal of Multiphase Flow*, 77, 271-284. Doi: <https://doi.org/10.1016/j.ijmultiphaseflow.2015.06.008>
- ❖ Emissions Gap Report, UN Environment Programme, <https://www.unep.org/resources/emissions-gap-report-2022>.

- ❖ Enweremadu, C.C., Mbarawa, M.M., 2009. Technical aspects of biodiesel production and analysis from used cooking oil – a review. *Renew. Sustain. Energy Rev.* 13 (9), 2205–2224. <https://doi.org/10.1016/j.rser.2009.06.007>.
- ❖ Fan, X., Liu, C., Mu, Y., Lu, H., Yang, J., & Xu, G. (2020). Experimental investigations of spray characteristics of a pressure-swirl atomizer. *Proceedings of the Institution of Mechanical Engineers, Part A: Journal of Power and Energy*, 234(5), 643-654. Doi: <https://doi.org/10.1177/0957650919875612>.
- ❖ Farooq, M., Ramli, A., Subbarao, D., 2013. Biodiesel production from waste cooking oil using bifunctional heterogeneous solid catalysts. *J. Clean. Prod.* 59, 131–140. <https://doi.org/10.1016/j.jclepro.2013.06.015>.
- ❖ Freitas SV, Oliveira MB, Lima AS, Coutinho JA. Measurement and prediction of biodiesel volatility. *Energy & fuels.* 2012 May 17;26(5):3048-53
- ❖ Gautam, R., & Kumar, N. (2015). Comparative study of performance and emission characteristics of Jatropha alkyl ester/butanol/diesel blends in a small capacity CI engine. *Biofuels*, 6(3-4), 179-190. Doi: 10.1080/17597269.2015.1068081
- ❖ Gautam, R., & Kumar, N. (2016). Effect of ethanol addition on the properties of Jatropha ethyl ester. *Energy Sources, Part A: Recovery, Utilization, and Environmental Effects*, 38(23), 3464-3469. doi: 10.1080/15567036.2016.1145766
- ❖ Gautam, R., & Kumar, N. (2018). Performance emission and combustion studies of diesel engine on Jatropha ethyl ester and its higher alcohol blends. *International Journal of Global Warming*, 14(2), 159-169. doi: 10.1504/IJGW.2018.090177
- ❖ Gautam, R., & Kumar, S. (2020). Performance and combustion analysis of diesel and tallow biodiesel in CI engine. *Energy reports*, 6, 2785-2793.
- ❖ Gautam, R., Ansari, N. A., Thakur, P., Sharma, A., & Singh, Y. (2022). Status of biofuel in India with production and performance characteristics: a review. *International Journal of Ambient Energy*, 43(1), 61-77.
- ❖ Gautam, R., Ansari, N. A., Thakur, P., Sharma, A., & Singh, Y. (2019). Status of biofuel in India with production and performance characteristics: a review. *International Journal of Ambient Energy*, 1-17.
- ❖ Gautam, R., Ansari, N., Sharma, A., & Singh, Y. (2020). Development of the ethyl ester from jatropha oil through response surface methodology approach. *Pollution*, 6(1), 135-147.

- ❖ Gautam, R., Chauhan, B. S., & Lim, H. C. (2022). Influence of variation of injection angle on the combustion, performance and emissions characteristics of jatropha ethyl ester. *Energy*, 254, 124436. doi: 10.1016/j.energy.2022.124436
- ❖ Gautam, R., Kumar, N., & Sharma, P. (2013). Comparative assessment of performance, emission and combustion characteristics of blends of methyl and ethyl ester of jatropha oil and diesel in compression ignition engine (No. 2013-01-2664). Doi: 10.4271/2013-01-2664
- ❖ Genzale, C. L., Pickett, L. M., & Kook, S. (2010). Liquid penetration of diesel and biodiesel sprays at late-cycle post-injection conditions. *SAE International Journal of Engines*, 3(1), 479-495. Doi: 10.4271/2010-01-0610
- ❖ Georjon, T. L., & Reitz, R. D. (1999). A drop-shattering collision model for multidimensional spray computations. *Atomization and Sprays*, 9(3). Doi: 10.1615/AtomizSpr.v9.i3.10
- ❖ Goodwin, M. S. and Wigley, G., A Fundamental Study of Liquid Sheet Breakup and its Relationship to GDI Sprays: 9th International Conference on Liquid Atomization and Spray Systems, Sorrento, Italy, 2003.
- ❖ Gui, M.M., Lee, K.T., Bhatia, S., 2008. Feasibility of edible oil vs. non-edible oil vs. waste edible oil as biodiesel feedstock. *Energy* 33 (11), 1646–1653. <https://doi.org/10.1016/j.energy.2008.06.002>.
- ❖ Han, Z., & Reitz, R. D. (1995). Turbulence modeling of internal combustion engines using RNG κ - ϵ models. *Combustion science and technology*, 106(4-6), 267-295.
- ❖ Hashiehbafe, A., & Romano, G. P. (2013). Particle image velocimetry investigation on mixing enhancement of non-circular sharp edge nozzles. *International journal of heat and fluid flow*, 44, 208-221. Doi: 10.1016/j.ijheatfluidflow.2013.05.017.
- ❖ Hawi, M., Kosaka, H., Sato, S., Nagasawa, T., Elwardany, A., & Ahmed, M. (2019). Effect of injection pressure and ambient density on spray characteristics of diesel and biodiesel surrogate fuels. *Fuel*, 254, 115674.
- ❖ Herbinet, O., Pitz, W. J., & Westbrook, C. K. (2010). Detailed chemical kinetic mechanism for the oxidation of biodiesel fuels blend surrogate. *Combustion and flame*, 157(5), 893-908.
- ❖ Hiroyasu, H., & Kadota, T. (1976). Models for combustion and formation of nitric oxide and soot in direct injection diesel engines. *SAE transactions*, 513-526.

- ❖ Hoang, A. T. (2018). Prediction of the density and viscosity of biodiesel and the influence of biodiesel properties on a diesel engine fuel supply system. *Journal of Marine Engineering & Technology*, 1-13.
- ❖ Hoang, A. T. (2020). Critical review on the characteristics of performance, combustion and emissions of PCCI engine controlled by early injection strategy based on narrow-angle direct injection (NADI). *Energy Sources, Part A: Recovery, Utilization, and Environmental Effects*, 1-15. Doi: 10.1080/15567036.2020.1805048
- ❖ Hosseinzadeh-Bandbafha, Homa, Meisam Tabatabaei, Mortaza Aghbashlo, Majid Khanali, and Ayhan Demirbas. "A comprehensive review on the environmental impacts of diesel/biodiesel additives." *Energy Conversion and Management* 174 (2018): 579-614.
- ❖ IEA, *World Energy Outlook 2022*, <https://www.iea.org/reports/world-energy-outlook-2022>.
- ❖ Imdadul, H. K., Masjuki, H. H., Kalam, M. A., Zulkifli, N. W. M., Alabdulkarem, A., Rashed, M. M., ... & How, H. G. (2016). Higher alcohol–biodiesel–diesel blends: an approach for improving the performance, emission, and combustion of a light-duty diesel engine. *Energy Conversion and Management*, 111, 174-185. doi: 10.1016/j.enconman.2015.12.066.
- ❖ Jedelský, J., Malý, M., Jícha, M., Sláma, J., & Wigley, G. (2021). Importance of Geometrical Factors on Spray Characteristics of Spray-Return Atomizers. *Journal of Propulsion and Power*, 37(3), 408-418. Doi: <https://doi.org/10.2514/1.B38066>.
- ❖ Jiang, Y. J., Umemura, A., & Law, C. K. (1992). An experimental investigation on the collision behaviour of hydrocarbon droplets. *Journal of Fluid Mechanics*, 234, 171-190. Doi: 10.1017/S0022112092000740.
- ❖ Jiang, Y., Zhang, Y., 2016. Supply chain optimization of biodiesel produced from waste cooking oil. *Transp. Res. Procedia* 12, 938–949. <http://creativecommons.org/licenses/by-nc-nd/4.0>
- ❖ Kalam, M. A., & Masjuki, H. H. (2002). Biodiesel from palmoil—an analysis of its properties and potential. *Biomass and Bioenergy*, 23(6), 471-479. Doi: 10.1016/S0961-9534(02)00085-5
- ❖ Kalghatgi, G. (2018). Is it really the end of internal combustion engines and petroleum in transport? *Applied energy*, 225, 965-974.
- ❖ Kannan, G. R., & Anand, R. (2012). Effect of injection pressure and injection timing on DI diesel engine fuelled with biodiesel from waste cooking oil. *Biomass and bioenergy*, 46, 343-352

- ❖ Kasyap, T. V., Sivakumar, D., & Raghunandan, B. N. (2009). Flow and breakup characteristics of elliptical liquid jets. *International journal of multiphase flow*, 35(1), 8-19. Doi: 10.1016/j.ijmultiphaseflow.2008.09.002
- ❖ Kim, H. J., Park, S. H., & Lee, C. S. (2010). A study on the macroscopic spray behavior and atomization characteristics of biodiesel and dimethyl ether sprays under increased ambient pressure. *Fuel processing technology*, 91(3), 354-363. doi: 10.1016/j.fuproc.2009.11.007.
- ❖ Kishna, R. S., Nanthagopal, K., Ashok, B., Srinath, R., Kumar, M. P., & Bhowmick, P. (2019). Investigation on pilot injection with low temperature combustion of Calophyllum inophyllum biodiesel fuel in common rail direct injection diesel engine. *Fuel*, 258, 116144. Doi: 10.1016/j.fuel.2019.116144
- ❖ Knothe, G., & Steidley, K. R. (2005). Kinematic viscosity of biodiesel fuel components and related compounds. Influence of compound structure and comparison to petrodiesel fuel components. *Fuel*, 84(9), 1059-1065. Doi: 10.1016/j.fuel.2005.01.016
- ❖ Körbitz, W. (1999). Biodiesel production in Europe and North America, an encouraging prospect. *Renewable Energy*, 16(1-4), 1078-1083. Doi: 10.1016/S0960-1481(98)00406-6
- ❖ Kostas, J., Honnery, D., & Soria, J. (2009). Time resolved measurements of the initial stages of fuel spray penetration. *Fuel*, 88(11), 2225-2237. Doi: 10.1016/j.fuel.2009.05.013.
- ❖ Kumar, M., Singh, V. K., Sharma, A., Ansari, N. A., Gautam, R., & Singh, Y. (2022). Effect of fuel injection pressure and EGR techniques on various engine performance and emission characteristics on a CRDI diesel engine when run with linseed oil methyl ester. *Energy & Environment*, 33(1), 41-63. Doi: 10.1177/0958305X20983477
- ❖ Kutti, O. A., Sarathy, S. M., & Nishida, K. (2020). Spray combustion simulation study of waste cooking oil biodiesel and diesel under direct injection diesel engine conditions. *Fuel*, 267, 117240. Doi: <https://doi.org/10.1016/j.fuel.2020.117240>
- ❖ Lakshmanan, T, and G Nagarajan. 2009. "Performance and Emission of Acetylene-Aspirated Diesel Engine." *Jordan Journal of Mechanical and Industrial Engineering* 3 (2): 125–30.
- ❖ Lam SS, Liew RK, Jusoh A, Chong CT, Ani FN, Chase HA. Progress in waste oil to sustainable energy, with emphasis on pyrolysis techniques. *Renew Sustain Energy Rev* 2016;53:741–53. <https://doi.org/10.1016/J.RSER.2015.09.005>.

- ❖ Lam, M.K., Lee, K.T., Mohamed, A.R., 2010. Homogeneous, heterogeneous and enzymatic catalysis for transesterification of high free fatty acid oil (waste cooking oil) to biodiesel: a review. *Biotechnol. Adv.* 28 (4), 500–518. <https://doi.org/10.1016/j.biotechadv.2010.03.002>.
- ❖ Lapuerta M, Villajos M, Agudelo JR, Boehman AL. Key properties and blending strategies of hydrotreated vegetable oil as biofuel for diesel engines. *Fuel Process Technol* 2011;92:2406–11. <https://doi.org/10.1016/j.fuproc.2011.09.003>
- ❖ Laurila, E., Koivisto, S., Kankkunen, A., Saari, K., Maakala, V., Järvinen, M., & Vuorinen, V. (2020). Computational and experimental investigation of a swirl nozzle for viscous fluids. *International Journal of Multiphase Flow*, 128, 103278. Doi: <https://doi.org/10.1016/j.ijmultiphaseflow.2020.103278>.
- ❖ Lešnik, L., Kegl, B., Bombek, G., Hočevár, M., & Biluš, I. (2018). The influence of in-nozzle cavitation on flow characteristics and spray break-up. *Fuel*, 222, 550-560. Doi: 10.1016/j.fuel.2018.02.144
- ❖ Li, T., Nishida, K., & Hiroyasu, H. (2011). Droplet size distribution and evaporation characteristics of fuel spray by a swirl type atomizer. *Fuel*, 90(7), 2367-2376.
- ❖ Li, T., Zhang, X. Q., Wang, B., Guo, T., Shi, Q., & Zheng, M. (2017). Characteristics of non-evaporating, evaporating and burning sprays of hydrous ethanol diesel emulsified fuels. *Fuel*, 191, 251-265. Doi: <https://doi.org/10.1016/j.fuel.2016.11.070>
- ❖ Lin, B. F., Huang, J. H., & Huang, D. Y. (2009). Experimental study of the effects of vegetable oil methyl ester on DI diesel engine performance characteristics and pollutant emissions. *Fuel*, 88(9), 1779-1785. doi: 10.1016/j.fuel.2009.04.006.
- ❖ Lin, Y. S., & Lin, H. P. (2010). Study on the spray characteristics of methyl esters from waste cooking oil at elevated temperature. *Renewable Energy*, 35(9), 1900-1907.
- ❖ Lingfa, P., Das, P., Das, L., & Naik, S. (2014). Effect of Injection Pressures and Injection Timings on the Engine Performance and Emissions on Single Cylinder Diesel Engine Operating with Tung Biodiesel Blends (No. 2014-01-2762). SAE Technical Paper. doi: 10.4271/2014-01-2762.
- ❖ Loizides, M.I., Loizidou, X.L., Orthodoxou, D.L., Petsa, D., 2019. Circular bioeconomy in action: collection and recycling of domestic used cooking oil through a social, reverse logistics system. *Recycling* 4 (16), 1–10. <https://doi.org/10.3390/recycling4020016>
- ❖ Luigi Di Angelo Luca Allocca, Angelo De Vita. Visualization and characterization of diesel spray wall-impingement. the 10th. International Symposium on Flow Visualization. 2002.

- ❖ Luo, Z., Plomer, M., Lu, T., Som, S., Longman, D. E., Sarathy, S. M., & Pitz, W. J. (2012). A reduced mechanism for biodiesel surrogates for compression ignition engine applications. *Fuel*, 99, 143-153.
- ❖ Ma, F., Hanna, M.A., 1999. Biodiesel production: a review. *Bioresour. Technol.* 70 (1), 1–15. [https://doi.org/10.1016/S0960-8524\(99\)00025-5](https://doi.org/10.1016/S0960-8524(99)00025-5).
- ❖ Manchanda T, Tyagi R, Sharma DK. Comparison of fuel characteristics of green (renewable) diesel with biodiesel obtainable from algal oil and vegetable oil. *Energy Sources, Part A Recover Util Environ Eff* 2018;40:54–9. <https://doi.org/10.1080/15567036.2017.1405109>.
- ❖ Markadeh, R. S., Arabkhalaj, A., Ghassemi, H., & Azimi, A. (2020). Droplet evaporation under spray-like conditions. *International Journal of Heat and Mass Transfer*, 148, 119049. Doi: 10.1016/j.ijheatmasstransfer.2019.119049.
- ❖ Marmesat, S., Rodriguez-Macado, E., Velasco, J., Dorbangarnes, M.C., 2007. Used frying fats and oils: comparison of rapid tests based on chemical and physical oil properties. *Int. J. Food Sci. Technol.* 42, 601–608. <https://doi.org/10.1111/j.1365-2621.2006.01284.x>.
- ❖ Marwaha, A., Rosha, P., Mohapatra, S. K., Mahla, S. K., & Dhir, A. (2018). Waste materials as potential catalysts for biodiesel production: Current state and future scope. *Fuel processing technology*, 181, 175-186.
- ❖ McKinley, G. H., & Renardy, M. (2011). Wolfgang von ohnesorge. *Physics of Fluids*, 23(12), 127101.
- ❖ Mittelbach, M., & Remschmidt, C. (2004). *Biodiesel: the comprehensive handbook*. Martin Mittelbach.
- ❖ Mittelbach, M., 1996. Diesel fuel derived vegetable oils, VI. Specifications and quality control of biodiesel. *Bioresour. Technol.* 56 (1), 7–11. [https://doi.org/10.1016/0960-8524\(95\)00172-7](https://doi.org/10.1016/0960-8524(95)00172-7).
- ❖ Moazeni, F., Chen, Y.C., Zhang, G., 2019. Enzymatic transesterification for biodiesel production from used cooking oil, a review. *J. Clean. Prod.* 216, 117–128. <https://doi.org/10.1016/j.jclepro.2019.01.181>.
- ❖ Mohan, B., Yang, W., Tay, K. L., & Yu, W. (2014). Experimental study of spray characteristics of biodiesel derived from waste cooking oil. *Energy conversion and management*, 88, 622-632.
- ❖ Mori, S. A., & Alexander, A. J. (1972). A investigation of paricle trajectories in two-phase flow systencs [J]. *Journal of Fluid Mechanics*, 55, 193-208. doi:10.1017/S0022112072001806.

- ❖ Naber, J. D., & Siebers, D. L. (1996). Effects of gas density and vaporization on penetration and dispersion of diesel sprays. *SAE transactions*, 82-111.
- ❖ Nagle, J. (1962). Oxidation of carbon between 1000-2000°C. In *Proceedings of Fifth Carbon Conference*, London, England, 1962.
- ❖ Najafi, S. M. A., Mikaniki, P., & Ghassemi, H. (2020). Microscopic and macroscopic atomization characteristics of a pressure-swirl atomizer, injecting a viscous fuel oil. *Chinese Journal of Chemical Engineering*, 28(1), 9-22.
- ❖ Omidvarborna, H., Kumar, A., & Kim, D. S. (2015). Recent studies on soot modeling for diesel combustion. *Renewable and Sustainable Energy Reviews*, 48, 635-647.
[org/files/dmfile/2019-annual-report-pages-FINAL.pdf](https://www.sciencedirect.com/org/files/dmfile/2019-annual-report-pages-FINAL.pdf).
- ❖ Ouanji, F., Kacimi, M., Ziyad, M., et al., 2016. Production of biodiesel at small-scale (10 L) for local power generation. *Int. J. Hydrogen Energy* 42, 8914–8921. <https://doi.org/10.1016/j.ijhydene.2016.06.182>.
- ❖ Patil, P., Deng, S., Isaac Rhodes, J., Lammers, P.J., 2010. Conversion of waste cooking oil to biodiesel using ferric sulfate and supercritical methanol processes. *Fuel* 89 (2), 360–364. <https://doi.org/10.1016/j.fuel.2009.05.024>.
- ❖ Payri, F., Payri, R., Salvador, F. J., & Martínez-López, J. (2012). A contribution to the understanding of cavitation effects in Diesel injector nozzles through a combined experimental and computational investigation. *Computers & Fluids*, 58, 88-101. doi: 10.1016/j.compfluid.2012.01.005.
- ❖ Payri, R., Salvador, F. J., Manin, J., & Viera, A. (2016). Diesel ignition delay and lift-off length through different methodologies using a multi-hole injector. *Applied Energy*, 162, 541-550.
- ❖ Payri, R., Viera, J. P., Gopalakrishnan, V., & Szymkowicz, P. G. (2017). The effect of nozzle geometry over the evaporative spray formation for three different fuels. *Fuel*, 188, 645-660. doi: 10.1016/j.fuel.2016.10.064
- ❖ Peraza, J. E., Salvador, F. J., Gimeno, J., & Ruiz, S. (2022). ECN Spray D visualization of the spray interaction with a transparent wall under engine-like conditions. Part I: Non-reactive impinging spray. *Fuel*, 307, 121699..
- ❖ Phankosol, S., Sudaprasert, K., Lilitchan, S., Aryasuk, K., & Krisnangkura, K. (2014). Estimation of surface tension of fatty acid methyl ester and biodiesel at different temperatures. *Fuel*, 126, 162-168. Doi: 10.1016/j.fuel.2014.02.054.
- ❖ Pickett, L. M., Kook, S., & Williams, T. C. (2009). Visualization of diesel spray penetration, cool-flame, ignition, high-temperature combustion, and soot formation using

- high-speed imaging. *SAE international journal of engines*, 2(1), 439-459. Doi: 10.4271/2009-01-0658
- ❖ Qian, J., & Law, C. K. (1997). Regimes of coalescence and separation in droplet collision. *Journal of fluid mechanics*, 331, 59-80. Doi: 10.1017/S0022112096003722
 - ❖ Qiu, T., Song, X., Lei, Y., Liu, X., An, X., & Lai, M. (2016). Influence of inlet pressure on cavitation flow in diesel nozzle. *Applied Thermal Engineering*, 109, 364-372. doi: 10.1016/j.applthermaleng.2016.08.046.
 - ❖ Quinn, W. R. (2005). Measurements in the near flow field of an isosceles triangular turbulent free jet. *Experiments in fluids*, 39(1), 111-126. Doi: 10.1007/s00348-005-0988-2.
 - ❖ Raheman, H., & Phadatare, A. G. (2003). Karanja esterified oil an alternative renewable fuel for diesel engines in controlling air pollution. *Bioenergy News*, 7(3), 17-23.
 - ❖ Rajamanickam, K., & Basu, S. (2017). Insights into the dynamics of spray–swirl interactions. *Journal of Fluid Mechanics*, 810, 82-126. Doi: <https://doi.org/10.1017/jfm.2016.710>
 - ❖ Raju, V. D., Venu, H., Subramani, L., Kishore, P. S., Prasanna, P. L., & Kumar, D. V. (2020). An experimental assessment of prospective oxygenated additives on the diverse characteristics of diesel engine powered with waste tamarind biodiesel. *Energy*, 203, 117821.
 - ❖ Rakopoulos, C. D., Rakopoulos, D. C., Giakoumis, E. G., & Kyritsis, D. C. (2004). Validation and sensitivity analysis of a two zone Diesel engine model for combustion and emissions prediction. *Energy conversion and management*, 45(9-10), 1471-1495.
 - ❖ Reitz, R. D. (1978). Atomization and other breakup regimes of a liquid jet. PhDT.
 - ❖ Reitz, R. D. (1996). Computer modeling of sprays. *Spray Technology Short Course*, Pittsburgh, PA.
 - ❖ Reitz, R. D., & Bracco, F. V. (1982). Mechanism of atomization of a liquid jet. *The physics of Fluids*, 25(10), 1730-1742. Doi: 10.1063/1.863650
 - ❖ Reitz, R. D., & Diwakar, R. (1986). Effect of drop breakup on fuel sprays. *SAE transactions*, 218-227
 - ❖ Sakthivel, R., Ramesh, K., Purnachandran, R., & Shameer, P. M. (2018). A review on the properties, performance and emission aspects of the third-generation biodiesels. *Renewable and Sustainable Energy Reviews*, 82, 2970-2992. doi: 10.1016/j.rser.2017.10.037.

- ❖ Salvador, F. J., Gimeno, J., De la Morena, J., & González-Montero, L. A. (2021). Experimental analysis of the injection pressure effect on the near-field structure of liquid fuel sprays. *Fuel*, 292, 120296
- ❖ Sarathy, S. M., Westbrook, C. K., Mehl, M., Pitz, W. J., Togbe, C., Dagaut, P., ... & Lu, T. (2011). Comprehensive chemical kinetic modeling of the oxidation of 2-methylalkanes from C7 to C20. *Combustion and flame*, 158(12), 2338-2357.
- ❖ Schadow, K. C., Gutmark, E., Parr, D. M., & Wilson, K. J. (2004). Selective control of flow coherence in triangular jets. *Experiments in Fluids*, 6(2), 129-135. Doi: 10.1007/BF00196464.
- ❖ Shahbandeh, M., 2020. Consumption of vegetable oils worldwide from 2013/14 to 2019/2020, by oil type (accessed 09/2020). <https://www.statista.com/statistics/263937/vegetable-oils-global-consumption>.
- ❖ Sharma, P., & Fang, T. (2014). Breakup of liquid jets from non-circular orifices. *Experiments in fluids*, 55(2), 1666. Doi: 10.1007/s00348-014-1666-z.
- ❖ Sharma, P., & Fang, T. (2015). Spray and atomization of a common rail fuel injector with non-circular orifices. *Fuel*, 153, 416-430. Doi: 10.1016/j.fuel.2015.02.119
- ❖ Sharma, Y., Yadav, R., Verma, S., Sehgal, M., & Gautam, R. (2019). Study About the Future of Electric Vehicles in the Current Indian Scenario (No. 2019-01-0922). SAE Technical Paper.
- ❖ Shlegel, N. E., Tkachenko, P. P., & Strizhak, P. A. (2020). Influence of viscosity, surface and interfacial tensions on the liquid droplet collisions. *Chemical Engineering Science*, 115639. Doi: 10.1016/j.ces.2020.115639
- ❖ Shu, Q., Wang, J., Peng, B., Wang, D., & Wang, G. (2008). Predicting the surface tension of biodiesel fuels by a mixture topological index method, at 313 K. *Fuel*, 87(17-18), 3586-3590. doi: 10.1016/j.fuel.2008.07.007.
- ❖ Singh, C. S., Kumar, N., & Gautam, R. (2021). Supercritical transesterification route for biodiesel production: Effect of parameters on yield and future perspectives. *Environmental Progress & Sustainable Energy*, 40(6), e13685. Doi: 10.1002/ep.13685
- ❖ Singh, D., Sharma, D., Soni, S. L., Inda, C. S., Sharma, S., Sharma, P. K., & Jhalani, A. (2021). A comprehensive review of biodiesel production from waste cooking oil and its use as fuel in compression ignition engines: 3rd generation cleaner feedstock. *Journal of Cleaner Production*, 307, 127299.

- ❖ Singh, D., Sharma, D., Soni, S.L., Sharma, S., Sharma, P.K., Jhalani, A., 2020. A review on feedstocks, production processes, and yield for different generations of biodiesel. *Fuel* 262, 116553. <https://doi.org/10.1016/j.fuel.2019.116553>.
- ❖ Singh, R. C., Chaudhary, R., Pandey, R. K., Maji, S., Babbar, A., Chauhan, B. S., ... & Mishra, C. (2012). Performance evaluation of an air cooled diesel engine fuelled with neat neem oil and diesel blends. Doi: 10.5958/j.0976-3015.3.1.006
- ❖ Singh, V., Agarwal, T., Saroha, N., & Gautam, R. (2019). Performance emissions and combustion analysis of CI engine using ethyl ester kusum oil and butanol blends (No. 2019-01-0568). SAE Technical Paper.doi: 10.4271/2019-01-0568
- ❖ Sosnowski, M., Krzywanski, J., & Gnatowska, R. (2017). Polyhedral meshing as an innovative approach to computational domain discretization of a cyclone in a fluidized bed CLC unit. In *E3S Web of Conferences* (Vol. 14, p. 01027). EDP Sciences.
- ❖ Spiegel, M., Redel, T., Zhang, Y. J., Struffert, T., Hornegger, J., Grossman, R. G., ... & Karmonik, C. (2011). Tetrahedral vs. polyhedral mesh size evaluation on flow velocity and wall shear stress for cerebral hemodynamic simulation. *Computer methods in biomechanics and biomedical engineering*, 14(01), 9-22.
- ❖ Stiesch, G. (2003). *Modeling engine spray and combustion processes*. Springer Science & Business Media.
- ❖ Suh, H. K., & Lee, C. S. (2016). A review on atomization and exhaust emissions of a biodiesel-fueled compression ignition engine. *Renewable and Sustainable Energy Reviews*, 58, 1601-1620. doi: 10.1016/j.rser.2015.12.329.
- ❖ Sun, Y., Alkhedhair, A. M., Guan, Z., & Hooman, K. (2018). Numerical and experimental study on the spray characteristics of full-cone pressure swirl atomizers. *Energy*, 160, 678-692.Doi: 10.1016/j.energy.2018.07.060.
- ❖ Taskiran, O. O. (2018). Investigation of the effect of nozzle inlet rounding on diesel spray formation and combustion. *Fuel*, 217, 193-201. doi: 10.1016/j.fuel.2017.12.031
- ❖ Venu, H., Raju, V. D., Subramani, L., & Appavu, P. (2020). Experimental assessment on the regulated and unregulated emissions of DI diesel engine fuelled with *Chlorella emersonii* methyl ester (CEME). *Renewable Energy*, 151, 88-102.
- ❖ Wan Omar, W.N.N., Nordin, N., Mohamed, M., Amin, N.A.S., 2009. A two-step biodiesel production from waste cooking oil: optimization of pre-treatment step. *J. Appl. Sci.* 9 (17), 3098–3103. <https://doi.org/10.3923/jas.2009.3098.3103>.

- ❖ Wang, H., Reitz, R. D., Yao, M., Yang, B., Jiao, Q., & Qiu, L. (2013). Development of an n-heptane-n-butanol-PAH mechanism and its application for combustion and soot prediction. *Combustion and Flame*, 160(3), 504-519.
- ❖ Wang, X., Huang, Z., Kuti, O. A., Zhang, W., & Nishida, K. (2010). Experimental and analytical study on biodiesel and diesel spray characteristics under ultra-high injection pressure. *International journal of heat and fluid flow*, 31(4), 659-666.
- ❖ Wang, Y., Ou, S., Liu, P., Xue, F., Tang, S., 2006. Comparison of two different processes to synthesize biodiesel by waste cooking oil. *J. Mol. Catal. Chem.* 252 (1–2), 107–112. <https://doi.org/10.1016/j.molcata.2006.02.047>.
- ❖ Wang, Z., Li, L., Wang, J., & Reitz, R. D. (2016). Effect of biodiesel saturation on soot formation in diesel engines. *Fuel*, 175, 240-248.
- ❖ Wierzbna, A. (1990). Deformation and breakup of liquid drops in a gas stream at nearly critical weber numbers. *Experiments in fluids*, 9(1-2), 59-64.
- ❖ Wierzbna, A., & Takayama, K. (1988). Experimental investigation of the aerodynamic breakup of liquid drops. *AIAA journal*, 26(11), 1329-1335. Doi: doi.org/10.2514/3.10044
- ❖ Yaakob, Z., Mohammad, M., Alherbawi, M., Alam, Z., & Sopian, K. (2013). Overview of the production of biodiesel from waste cooking oil. *Renewable and sustainable energy reviews*, 18, 184-193. Doi: [10.1016/j.rser.2012.10.016](https://doi.org/10.1016/j.rser.2012.10.016).
- ❖ Yadav, P. S., & Gautam, R. (2022). Experimental and theoretical assessment of surface tension using different biodiesels at elevated temperature. *Proceedings of the Institution of Mechanical Engineers, Part E: Journal of Process Mechanical Engineering*, 09544089221133252.
- ❖ Yadav, P. S., & Gautam, R. (2022). Numerical and experimental analysis on spray characteristics of biodiesel (waste cooking oil) using pressure swirl atomizer. *Environmental Progress & Sustainable Energy*, 41(3), e13761.
- ❖ Yadav, P. S., Chaturvedi, A. A., Sahu, A., Yadav, A., Fraynjiya, A., & Gautam, R. (2023). Effect of Nozzle Geometry and Fuel Modification on Atomization and Emission Characteristics in CI Engine: A Review. *Emerging Trends in Mechanical and Industrial Engineering: Select Proceedings of ICETMIE 2022*, 13-32. doi: [10.1007/978-981-19-6945-4_2](https://doi.org/10.1007/978-981-19-6945-4_2)
- ❖ Yadav, P. S., Said, Z., Gautam, R., Raman, R., & Caliskan, H. (2023). Novel investigation on atomization, performance, and emission characteristics of preheated jatropha oil methyl ester and ethyl ester. *Energy*, 126870. doi: [10.1016/j.energy.2023.126870](https://doi.org/10.1016/j.energy.2023.126870)

- ❖ Yadav, P., Kumar, N., & Gautam, R. (2021). Improvement in performance of CI engine using various techniques with alternative fuel. *Energy Sources, Part A: Recovery, Utilization, and Environmental Effects*, 1-27.
- ❖ Yoon, S. H., Park, S. H., & Lee, C. S. (2008). Experimental investigation on the fuel properties of biodiesel and its blends at various temperatures. *Energy & Fuels*, 22(1), 652-656. Doi: 10.1021/ef7002156.
- ❖ Yu, S., Yin, B., Deng, W., Jia, H., Ye, Z., Xu, B., & Xu, H. (2018). Experimental study on the spray characteristics discharging from elliptical diesel nozzle at typical diesel engine conditions. *Fuel*, 221, 28-34. Doi: 10.1016/j.fuel.2018.02.090
- ❖ Yu, S., Yin, B., Deng, W., Jia, H., Ye, Z., Xu, B., & Xu, H. (2019). Experimental study on the spray and mixing characteristics for equilateral triangular and circular nozzles with diesel and biodiesel under high injection pressures. *Fuel*, 239, 97-107. Doi: 10.1016/j.fuel.2018.10.146
- ❖ Yunyi, G., Changwen, L., Yezhou, H., & Zhijun, P. (1998). An experimental study on droplet size characteristics and air entrainment of elliptic sprays (No. 982546). Doi: 10.4271/982546
- ❖ Zhang, T., Dong, B., Chen, X., Qiu, Z., Jiang, R., & Li, W. (2017). Spray characteristics of pressure-swirl nozzles at different nozzle diameters. *Applied thermal engineering*, 121, 984-991. Doi: <https://doi.org/10.1016/j.applthermaleng.2017.04.089>
- ❖ Zhang, T., Dong, B., Chen, X., Qiu, Z., Jiang, R., & Li, W. (2017). Spray characteristics of pressure-swirl nozzles at different nozzle diameters. *Applied thermal engineering*, 121, 984-991.
- ❖ Zhang, X., He, Z., Wang, Q., Tao, X., Zhou, Z., Xia, X., & Zhang, W. (2018). Effect of fuel temperature on cavitation flow inside vertical multi-hole nozzles and spray characteristics with different nozzle geometries. *Experimental Thermal and Fluid Science*, 91, 374-387. doi: 10.1016/j.expthermflusci.2017.06.006.
- ❖ Zheng, H., Liu, Z., Wang, K., Lin, J., & Li, Z. (2020). Influence of orifice geometry on atomization characteristics of pressure swirl atomizer. *Science Progress*, 103(3), 0036850420950182.

List of Publications

Internation Journal:

1. **Yadav, P. S.**, Said, Z., Gautam, R., Raman, R., & Caliskan, H. (2023). Novel investigation on atomization, performance, and emission characteristics of preheated jatropha oil methyl ester and ethyl ester. *Energy*, 126870. Doi: 10.1016/j.energy.2023.126870
2. **Yadav, P. S.**, & Gautam, R. (2022). Experimental and theoretical assessment of surface tension using different biodiesels at elevated temperature. *Proceedings of the Institution of Mechanical Engineers, Part E: Journal of Process Mechanical Engineering*, 09544089221133252. Doi: <https://doi.org/10.1177/09544089221133252>
3. **Yadav, P. S.**, & Gautam, R. (2022). Numerical and experimental analysis on spray characteristics of biodiesel (waste cooking oil) using pressure swirl atomizer. *Environmental Progress & Sustainable Energy*, 41(3), e13761. Doi: 10.1002/ep.13761
4. **Yadav, P.**, Kumar, N., & Gautam, R. (2021). Improvement in performance of CI engine using various techniques with alternative fuel. *Energy Sources, Part A: Recovery, Utilization, and Environmental Effects*, 1-27. Doi: 10.1080/15567036.2020.1864517

Book chapter:

1. **Yadav, P. S.**, Chaturvedi, A. A., Sahu, A., Yadav, A., Fraynjiya, A., & Gautam, R. (2023). Effect of Nozzle Geometry and Fuel Modification on Atomization and Emission Characteristics in CI Engine: A Review. *Emerging Trends in Mechanical and Industrial Engineering: Select Proceedings of ICETMIE 2022*, 13-32. Doi: 10.1007/978-981-19-6945-4_2

Conference Paper:

1. **Title** “Experimental and theoretical assessment on spray characteristics of waste cooking oil at varying injection Pressure”, **ICETMIE**, 4-5 March, **2022**.
2. **Title** “Effect of higher injection pressure on biodiesel for spray formation”, **ISFT** 4-5 January, **2020**.

A Brief Biographical Sketch

Prem shanker Yadav was born on 03 July 1985 in Ghazipur, Uttar Pradesh, India. He did his B.Tech in Department of Mechanical Engineering from JSS Academy of Technical Education Noida Uttar Pradesh India in the Year 2009; M.Tech in Applied Mechanics Engineering from Indian Institute of Technology, Delhi, India in 2011. Further, He joined Department of Mechanical Engineering Delhi Technological University as Ph. D Scholar.

Mr. Prem shanker Yadav conducted research on 3-hole probe, 5-hole probe in wind tunnel study and single phase, multiphase flow on computational fluid dynamics. His M.Tech research was based on determination of flow characteristics on war ship. The PhD work work is focused on spray characteristics to emphasis on cleaner combustion with alternative fuel. he mainly emphasis on state-of -the art on nozzle geometry reformation technique, which purposes to employ an enhanced spray behavior of biodiesel, diesel and blends. His research also exhibits the waste to wealth policy, modification in fuel and heat transfer. However, the major goal is to enhance combustion, performance and emission characteristics with improvement in spray characteristics.

He has published four SCI and two Scopus indexed scientific research papers. Besides, one book chapter is published for a known publisher such as Springer. He also works as a reviewer for many reputed journals such as Springer, Elsevier etc. In recognition of his excellent research contribution, he has also been awarded the DTU Research Excellence award for executing commendable research work in the year 2023 and eligible in 2024.

Curriculum Vitae

Personal detail

Surname, First name:	Yadav, Prem shanker
Father's name:	Rajendra Singh Yadav
Mother's name:	Indravati Devi
Nationality	Indian
Date of Birth	3rd July 1985
Languages known:	English & Hindi
Permanent Address:	Vill-Dillachawar, P.O- Tokawan, Dist-Ghazipur, (U.P) 232331, India
Contact No:	+91-9968759147
Email Id:	prem0jss@gmail.com
Orcid id:	https://orcid.org/0000-0003-0777-4423

Education:

Degree	Specialization / Major	Year	Board/University	Marks percentage/CGP A
Ph.D.	Mechanical Engineering	2018 - 2023	Delhi Technological University, Delhi	NA
M.Tech	Applied Mechanics Engineering	2009 - 2011	Indian Institute of Technology, Delhi	7.0
B.Tech	Mechanical Engineering	2009 - 2005	JSS Academy of Technical, Noida	7.0

Research Focusses/Title of Dissertation:

- Biodiesel: Production, characterization & Utilization, fuel modification, spray characteristics, combustion & emission control, fuel-reformulation techniques, Thermo-fluids Heat transfer.
- Some studies on spray characteristics of alternative fuel and its effect on combustion, performance and emissions.

ACADEMIC PROJECTS:

- ❖ CNC part programming from various operation using CATIA.
- ❖ Transient analysis of metro bridge using ANSYS.
- ❖ Modification in geometry of Mast to reduce smoke ingress problem in war ship using CFD..

Publications:

Internation Journal:

5. **Yadav, P. S.**, Said, Z., Gautam, R., Raman, R., & Caliskan, H. (2023). Novel investigation on atomization, performance, and emission characteristics of preheated jatropa oil methyl ester and ethyl ester. *Energy*, 126870. Doi: 10.1016/j.energy.2023.126870
6. **Yadav, P. S.**, & Gautam, R. (2022). Experimental and theoretical assessment of surface tension using different biodiesels at elevated temperature. *Proceedings of the Institution of Mechanical Engineers, Part E: Journal of Process Mechanical Engineering*, 09544089221133252. Doi: <https://doi.org/10.1177/09544089221133252>
7. **Yadav, P. S.**, & Gautam, R. (2022). Numerical and experimental analysis on spray characteristics of biodiesel (waste cooking oil) using pressure swirl atomizer. *Environmental Progress & Sustainable Energy*, 41(3), e13761. Doi: 10.1002/ep.13761
8. **Yadav, P.**, Kumar, N., & Gautam, R. (2021). Improvement in performance of CI engine using various techniques with alternative fuel. *Energy Sources, Part A: Recovery, Utilization, and Environmental Effects*, 1-27. Doi: 10.1080/15567036.2020.1864517

Book chapter:

2. **Yadav, P. S.**, Chaturvedi, A. A., Sahu, A., Yadav, A., Fraynjiya, A., & Gautam, R. (2023). Effect of Nozzle Geometry and Fuel Modification on Atomization and Emission Characteristics in CI Engine: A Review. **Emerging Trends in Mechanical and Industrial Engineering: Select Proceedings of ICETMIE 2022**, 13-32. Doi: 10.1007/978-981-19-6945-4_2

Reviewer:

1. Journal of thermal engineering (Yildiz Technical University)
2. Fuel (Elsevier)
3. Biomass Conversion and Biorefinery (Springer)
4. IET Renewable Power Generation (Wiley)

Technical Skills:

- ★ Experience of product design via. Solid Edge, Solid Works, Pro-E and CATIA software
- ★ Good hands-on simulation softwares such as Computational fluid dynamics, CATIA, FEM.
- ★ Basic Knowledge of C, C++, Blue java
- ★ Experience in operating analytical instruments such as GC/MS, TGA, FTIR, XRD, FESEM, Flame Spray Pyrolysis System, AVL DITEST MDS 205, KiBoX Kistler Combustion. Analyzer

Awards/ Funding:

- ★ Awarded the DTU Research Excellence Award for commendable Research in the academic year 2022- 23, and eligible for 2023-24

References:

- | | |
|--|--|
| ❖ Dr. Raghvendra Gautam
Assistant Professor
Department of Mechanical Engineering
Delhi Technological University
raghvendrag80@yahoo.com | Dr. Sidhnath Singh
Professor
Applied mechanics department
IIT Delhi
sidhnathsingh@hotmail.com |
|--|--|

I hereby declare that the information furnished above is true to the best of my knowledge and belief.

Place: Delhi

(Prem shanker Yadav)